63-3-1

RADC-TDR-63-15

MEASUREMENT OF DIFFRACTION FIELDS OF FINITE CONES BY A SCATTERING TECHNIQUE USING LIGHT MODULATION

By
Ayhan Vural

TASK REPORT NO. 3
JANUARY 1963

ROME AIR DEVELOPMENT CENTER
Air Force Systems Command
Griffiss Air Force Base
Rome, New York

Project No. 4506, Task No. 450604

PREPARED UNDER CONTRACT NO. AF 30(602)-2646
By
ELECTRICAL ENGINEERING DEPARTMENT
COLLEGE OF ENGINEERING
Report EE 957-6301T3

SYRACUSE UNIVERSITY RESEARCH INSTITUTE
SYRACUSE 10, NEW YORK

RADC-TDR-63-15

MEASUREMENT OF DIFFRACTION FIELDS OF FINITE CONES BY A SCATTERING TECHNIQUE USING LIGHT MODULATION

Task Report No. 3

Contract No. AF 30(602)-2646

Project No. 4506 Task No. 450604

By

Ayhan Vural

SYRACUSE UNIVERSITY RESEARCH INSTITUTE

Approved by:
David K. Cheng
Project Director

Sponsored by:
Rome Air Development Center
Air Force Systems Command
Griffiss Air Force Base
Rome, New York

S.U.R.I. Report No.
EE 957-6301T3

Date:
2 January 1963

MEASUREMENT OF DIFFRACTION FIELDS OF FINITE CONES BY A SCATTERING TECHNIQUE USING LIGHT MODULATION

ABSTRACT

The present investigation perfects a new method for measuring microwave near-fields and applies the techniques thus developed to the measurement of diffraction fields around finite cones.

A small photoconductive scatterer is employed in a light-modulated scattering technique, which is modulated by light pulses at a chosen rate. Complete electrical isolation is achieved and all complications and sources of error due to connection disturbance and scatterer movement are thereby eliminated.

The results of the measurements with a circular aperture and its disk complement were in complete agreement with the data obtained by more conventional methods, thus validating the operation of the system.

Extensive data on the diffraction field of finite cones have been obtained, verifying the advantages and usefulness of this method. Measurements have been largely confined to the principal component of the electric field distributions but not limited to the principal planes. The cross-polarized component of the diffraction field was also measured. In all cases it was insignificant in comparison with the principal component. The results of the principal plane measurements have also been plotted in three-dimensional contours which afford a better perspective.

TABLE OF CONTENTS

		Page
	ABSTRACT	ii
	TABLE OF CONTENTS	iii
I	INTRODUCTION	
	I-1 Statement of the Problem	1
	I-2 Field Measurements by Modulated Scattering Technique	2
	I-3 Scattering by Light Modulation	5
II	THE SCATTERING TECHNIQUE BY LIGHT MODULATION	
	II-1 Theory of Operation	7
	II-2 Choice of Photoconductive Devices	9
	II-3 Spectral Response	13
	II-4 Selection of Modulation Frequency	14
	II-5 Summary of Selection Rules	16
III	THE OPTICAL SYSTEM	
	III-1 The Light Source	22
	III-2 The Focusing Assembly	22
	III-3 Chopper Design	23
IV	PRELIMINARY EXPERIMENTS	
	IV-1 The Experimental Setup	26
	IV-2 Measurement Procedure	28
	IV-3 Determination of the Phase Center Location	30
	IV-4 Diffraction by a Circular Aperture	30
V	DIFFRACTION BY A CONE	
	V-1 Discussion of the Analytical Problem	39
	V-2 Scattering by a Semi-Infinite Cone	40

VI EXPERIMENTAL RESULTS

VI-1 Cone Design Considerations. 53

VI-2 Measurement of Diffraction Fields in the H-Plane. . . 53

VI-3 On-Axis Field Measurements. 81

VI-4 Discussion of Results 81

VII CONCLUSIONS 88

APPENDIX. 89

BIBLIOGRAPHY. 92

ACKNOWLEDGEMENT 94

DISTRIBUTION LIST 95

I. INTRODUCTION

I-1. Statement of the Problem

The broad field of scattering and diffraction of waves from obstacles in a homogenous medium has been long investigated in the field of optics. The interest in this subject has notably increased during the past decade because of its relevance in the application of more general electromagnetic phenomena to radar, which operates essentially on the basis of the scattering properties of an obstacle, namely, the target, and advanced antenna design.

Diffracted field in an environment where an incident wave impinges on an obstacle is defined as the total field in the presence of the obstacle, and scattered field is the difference between the total field and the field that would exist if the obstacle were absent. The scattering properties of an object are important in two different but related problems. The first of these deals with the determination of the diffraction field in the vicinity (near zone) of an obstacle of any shape; the second relates the properties of the back-scattered waves from a distant (far zone) object to a quantity called the radar cross section. Analytical solutions to both of these problems may be obtained, in principle, by solving the equations governing the problems with suitable mathematical methods subject to appropriate boundary conditions. However, analytical solutions are limited to idealized situations and in many cases, a variety of approximations must be made. The degree of the approximations necessary both in order to formulate the problem and to obtain a numerical result from the solution depends on the class of the problem and on the particular method used. In general, the evaluation

of far-zone fields is relatively easy to handle both analytically and experimentally, although it usually still is a formidable task. Many mathematical techniques and experimental methods have been proposed in recent years, but analytical solutions have been obtained only for a few simple geometric shapes and many of the approximate solutions remain inadequate for more general problems.

In the study of the diffraction of electromagnetic waves from obstacles of complex shapes, an exact analytical approach is usually not possible and approximate mathematical solutions are generally remote from actual physical conditions. In these instances, experimental results obtained with the aid of carefully designed apparatus are of great importance.

The purposes of this project are:

1. To develop a new experimental technique based on the modulation of a photoconductive scatterer for measuring microwave near fields.
2. To check the validity of this technique by measuring a known field for which exact solutions exist and accurate experimental results are available.
3. To apply this technique to the measurement of unknown fields.

1-2. Field Measurements by Modulated Scattering Technique

A complete determination of the diffraction field of an obstacle requires a knowledge of the field distributions at every point in the space surrounding the obstacle. In an experimental study, this can only be

done with the aid of an auxiliary detection device located at the particular points. The existence of this device disturbs the ideal problem. However, this approximation is inevitable. The main difference between the various measurement techniques lies in the principle of operation of the detection device which is generally in the form of a miniature dipole or a receiving loop. In order to correlate experimental results with theoretical predictions quantitative theory of such devices is necessary.

The most common of these experimental techniques is the so-called probing technique, which employs a receiving antenna in the form of a dipole or a loop at the point of observation connected with a transmission line to the receiving system.

To overcome the difficulties involved in this technique due to disturbances caused by the trailing transmission line, a scattering technique was introduced for the measurement of electric field distributions.[1] The principle of this method is to relate the detected signal scattered back from a very short, thin straight wire to the square of the component of the electric field along the wire. Although this system eliminated the transmission line connections, a very high degree of stability and strict tuning requirements limited the usefulness of the system from a practical point of view.

The modulated scattering technique[2] is an extension of the scattering technique to relax the tuning and stability requirements and to increase the sensitivity of the measurements by simply coding the scattered signal from a dipole. The amplitude modulation of the scattered field, which is set up by the induced currents on the scatterer may be achieved in several

ways. The original and most common method, as it was introduced by Richmond,[2] employed the non-linear characteristic of a miniature semiconductor diode fed by an audio modulating signal. The change of the impedance of the diode under the modulating current causes periodic changes of the current distribution induced on the diode by the total field of interest. The amplitude of the scattered field which is set up by these currents, is then modulated at the same rate. This modulated signal is reflected back to the source, separated from the transmitted signal by means of a hybrid junction, and subjected to coherent detection. It may be shown[1] that when the diode satisfies certain requirements, which will be discussed later, the magnitude of the detected signal is proportional to the square of the magnitude of the tangential component of E along the diode and the phase is twice the phase of this component of E within an additive constant.

Recently this system was revised and extended to the independent measurements of magnetic field distributions.[3] The modulated scattering technique employing diode scatterers has gained unique features of application with this latest development. However, the electrical connections to the diodes carrying modulating current still require consideration. In an experiment where it is possible or required to use a conducting ground plane these connections may be located in their major part behind the plane. The disturbances that would be caused by the exposed part may be reduced considerably by using cotton threads coated with highly resistive material. Yet in a more general experiment this would be a questionable problem and also introduce practical difficulties.

Thus a scatterer which is completely isolated in the measurement space with the possibility of being modulated still remain a desirable device.

I-3. Scattering by Light Modulation

In recent years various modulation methods of scattered fields for microwave diffraction field measurements have been proposed. These included mechanically modulated scatterers[4] and small resonant scatterers.[5] The most common of these methods, from a practical point of view, employs electronic modulation of the impedance of a diode located in the diffraction field as discussed previously. However, the existence of leads connecting the diode to the modulator involved special considerations as well as experimental difficulties.

This report presents another type of modulating mechanism utilizing periodic changes in the conductivity of a photoelectric material located in the field under measurement upon which light pulses shine at a fixed rate. The diffraction field is thus subjected to modulation at the pulse repetition rate. By the use of this system, it is possible to isolate the scatterer completely at any point in the diffraction field, thereby eliminating all the complications due to connection disturbances and scatterer movement.

The principle of the modulation mechanism is much the same as that of the regular diode dipole; only the manner in which modulation is applied to the scatterer is different. A small dipole is centrally loaded by an

element of photoconductive material. Under the influence of the incident electric field a current distribution results on the dipole. When the dipole is illuminated by a light source whose intensity changes periodically, the resistance of the photoconductive material follows this variation. If the magnitude and the level of this resistance variation satisfies certain requirements, to be discussed later, this causes the current distribution on the dipole to vary periodically. In turn, the scattered field which is set up by the current distribution becomes modulated at the frequency of the light pulses.

This feature of the light modulation method has distinct advantages in that it makes possible the use of the isolated scatterer, and that it reduces the error and the effort involved in measurement.

II. THE SCATTERING TECHNIQUE BY LIGHT MODULATION

II-1. Theory of Operation

When an obstacle is placed in the radiation zone of a source a total field E which is the sum of the incident field E^i and the scattered field E^s results in the space containing the source and the obstacle. The problem is to determine the diffraction field near or at the surface of the obstacle. This involves the determination of the phase, magnitude and the polarization of the electric and magnetic fields at all desired points. As it was mentioned earlier, this can only be done, in an experimental investigation, in reference to an auxiliary small scatterer. Then the operation of the system as a whole is based on the theory of operation of this scatterer.

When the conducting scatterer is placed at some point in the total field to be measured, a current distribution is induced on the scatterer such that the field set up by the current cancels the component of the original field tangent to its surface. Naturally, there is a disturbance of the field caused by the scatterer. If this disturbance is not large in magnitude to affect the original field then the field cancelled by the induced current is the tangential component of the total field at that point in the absence of the scatterer but in the presence of the obstacle. Under this condition the current on the scatterer, and hence the back-scattered signal, can be related to that component of the total field along the dipole.

The formulation of the back-scattered signal is essentially the same as the diode scatterer case except the fact that the resistance change is now a function of modulating light rather than current. With an analysis using the superposition of the back-scattered signals from an open-

circuited dipole and from a radiating dipole, it was shown that[6] the received signal may be expressed as

$$V = V_o - K \frac{E_d^2 l_d^2}{Z + Z_L} \tag{1}$$

where V_o is the contribution of the open-circuited dipole, E_d is the component of the electric field along the scatterer, l_d is the effective length of the scatterer, Z and Z_L are the input and junction impedances respectively. K is a constant if the source excitation is kept constant. Only the second term in this equation is modulated and detected because the junction impedance Z_L is the only quantity which is affected by the modulation. This result may be summarized as follows:

a) The magnitude of the detected signal is proportional to the square of the magnitude of the E component along the scatterer.

b) The phase of the detected signal is equal to twice the phase of E component along the scatterer plus a constant phase shift.

It should be noted that this analysis is valid only when the scatterer is small, with respect to wavelength, and thin. Secondly, because of the finite dimensions of the scatterer, however small, the field measured is the average value about the point of interest. The measurement of components of total field is based on this result. When the scatterer is moved through the field with any predesigned orientation, the back scattered signal is proportional to the square of that component of E parallel to the scatterer which exists in the absence of the scatterer.

II-2 Choice of Photoconductive Devices

Photoelectrical transducers are designed to convert optical impulses into electrical signals. There are three major categories under the title of photoelectrical devices. The first class behaves primarily as variable resistors. A change in the intensity of incident light results in a change in the conductivity of the device. These are called photoconductors. The second class produces an open-circuited voltage which is proportional to the light intensity. Finally, for the last class, the response is in the form of a photo-current proportional to the light intensity.

The photoelectrical device used in this experiment belongs to the first class, since the modulation mechanism is controlled by the variation of resistance of the scatterer. Photoconductivity is the phenomenon of an increase in the conductivity of a material when it is illuminated by light of sufficiently small wavelength. Although this effect is observed in almost all semiconductor materials and PN junctions, the magnitude and the level of this variation change from material to material. This phenomenon is simply caused by the creation of extra free carriers, hole-electron pairs, upon irradiation. This can only occur if the absorbed photons have sufficient energy, i.e. $hf \geq E_g$ where E_g is the energy gap between the conduction and valence bands, h is the Planck's constant, and f is the frequency.

By considering the motion of a free electron under the influence of a time-harmonic electric field, the electromagnetic conductivity of a semiconductor material may be expressed as[7]

$$\sigma = \frac{N e^2}{m\left(\omega^2 + \frac{1}{\tau^2}\right)} \left[\frac{1}{\tau} + j\,\omega\right]$$

where N = Free electron density
e = Electronic charge
m = Mass of an electron
τ = Time between scattering collisions

Since N is proportional to light intensity, conductivity changes as the intensity of the exciting light changes.

An extensive study of semiconductor crystals, films and PN junctions has been made to determine the characteristics appropriate for use as a modulated scatterer. Most of these determinations were made from an experimental point of view. The complexity of requirements for a photoconductive material to be used for such a purpose in the experiments included the following:

Silicon crystals
Germanium crystals
Lead-Sulfide films
Cadmium-Sulfide "
Cadmium-Selenide "
PN junctions (silicon and germanium)
Photo diodes (semiconductor)

Generally, the requirements for materials to be used as a modulated scatterer arise from two distinct considerations.

1. Operation of the device as a dipole. This is primarily related to the geometric shape and size of the object.

a) The scatterer must be sufficiently small with respect to wavelength to provide a point representation on the average.

This rather constrains the length of the dipole to be short to indicate the field at a point.

b) It must be slender to discriminate against orthogonal polarization. It has been shown that[2] for an unmodulated scatterer a length-to-width ratio of at least 50 must be provided. However, for a modulated scatterer this restriction may be relaxed since the scattered field due to the orthogonal component is not modulated.

c) The perturbing effect of the scatterer to the original field by its existence might be reduced by using detectors made of thin films of photosensitive materials.

d) Finally, the fact that the photodetector in question must be operated under unbiased conditions in order to provide isolation places some degree of restriction on the selection.

2. Factors to be considered from the point of view of modulation and detection. These originate from the physical and electrical parameters used to differentiate between different photoconductive detectors.

a) Spectral response. This must yield a maximum value at or near visible light frequencies. It should also match the effective region of the spectral energy distribution of the light source.

b) Frequency response. The speed of response is related to the time constants of the detector. Good frequency behavior permits the use of higher modulation frequencies which are more desirable for practical purposes.

c) Sensitivity. This is measured in terms of the ratio of dark to light resistance values. A resistance variation of at least 100 Kohm must be provided by the material used upon illumination from a source of variable intensity. What is more important is the level of this resistance variation. Materials with light resistances as small as possible are preferred. This is true since the percentage of modulation depends upon how closely the loaded dipole may be approximated by a short and an open circuit at its center when the incident light is on and off.

d) Noise equivalent power and detectivity. This is defined as the power which produces a signal equal in magnitude to the noise of a detector. As a figure of merit of a detector the quantity called detectivity might be useful. This is defined as the signal to noise ratio for a 1cps. amplifier bandwidth produced by 1w. ave. power falling onto a detector of 1 cm^2 area.

e) Behavior at microwave frequencies. This is determined by the change in detector parameters at microwave frequencies.

f) Possibility of tuning the scatterer to the operating frequency. This is desirable if it can be achieved without affecting the operation of the scatterer as a dipole. It has been shown that[5] the scattered field from a resonant scatterer may be in the order of 30 db. stronger than from those which are non-resonant.

A clear understanding of the aforementioned factors makes it possible to develop photoconductive scatterers with desired characteristics.

Experiments were conducted to determine the parameters associated with the listed photoconductive materials. While theoretically all these requirements must be satisfied by the selected material, it is practically impossible to control production techniques to such an extent that all the desired characteristics are obtained. In this case the only approach would be first to select a material satisfying the physical and electrical requirements, then to construct a scatterer from this material having the best possible geometry.

II-3. Spectral Response

Spectral sensitivity is essentially set by the basic material used in the detector. The maximum wavelength to which a photoconductor is sensitive is determined by the minimum photon energy required to free a charge carrier.

The relative spectral response of a detector is determined by measuring the detector signal as a function of wavelength of the incident light. It may be obtained by illuminating the cells with monochromatic radiation from a calibrated monochromator equipped with a tungsten light source.

The ac signal, S, across a load resistor, R_L, of a series circuit containing the detector and battery, E, is determined as follows: When there is no modulation the voltage across R_L is

$$E_L = \frac{E\, R_L}{R_D + R_L} \tag{3}$$

where R_D is the resistance of the detector. By the action of the modulated radiation an ac signal is produced across R_L such that

$$S = \Delta E_L = \frac{d\,E_L}{d\,R_D}\ \Delta R_D$$

performing the operation one has

$$S = E\,\frac{R_D\,R_L}{(R_D + R_L)^2}\ \frac{\Delta R_D}{R_D} \qquad (4)$$

If $\Delta R_D/R_D$ is replaced by $\Delta n/n$, the fractional change in the carrier density, and use is made of the equation $\Delta n = G\tau$ where G represents the rate of generation of charge carriers per unit volume and τ is the lifetime of a free carrier, then the expression for the signal becomes

$$S = E\,\frac{R_L\,R_D}{(R_L + R_D)^2}\ \frac{G\tau}{n} \qquad (5)$$

The spectral responses of different materials used in the experiments are illustrated in Fig. 1., as given in the technical publications of Clairex Corp. and Texas Instruments Inc.

II-4. Selection of Modulation Frequency.

Frequency response is determined by the time constant of the photoconductive material, which in turn is a function of light level.

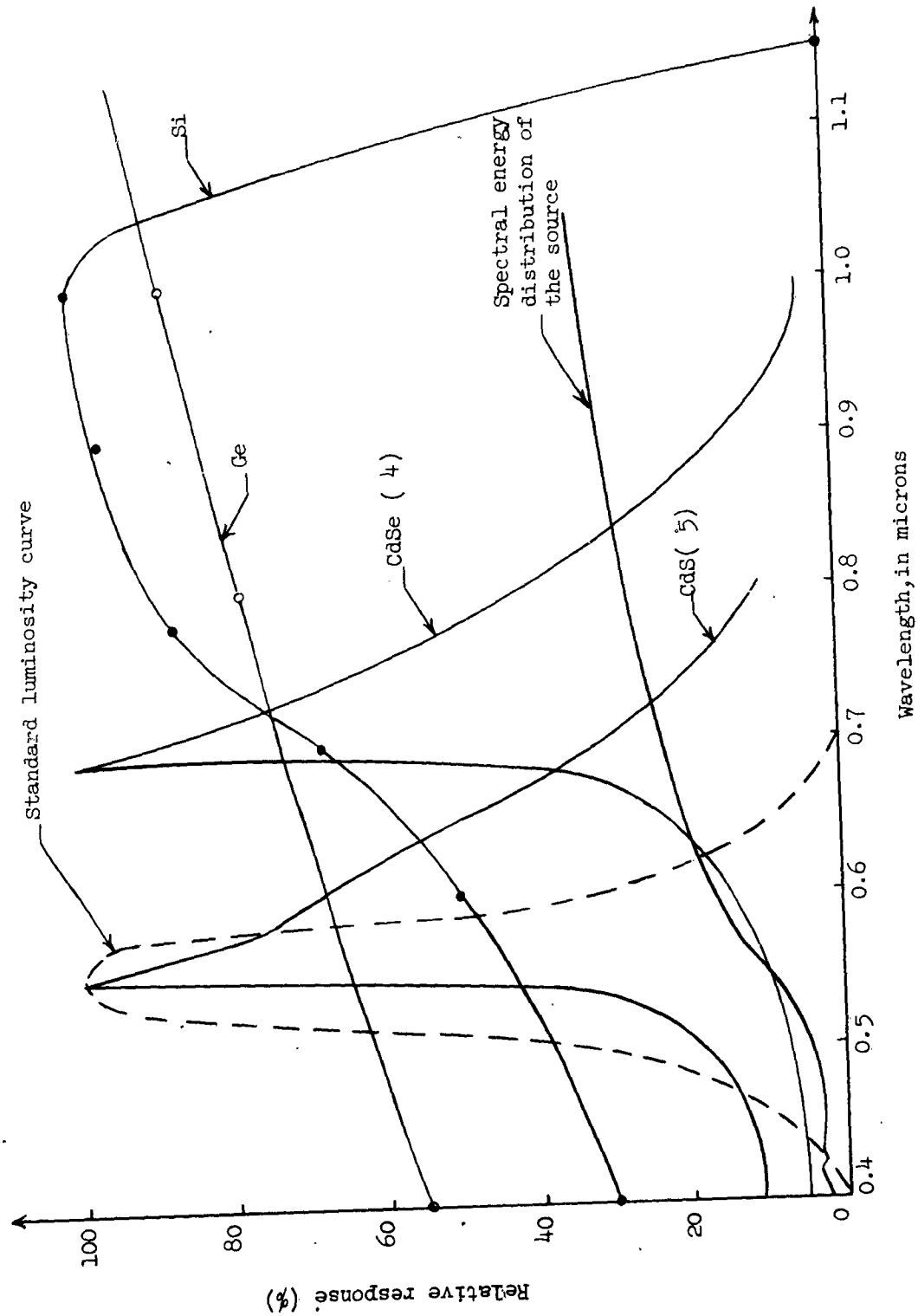

Fig. 1. Spectral responses of various photoconductive materials

It is essentially limited by the decay time that can be directly related to the recovery time of the semiconductor material. It takes a finite time for charge carriers to recombine after the excitation has been removed.

The speed of response may be determined by subjecting the detector to a square radiation pulse and observing the rise and decay of the signal. The square radiation pulse may be obtained by focusing the energy from a globar source onto a slit which is placed in front of a rotating sector disc. If the decay is exponential the time constant is given by the time taken for the signal to decay from its equilibrium value under exposure to radiation to 1/e of this value. Fig. 2. illustrates the behavior of the time constants of CdS and CdSe detectors as functions of light level.

As a more practical experiment the amplitude of the ac signal produced by the detector under the action of different modulation frequencies was determined. Signal was measured across a load resistor in series with a battery and the detector. Amplitude curves for CdS and CdSe detectors are shown in Fig. 3. as functions of modulating frequency. It is clear that in order to obtain large signal amplitudes a reasonably low modulation frequency must be used with these materials. However, considering the overall frequency response of the system a modulation frequency of 300 cps was selected.

II-5. Summary of Selection Rules.

Most of the materials listed in Section II-2, except CdS and CdSe, were eliminated in the preliminary experiments because of their poor

It is essentially limited by the decay time that can be directly related to the recovery time of the semiconductor material. It takes a finite time for charge carriers to recombine after the excitation has been removed.

The speed of response may be determined by subjecting the detector to a square radiation pulse and observing the rise and decay of the signal. The square radiation pulse may be obtained by focusing the energy from a globar source onto a slit which is placed in front of a rotating sector disc. If the decay is exponential the time constant is given by the time taken for the signal to decay from its equilibrium value under exposure to radiation to 1/e of this value. Fig. 2. illustrates the behavior of the time constants of CdS and CdSe detectors as functions of light level.

As a more practical experiment the amplitude of the ac signal produced by the detector under the action of different modulation frequencies was determined. Signal was measured across a load resistor in series with a battery and the detector. Amplitude curves for CdS and CdSe detectors are shown in Fig. 3. as functions of modulating frequency. It is clear that in order to obtain large signal amplitudes a reasonably low modulation frequency must be used with these materials. However, considering the overall frequency response of the system a modulation frequency of 300 cps was selected.

II-5. Summary of Selection Rules.

Most of the materials listed in Section II-2, except CdS and CdSe, were eliminated in the preliminary experiments because of their poor

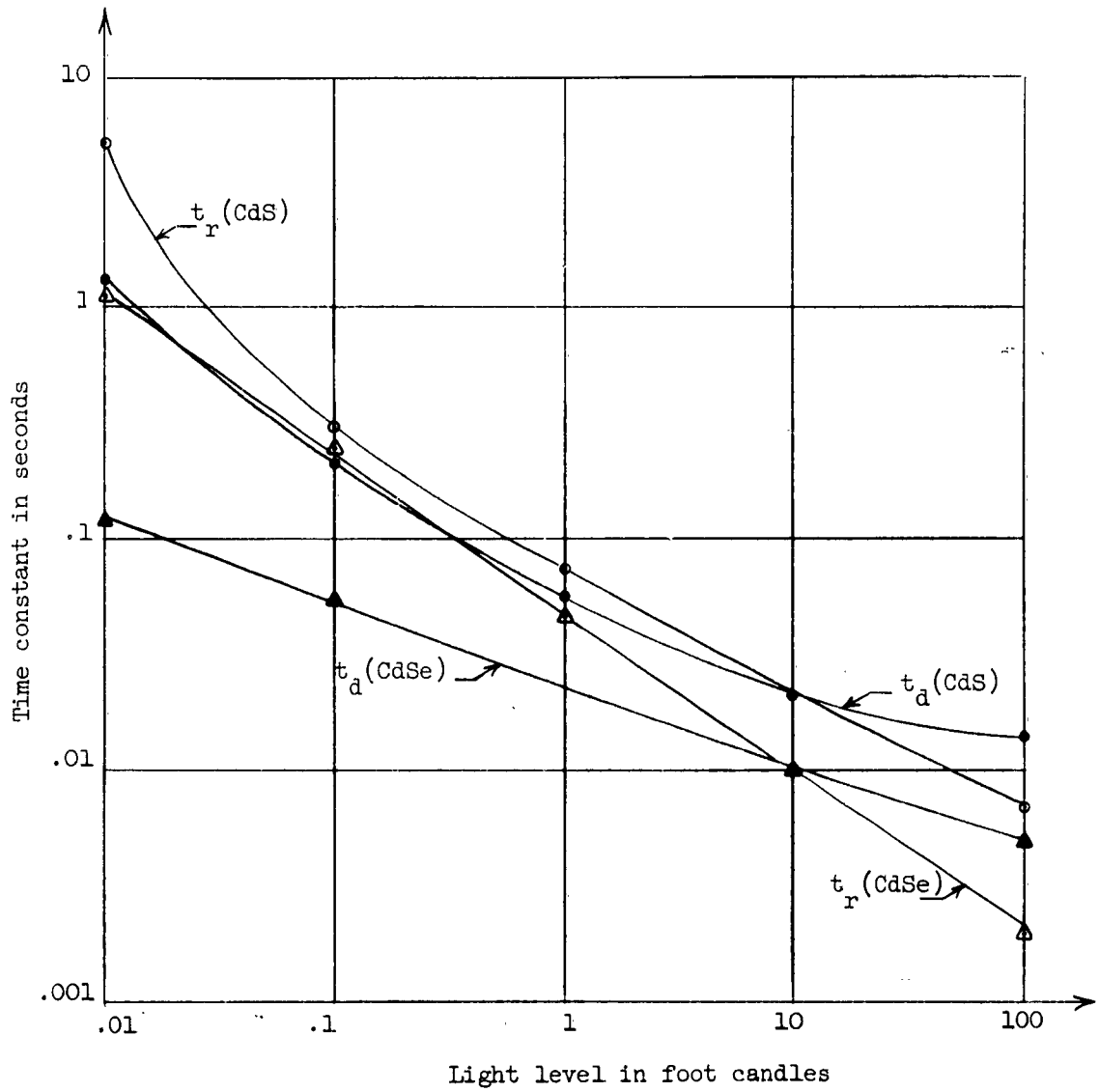

Fig. 2. Time constants of CdS and CdSe materials (plotted from the published data of Clairex Corporation)

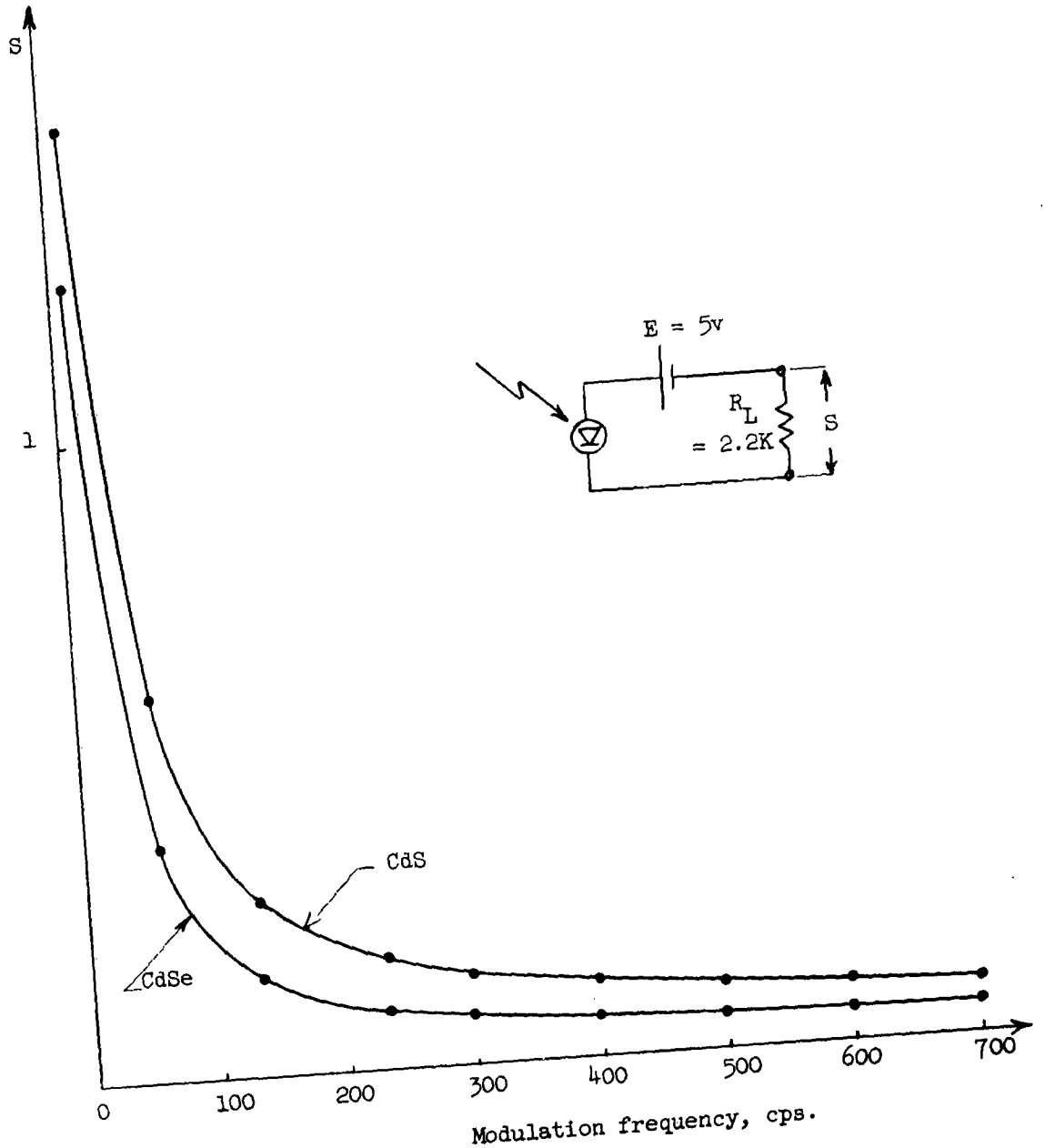

Fig. 3. Signal amplitude, S, at various chopping frequencies

microwave behaviour. A scatterer made of CdSe material was used in the experiments in consideration of its higher sensitivity and faster speed of response. Resistance curves for commerically available photoconductive cells CL604L (CdSe) and CL605L (CdS) (products of Clairex Corp.) are plotted in Fig. 4. versus light level. As it may be seen from the figure, CdSe has relatively low light resistance. This was the main factor for its selection, as has been emphasized before.

The scatterer was constructed from a combination of very thin CdSe film elements having dimensions of approximately .25 by .02 cm. The electrodes of a CL604L (CdSe) photoconductive cell were used as sensitive elements. Two axial leads of lengths less than $\lambda/8$ were attached to the perfectly conducting electrodes connecting the elements at the top and bottom. The elements were hermetically sealed into a glass enclosure. To increase the response a resonant scatterer was later devised. This was accomplished by using two quarter-wavelength leads perpendicular to the axis of the elements instead of axial leads. Then the scatterer was used to tune up to the operating frequency by changing the geometry of the leads. Thus an increase in response of 10 db. was obtained.

It has been shown that[7], in the case of CdS, the expression for conductivity in Eq.2. may be simplified at X-band frequencies. This was done by using the approximation $1/\tau \gg w$ due to the calculated value of $\tau = 2.8 \times 10^{-14}$ seconds. With this approximation, the electromagnetic conductivity of CdS may be expressed as,

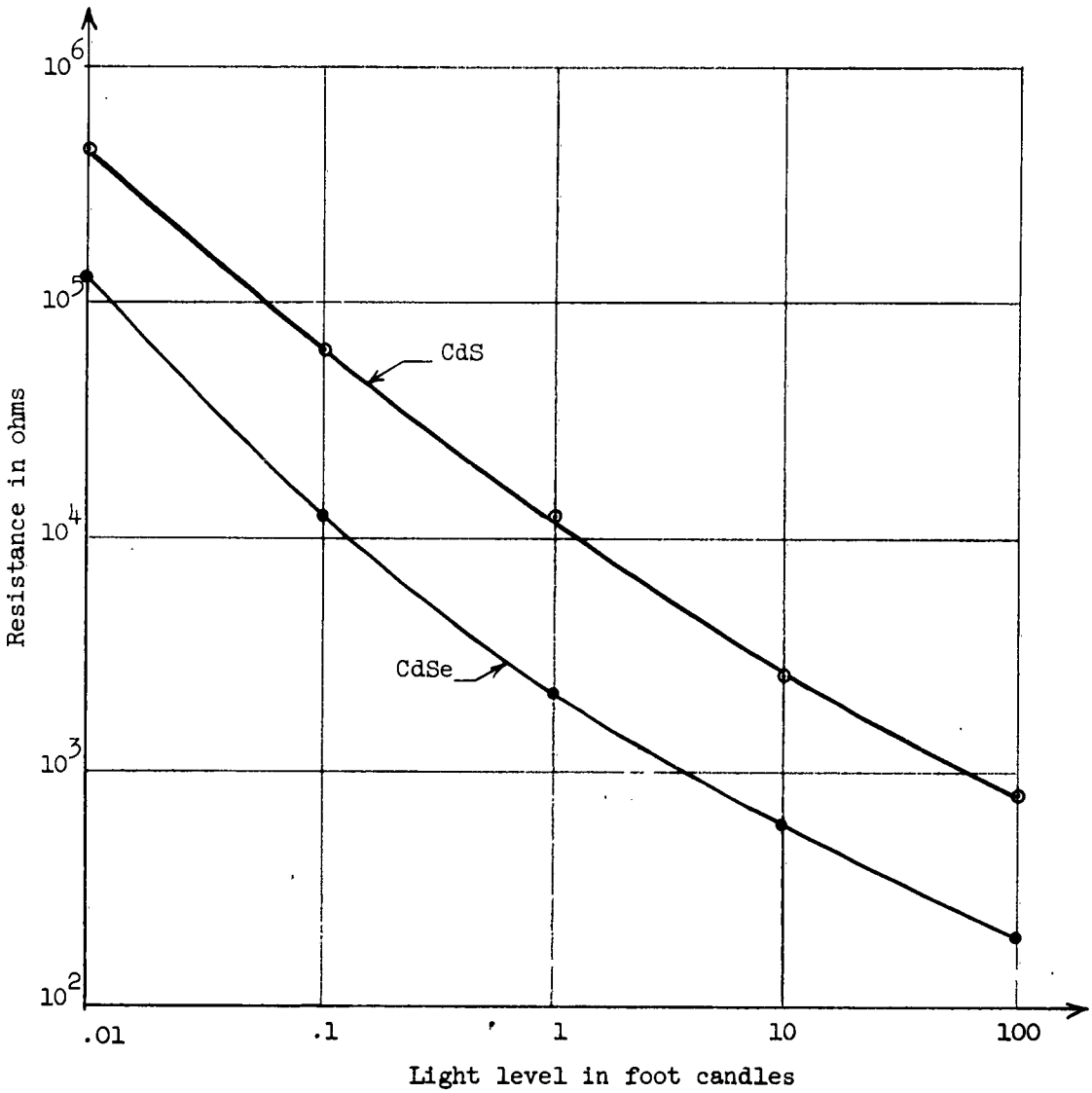

Fig. 4. Resistance of CdS and CdSe scatterers as function of light level

$$\sigma \doteq \frac{Ne^2 \tau}{m} \qquad (6)$$

The fundamental nature of CdSe cyrstals is exactly the same as that of CdS. The mobility of electrons in CdSe is of the same order of magnitude as in CdS[8]. The small difference between the conductivities of CdS and CdSe materials is due to the difference in the value of free electron density, N. This density depends on the amount of doping of the material.

III. THE OPTICAL SYSTEM

The performance of a photoconductive modulation system once the scatterer has been selected depends upon the design of a proper optical system. The optical system which was specially constructed in accordance with the needs of this experiment consists of three main parts: a light source, a chopper and a focusing assembly.

III-1. The Light Source

A high power concentrated arc lamp (Sylvania, type K-300) was used as the light source. The spectral energy distribution of the lamp is illustrated in Fig. 1. A special feature of this lamp is its essentially point-source characteristic with a brightness of 29,000 candles per square inch. The high-intensity narrow beam emitted by the lamp results in a uniform, compact spot over the surface of the scatterer upon focusing. These characteristics made it possible to relax the focusing requirements to some extent. It was observed that the response of the photoconductive scatterer remained approximately constant over a distance of $\mp$ 5 wavelengths (λ=3.2 cm.) about the focusing point.

III-2. The Focusing Assembly

Concentrated arc lamps usually do not require complicated optics. In this system focusing was accomplished by means of two sets of lenses. The condensing lens was located at the aperture of a ventilated box containing the light source. At this stage the uniform light beam emerging from the condensing lens was chopped by a rotating chopper blade before it reached the focusing lens. A focusing lens of 508 mm. focal length was used to focus the modulated light energy upon the scatterer.

III-3 Chopper Design

The design of the chopper was based on a Fourier analysis determining the spectrum of the modulating frequency and its harmonics, and relating them to the radiation power emanating from the light source. It has been shown that[9] by this analysis a relationship between the aperture radius-to-chopper wheel radius ratio and the number of notch-tooth pairs may be established to produce a fundamental amplitude equal to the ideal sinusoidal modulation of radiation emanating from the same aperture. The same relationship holds also for the equality of the rms value of the radiation modulated in the assumed manner to the rms value of the radiation modulated in an ideal sinusoidal manner. This relationship between the number of notch-tooth pairs and the radii ratio is plotted in Fig. 5.

The chopper blade was driven by a hysteresis synchronous motor operating at fixed speed of 1800 rpm. A sequence of light pulses of frequency 300 cps resulted from the chopping action of the blade containing 10 notch-tooth pairs. The geometry of the chopper blade is illustrated in Fig. 6.

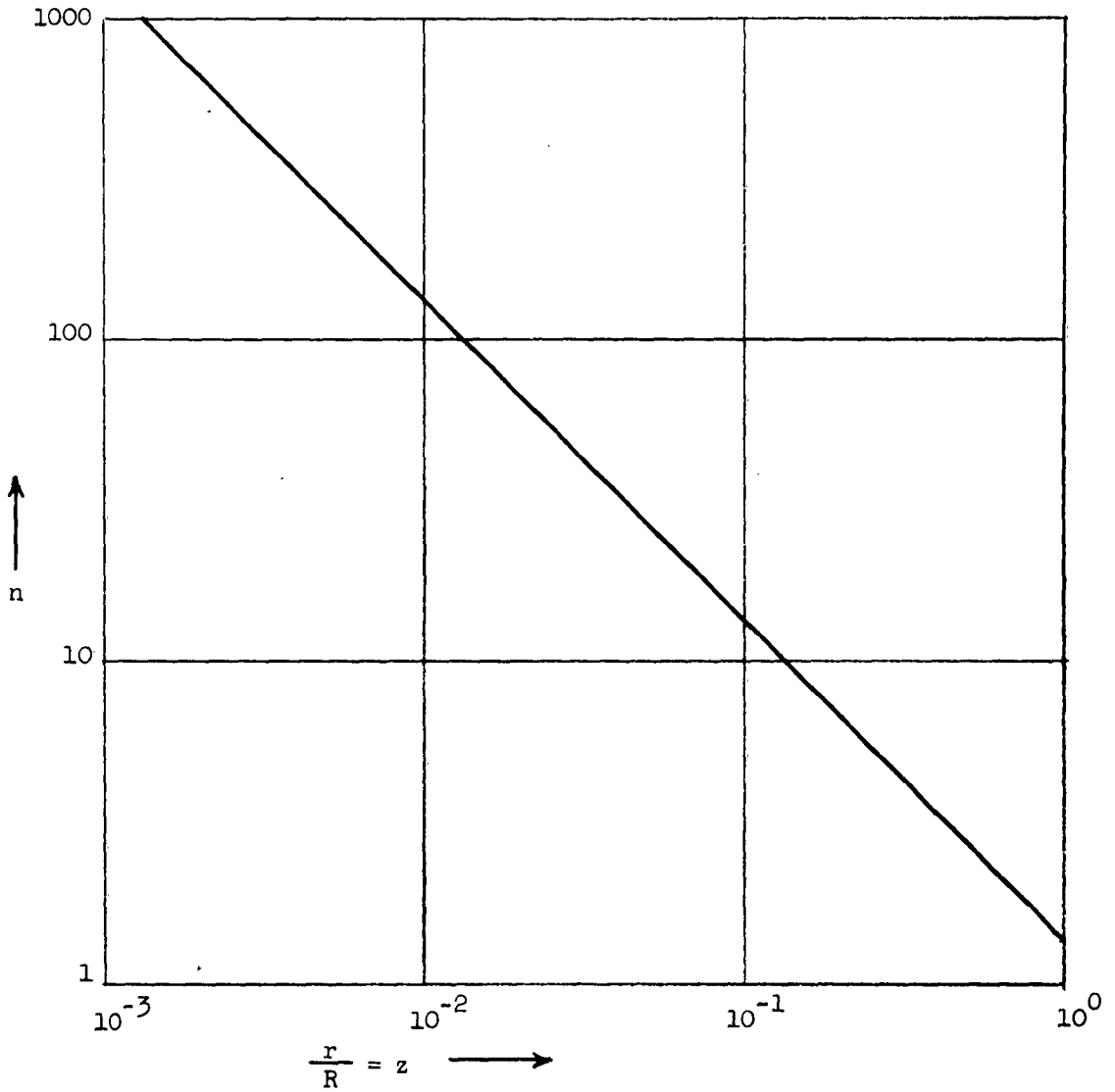

Fig. 5. The number of notch-tooth pairs, n, as a function of aperture radius-to-chopper wheel radius ratio, z, that will produce a fundamental equal to that produced by the ideal sinusoidal modulation of radiation emanating from the same aperture.

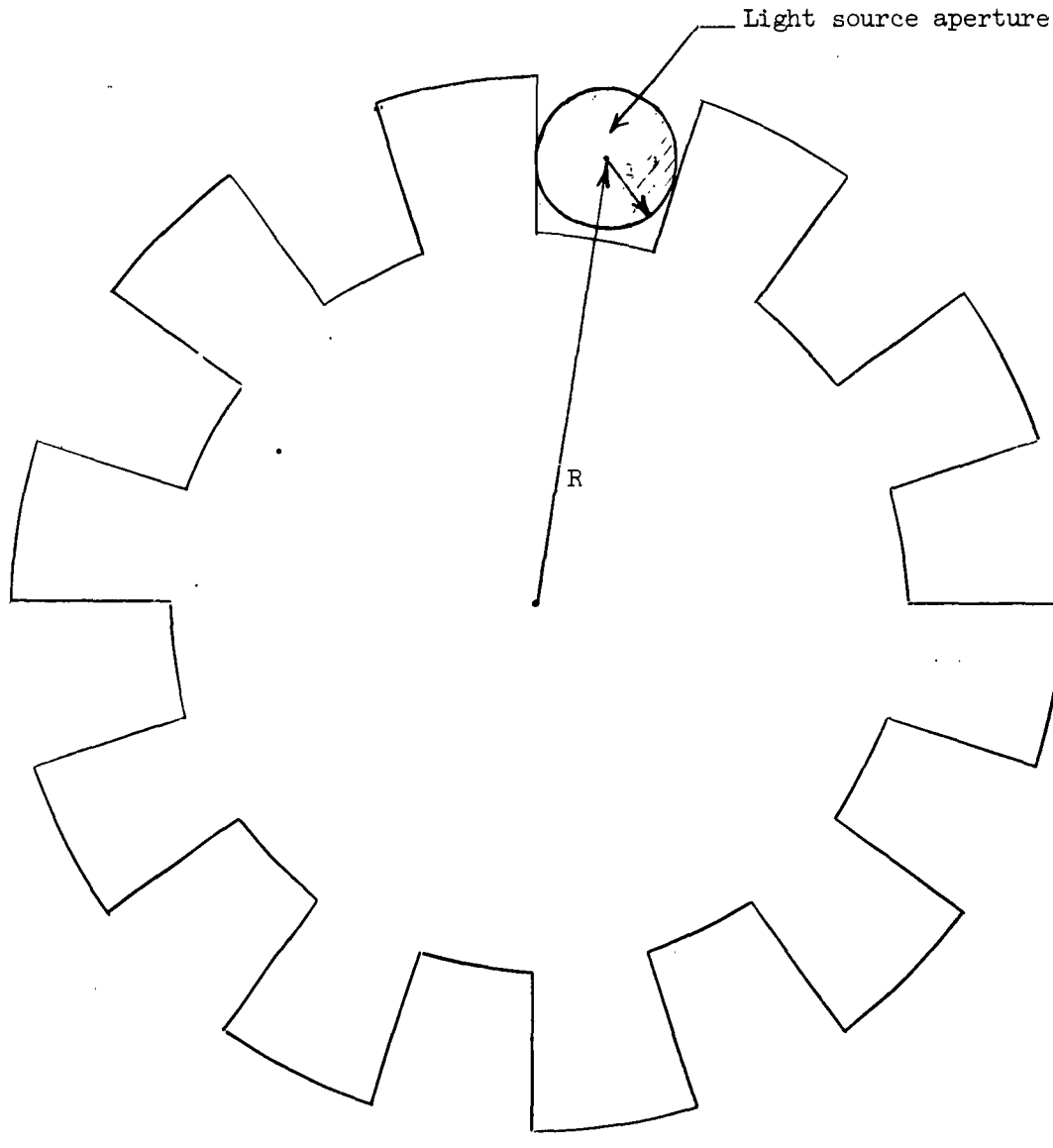

Fig. 6. The geometry of the chopper blade.

IV. PRELIMINARY EXPERIMENTS

IV-1. The Experimental Setup

The experiments were performed in a microwave anechoic chamber. The room was a modification of Emerson and Cumings Inc. eccosorb anechoic chamber no. 205 with longitudinal baffles. The obstacles and the scatterer were located in the quiet-zone surrounding the long axis of the chamber. The room was air conditioned for temperature control. The experimental apparatus were located on a stand at one end of the chamber separated from the radiation zone by a wall of eccosorb material. A 20 db. horn representing the antenna was used to radiate into the room from an aperture centered on the axis of the chamber. Light illumination was obtained through another aperture in the absorbent wall. The block diagram of the apparatus used in the experiment is shown in Fig. 7. The use of many of the devices in the diagram is self-explanatory. The source was a Varian V-63 klystron immersed in a large oil bath to maintain frequency stability. The frequency of operation was 9375 Mc (λ=3.2 c.m.). System performance was monitored by the frequency meter and the power meter.

Isolation between the transmitted and the back-scattered signal is accomplished by the properties of a transmitter-receiver hybrid junction. If a perfect match is obtained between the antenna and the load, the transmitted power is divided evenly between them and none enters the receiver, the received power is directed to a detector hybrid junction by the same property. This received signal and a reference signal taken from the reference arm of a 20 db coupler are then divided between the two collinear arms (in phase in one arm out of phase in the other arm) of the detector hybrid junction in which the barretters are mounted. Some unmodulated error signal resulting from slight detuning of the transmitter-receiver hybrid junction will also be transferred to the detector junction. These signals

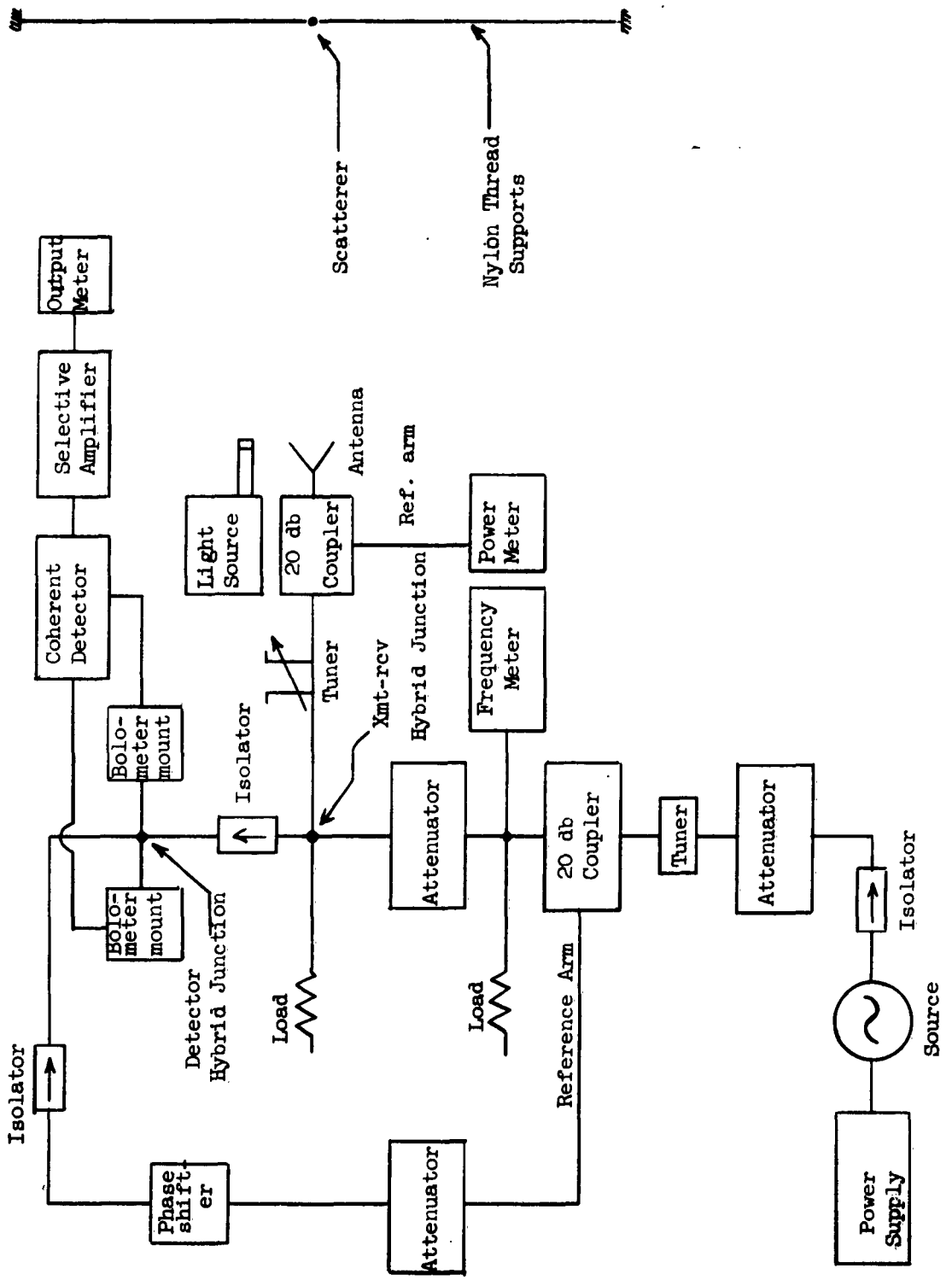

Fig. 7 —Block diagram of experimental set-up

are processed in a receiving system consisting of a coherent detector, a selective amplifier of 4 cps bandwidth about 300 cycles and an output meter.

The output of the coherent detector can be shown to be[3]

$$V = |E_o| \; |E_d|^2 \; \cos(2\gamma - \beta) \tag{7}$$

Where E_o/β is the reference signal, E_d/γ is the component of E along the scatterer. The performance of the system depends on a good tuning procedure. This procedure was explained in detail by Strait[3] previously.

The scatterer was supported by thin nylon threads attached to a large frame. The disturbance of the field due to the supporting threads was completely negligible. The motion of the scatterer through the field was accomplished by the sliding contacts on the frame. Since the signal scattered back from the frame is not modulated, it does not affect the accuracy of the experiment. However, the frame was constructed as large as possible in accordance with the dimensions of the room and was covered with absorbant material to minimize reflection.

IV-2. Measurement Procedure

The measurements were made relative to a reference point by assigning an amplitude and a phase angle to the electric field at that point. The output of the coherent detector was given by Eq. 7. When the phase shifter in the reference arm is adjusted so that the reading of the output meter is a maximum ($\beta = 2\gamma$) then

$$V = |E_o| \; |E_d|^2 \tag{8}$$

Since E_o is constant, both the amplitude and the phase of E_d can be determined.

The optical system was located just behind the stand carrying the experimental apparatus. Light was directed to the scatterer through an aperture in the absorbent wall which divided the room. Since it is impossible to focus the same amount of light energy onto a distant small scatterer at each location, light was focused onto a convenient point in the measurement space and the necessary distance corrections were made through the calibrated movement of the optical unit. However, as it was explained in the previous chapter, it is sufficient to make the distance corrections once every five wavelength intervals.

One complication arises in the experiments in which the obstacle is a part of, or related to, a large conducting plane. In such an experiment a standing wave is set up in the space between the radiating horn and the conducting plane. Part of the reflected wave finds its way back into the light unit through the lens aperture. Consequently, this portion of the reflected wave becomes mechanically modulated by the rotation of the chopper blade and detected by the receiving system upon returning into the measurement space. An analytical evaluation of the detection mechanism shows that (see Appendix I) chopper modulation contributes an additive term to the final reading. It is then possible to evaluate the signal resulting from chopper modulation separately and subtract it from the total reading. This may be done by turning off the light and reading the amount contributed by chopper modulation. It was found that this effect was completely negligible in experiments which did not require the use of a large conducting plane.

IV-3. Determination of Phase Center Location

The phase center of a scatterer built completely in an axial manner lies on the axis. However, because of the difficulty in constructing small photoconductive scatterers having axial symmetry, a shift in the phase center location from the axis of the sensitive surface may result. For the scatterer used in this experiment such a shift resulted from the existence of the short resonating leads. The location of the phase center was determined by amplitude measurements, in comparison with a current modulated diode scatterer, over a standard configuration.

IV-4. Diffraction by a Circular Aperture

To check the validity of the system an experiment was performed to determine the diffraction field of a circular aperture for which exact solutions exist and accurate experimental results are available[3]. Since the theory of diffraction by a circular aperture is not the major concern of this paper only the experimental results will be presented in this section.

The conducting plane having dimensions 80λ by 46λ was located at a distance 63λ from a radiating horn. An aperture of 5λ in diameter was used in the experiments. A plane wave was assumed to exist at 63λ. The electric field was y-polarized and the magnetic field was x-polarized. The geometry is illustrated in Fig. 8.

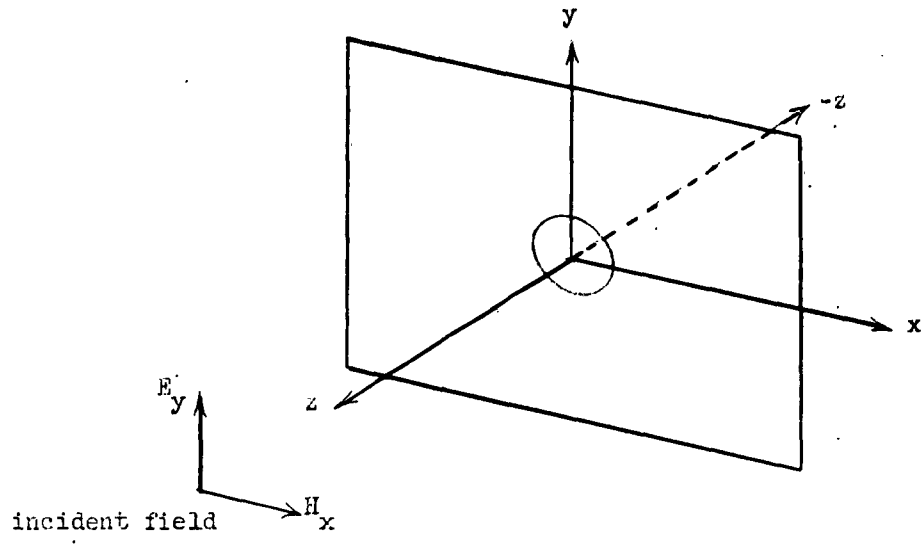

Fig. 8. Coordinates of diffraction experiment

Three sets of measurements were made for the electric field distribution in relation to the circular aperture:

a) Measurements in the aperture plane

b) Measurements behind the aperture plane ($z < 0$)

c) On-axis measurements

Figs. 9, 10, and 11 show the results of these measurements. A comparison of these results with those obtained previously shows complete agreement, thus validating the operation of the system.

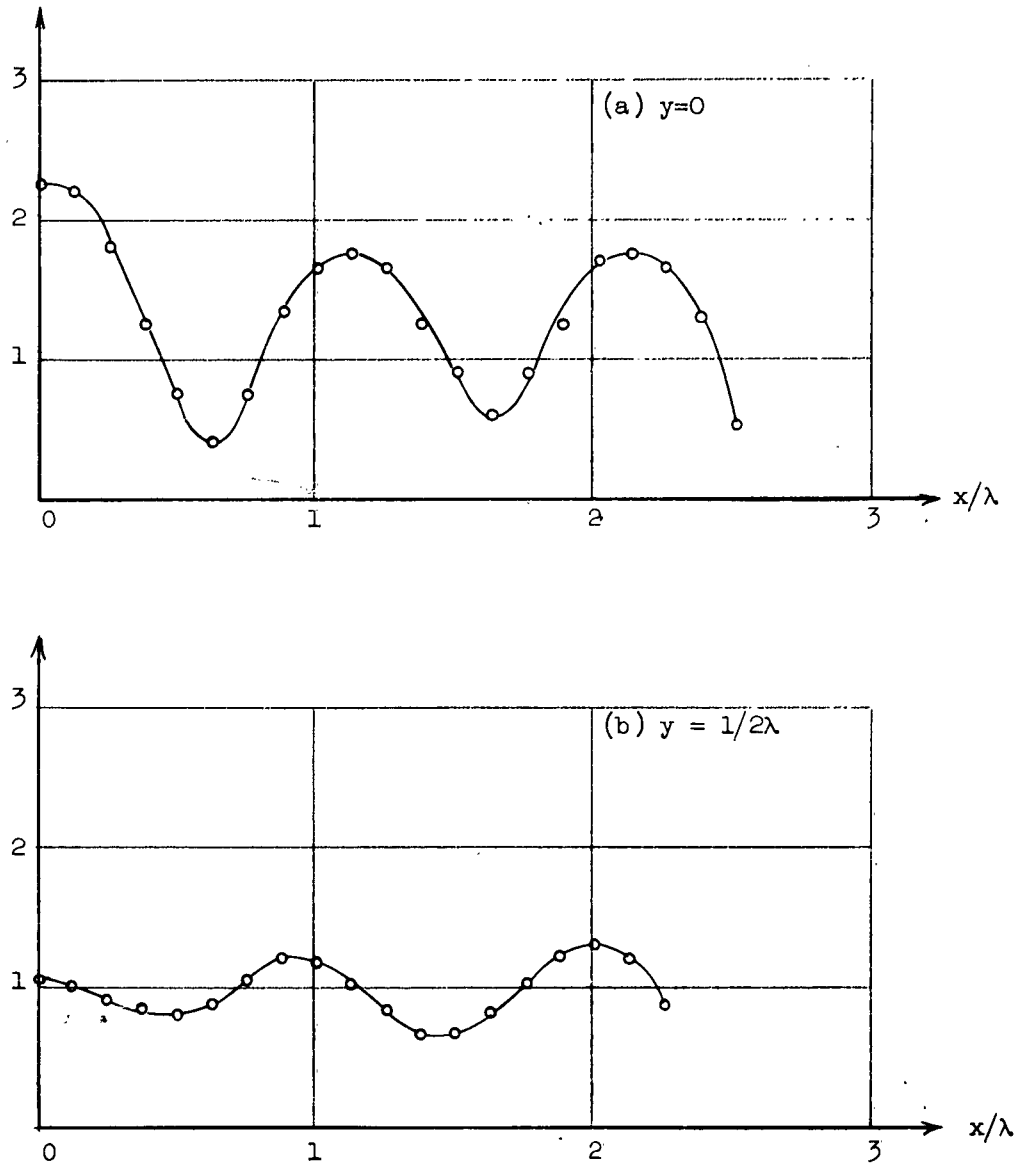

Fig. 9. Amplitude distribution, $\left|\frac{E_y}{E_i}\right|^2$, in the aperture plane (z=0)

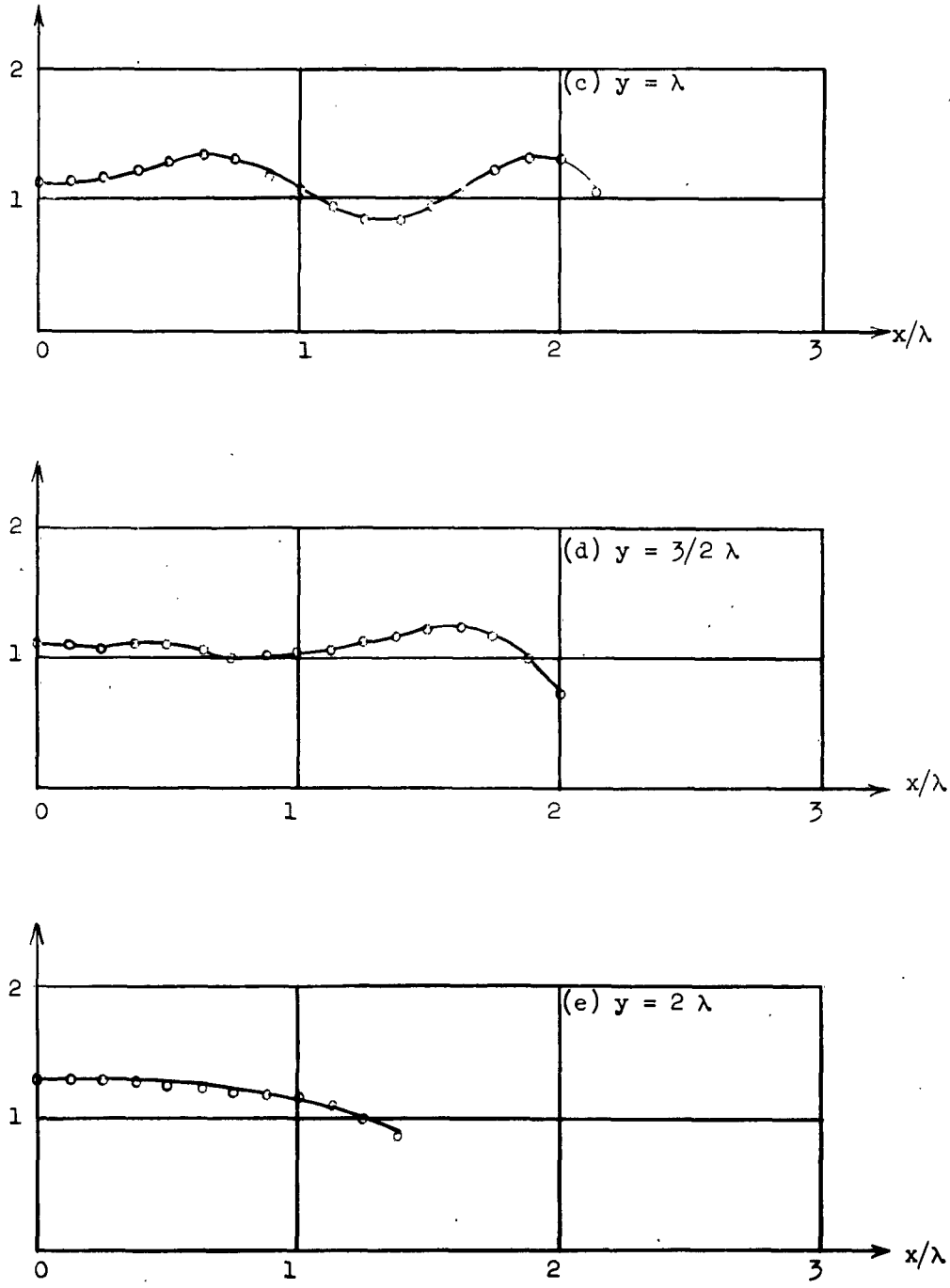

Fig. 9. (continued)

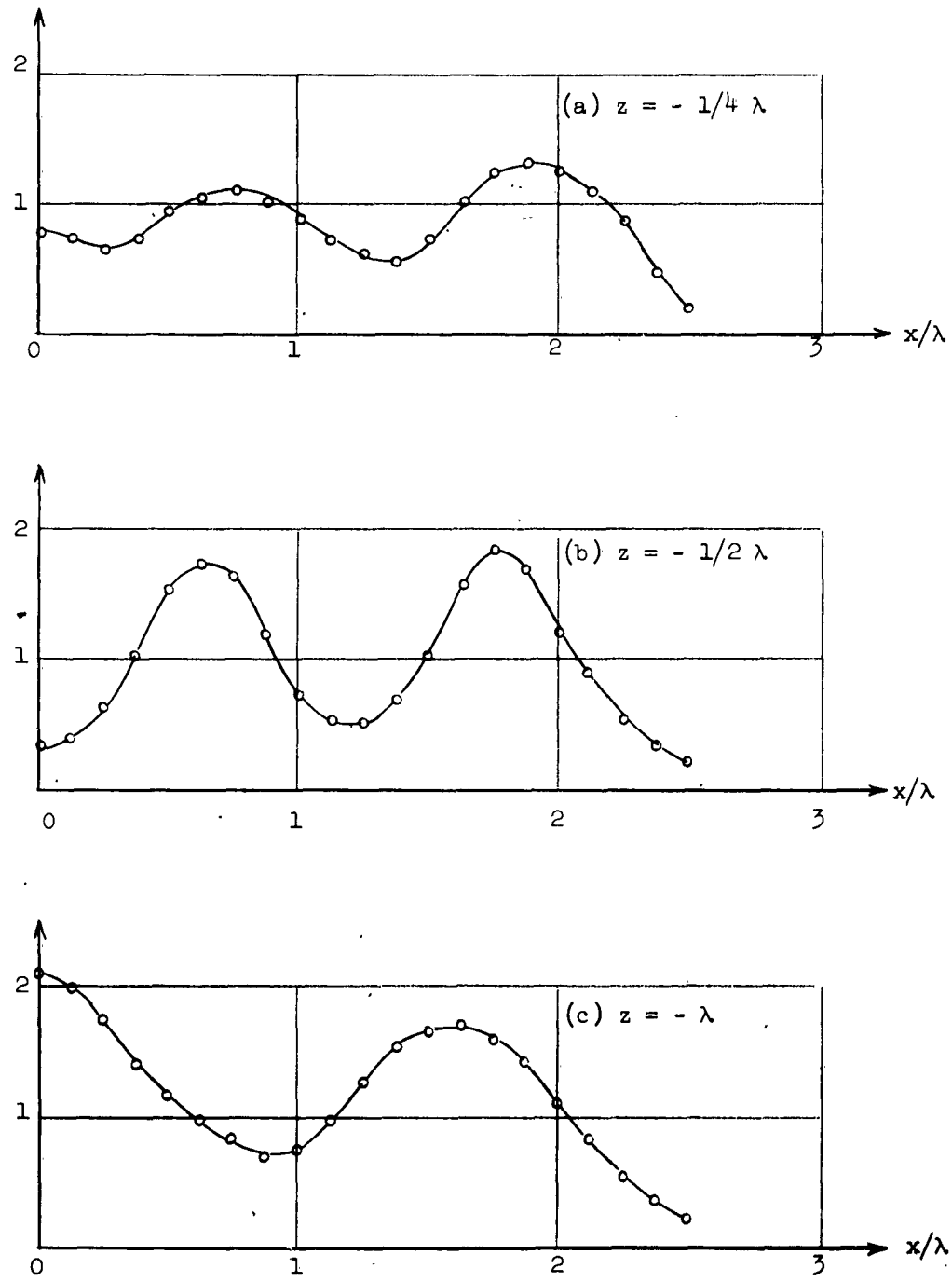

Fig. 10. Amplitude distribution, $\left|\frac{E_y}{E_i}\right|^2$, in the H-plane for various values of z (x=0; z<0)

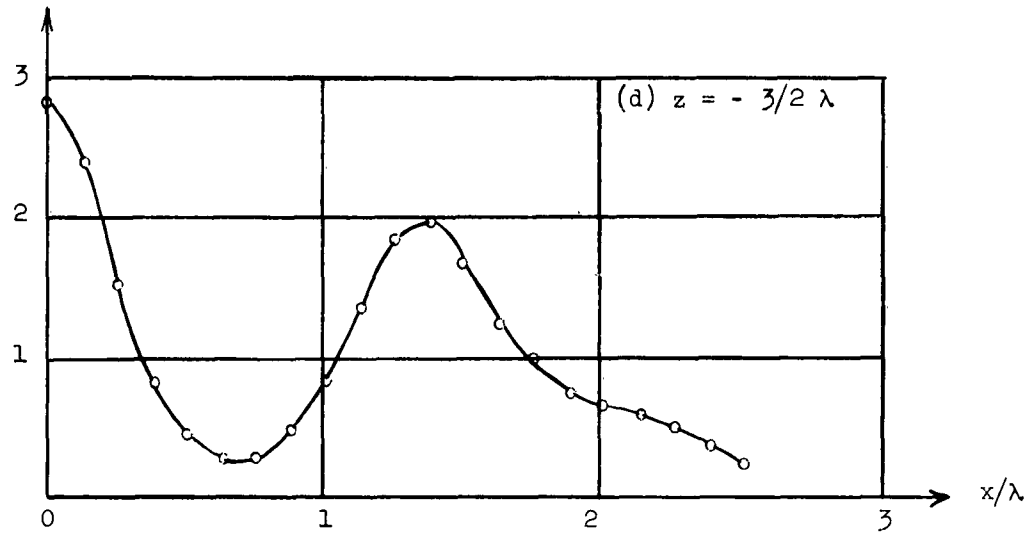

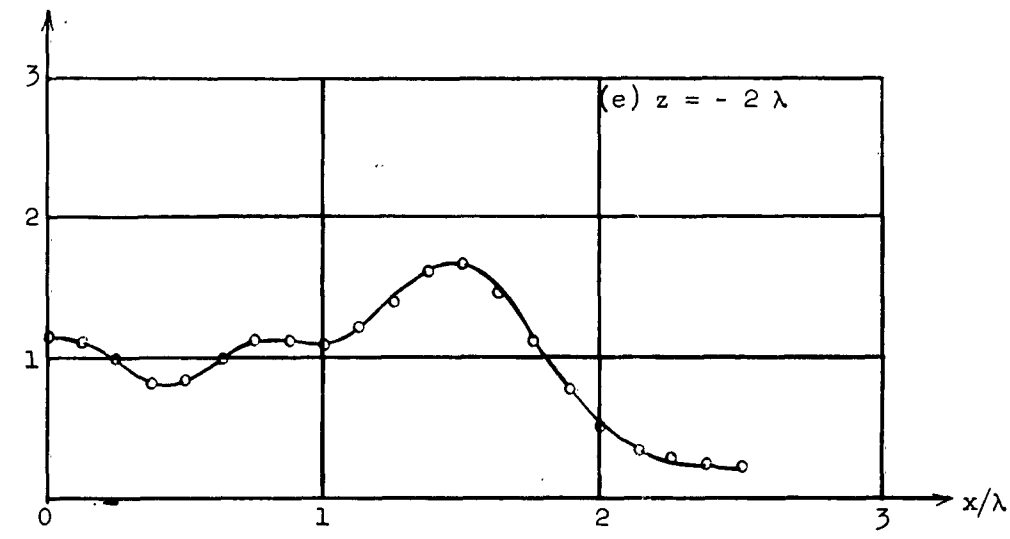

Fig. 10. (continued)

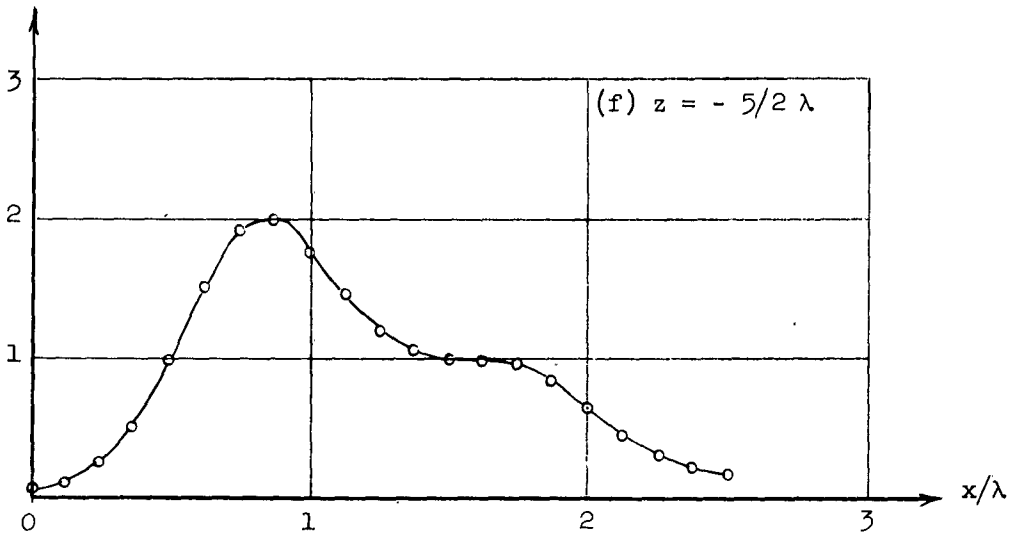

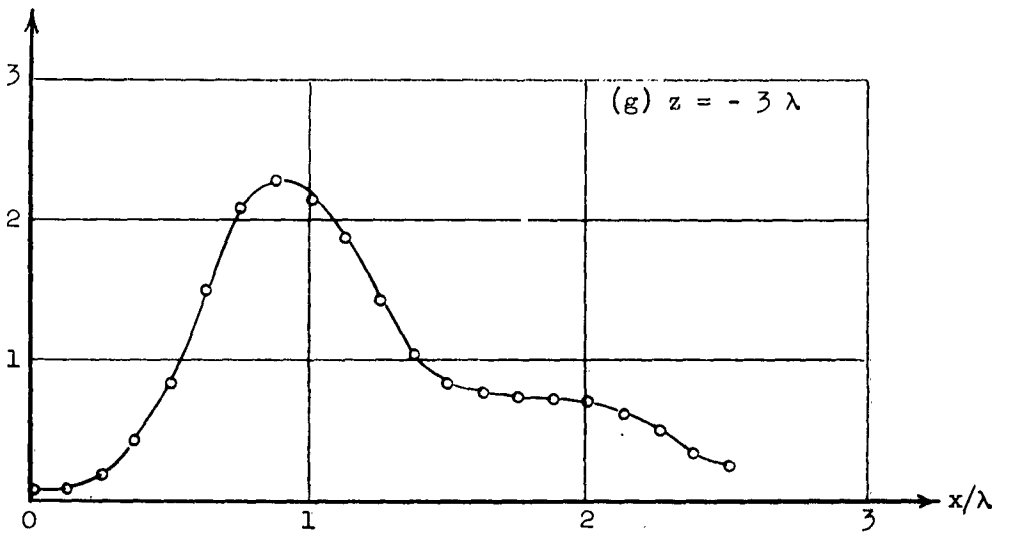

Fig. 10 (continued)

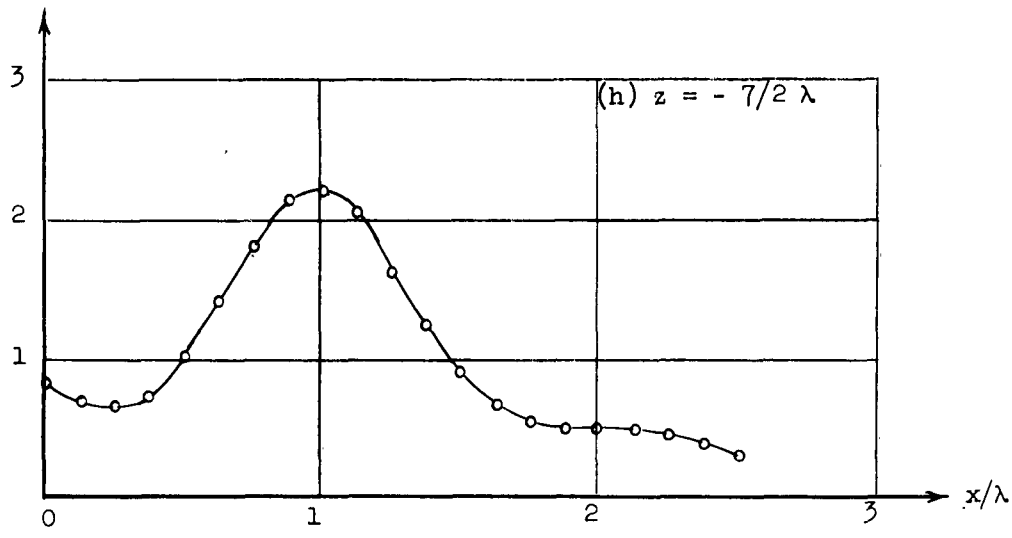

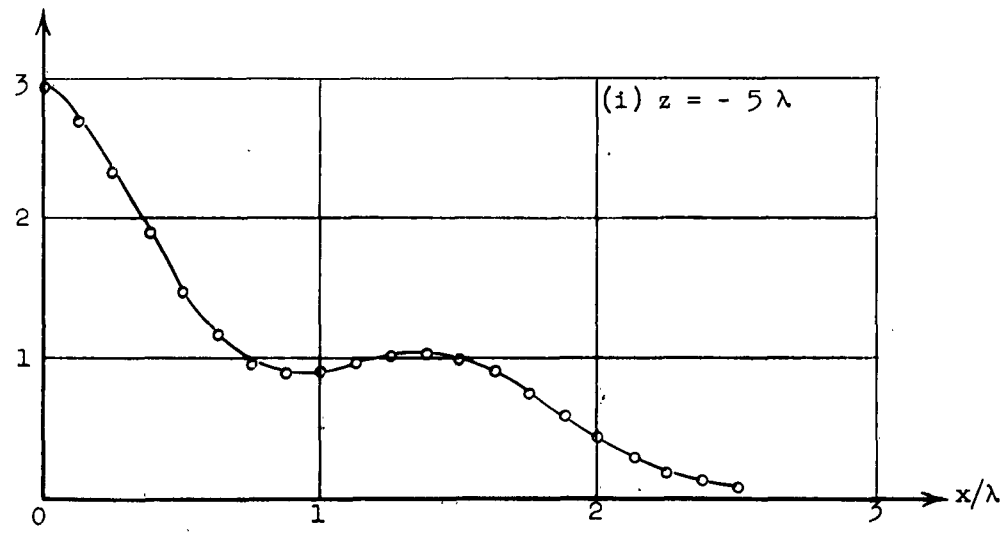

Fig. 10. (continued)

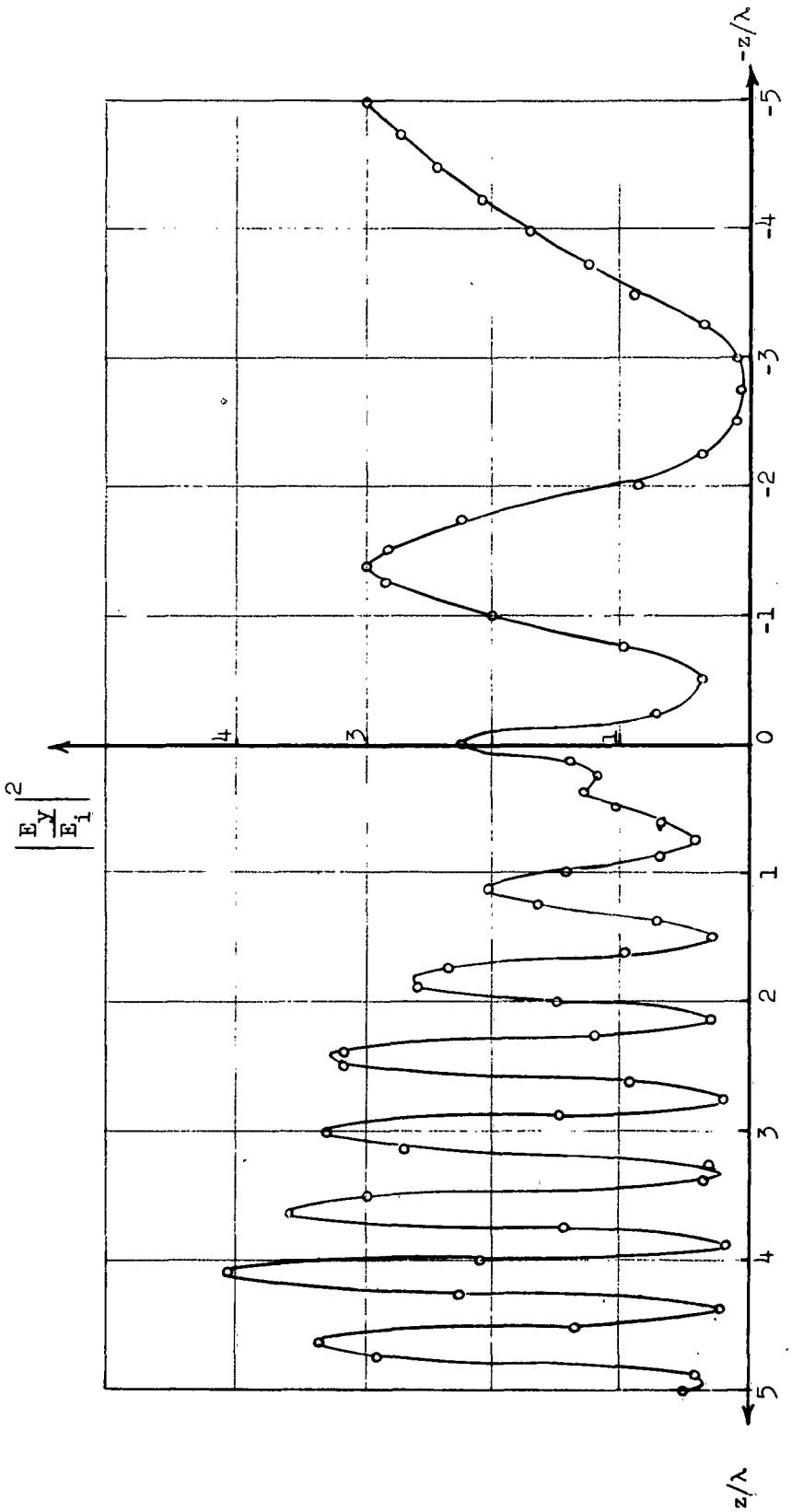

Fig. 11. Amplitude distribution of $\left|\frac{E_y}{E_i}\right|^2$ versus z/λ.

V. DIFFRACTION BY A CONE

V-1. Discussion of the Analytical Problem

Scattering of electromagnetic and acoustic waves by cones have been investigated in the literature. However, most of the previous efforts on this subject was concentrated on the evaluation of the back-scattered fields in relation to the radar cross sections of semi-infinite cones. Exact solutions originally were obtained by Carslaw[10] and by Hansen and Schiff[11] for the acoustic and electromagnetic back-scattering from the tip of a semi-infinite cone. Even in this simplified problem the difficulty in evaluating numerical results from the solutions which were in terms of infinite series or integrals limited their practical use. To increase the rapidity of convergence of the series special summation techniques and transformation methods[12] were later devised. However, even the rapidly convergent representations introduced difficulties because of the complicated nature of the functions involved. Approximate closed-form solutions were obtained by Siegel[13,14] and Felsen[15,16] for the problem of axial plane wave back-scattering from the tip of a semi-infinite cone of large and small angles. Later the problem was somewhat generalized by Felsen to include off-axial incidence on small-angle cones[17] and axial incidence on a cone of any angle[18]. Because of the difficulty in obtaining numerical results from the solutions of scalar or vector wave equations, various approximate methods were employed according to the dimensions of the cone relative to the wavelength. When the wavelength of the incident field is small in comparison with the characteristic dimensions of the obstacle the method of physical optics may be used. Although this method may not be applicable when the scattering body contains a vertex such as

the tip of the cone, the results obtained by Siegel[13] were in good agreement with the electromagnetic theory in the case of back-scattering from semi-infinite cones. Siegel also employed the method of physical optics to determine the radar cross-section of a finite cone[13].

When the wavelength is very small, the method of geometric optics is applicable. Ordinary geometric optics methods were generalized by Keller[19] to include diffracted rays. Then the diffracted electromagnetic field associated with these rays was constructed from the usual Luneburg's method and from the asymptotic behavior of the field at very small wavelengths near an edge or vertex. Later Keller applied the geometrical theory of diffraction to the problem of plane wave back-scattering from a finite cone[20].

All of these results pertained to the back-scattering fields and a majority of them were formulated under the assumption of a semi-infinite cone. The numerical results are fair approximations only for a limited range of values of obstacle parameters. Near-zone diffraction field due to finite cones are not available. One of the aims of this project was to apply the photoconductive modulation technique to near-field measurements around a scattering obstacle chosen to be a conducting finite cone.

V-2. Scattering by a Semi-Infinite Cone

In this section , a short formulation of the electromagnetic scattering problem from a semi-infinite cone is presented. The formulation is similar to some published work[21], but it helps the understanding of the problem. The semi-infinite cone problem is easier to solve, and it is a good approximation to the solutions of certain bodies of revolutions

which do not contain sharp edges like the ogive.

Consider a plane wave incident on a perfectly conducting semi-infinite cone located with its tip at the origin of a spherical coordinate system as indicated in Fig. 12.

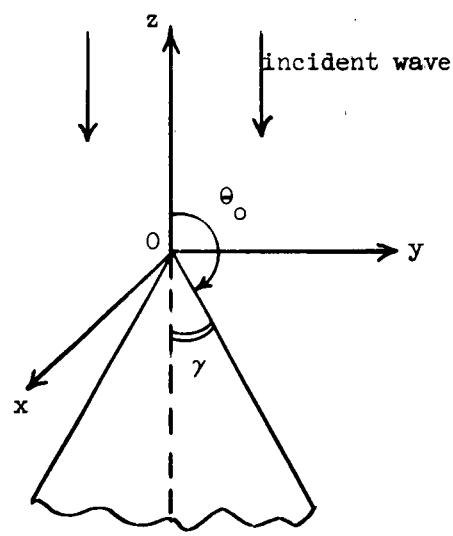

Fig. 12. A plane wave incident on a semi-infinite cone.

It is assumed that the incident plane wave is linearly polarized in y-direction and travels along the (-z) direction.

A series solution in terms of angular modes (transmission in radial direction) has been shown to be rapidly convergent[16] when either the source point or the observation point is located near the cone tip. To represent an arbitrary electromagnetic field in spherical coordinates as the superposition of components TM and TE to r the vector potentials are chosen as

$$\bar{A} = \hat{u}_r A_r = \hat{u}_r r \psi_a$$
$$\bar{F} = \hat{u}_r F_r = \hat{u}_r r \psi_f \qquad (9)$$

Where $\hat{u}_r$ is a unit vector in r-direction and the scalar potentials Ψ_a and Ψ_f are solutions to the Helmholtz equation[22].

$$(\nabla^2 + k^2)\,\Psi = 0$$

subject to the boundary conditions which have to be satisfied by $\bar{E}$. Then the components of the field are given by

$$\begin{aligned}
E_r &= \frac{1}{\tilde{y}} \left(\frac{\partial^2}{\partial r^2} + k^2\right) A_r \\
E_\theta &= -\frac{1}{r \sin\theta} \frac{\partial F_r}{\partial \phi} + \frac{1}{\tilde{y} r} \frac{\partial^2 A_r}{\partial r \partial \theta} \\
E_\phi &= \frac{1}{r} \frac{\partial F_r}{\partial \theta} + \frac{1}{\tilde{y} r \sin\theta} \frac{\partial^2 A_r}{\partial r \partial \phi} \\
H_r &= \frac{1}{\tilde{z}} \left(\frac{\partial^2}{\partial r^2} + k^2\right) F_r \\
H_\theta &= \frac{1}{r \sin\theta} \frac{\partial A_r}{\partial \phi} + \frac{1}{\tilde{z} r} \frac{\partial^2 F_r}{\partial r \partial \theta} \\
H_\phi &= -\frac{1}{r} \frac{\partial A_r}{\partial \theta} + \frac{1}{\tilde{z} r \sin\theta} \frac{\partial^2 F_r}{\partial r \partial \phi}
\end{aligned} \tag{10}$$

where $\tilde{y} = j\omega\epsilon_o$ and $\tilde{z} = j\omega\mu_o$.

The boundary conditions of the problem are:

1) $E_r = E_\phi = 0$ when $\theta = \theta_o$

2) $E_y \rightarrow e^{jkr\cos\theta}$ as $r \rightarrow \infty$

At large distances from the cone the total solution must have the character of an incoming plane wave plus an outgoing spherical wave which appears to diverge from the scattering body. Then the second boundary condition implies that

$$\Psi \Big|_{r\to\infty} \longrightarrow \Psi^i + \left[\frac{e^{-jkr}}{r}\right] f(\theta,\phi) = \Psi^i + \Psi^s$$

where Ψ^i denotes the incident field, (A time variation of $e^{j\omega t}$ is assumed throughout) and the scattered wave, Ψ^s, must satisfy the Sommerfeld radiation condition

$$\lim_{r\to\infty} r\left[\frac{\partial \Psi^s}{\partial r} + jk\Psi^s\right] = 0$$

The general solution to the Helmholtz equation in spherical coordinates will be

$$\Psi = \begin{bmatrix} \sin m\phi \\ \cos m\phi \end{bmatrix} \begin{bmatrix} P_{n_i}^m(\cos\theta) \\ Q_{n_i}^m(\cos\theta) \end{bmatrix} \left[b_{n_i}(kr)\right]$$

where $b_{n_i}(kr)$ represents any one of the spherical radial functions $j_{n_i}(kr)$, $n_{n_i}(kr)$, $h_{n_i}^{1,2}(kr)$. $P_{n_i}^m(\cos\theta)$ and $Q_{n_i}^m(\cos\theta)$ are associated Legendre polynomials of the first and second kind respectively. The functions $Q_{n_i}^m(\cos\theta)$ have to be eliminated from the solution because of their singularities at $\theta = o,\pi$. Similarly the Neumann's and Hankel's functions may not be used on account of their singularities at the origin. The radial functions are not orthogonal. But the functions $P_{n_i}(\cos\theta)$ and

$P_{n_i}^{1}(\cos\theta)$ are orthogonal in $(0,\theta_o)$. The unperturbed incident field has a limited ϕ variation and since the cone does not disturb the symmetry in ϕ, the total field must have this variation as well. This constraints the index m to be taken as unity.

With this argument solutions for Ψ_a and Ψ_f may be synthesized as

$$\Psi_a = \sum_{i=1}^{\infty} B_i \, j_{n_i}(kr) \quad P_{n_i}^{1}(\cos\theta) \quad \sin\phi \tag{11}$$

$$\Psi_f = \sum_{i=1}^{\infty} C_i \, j_{l_i}(kr) \quad P_{l_i}^{1}(\cos\theta) \quad \cos\phi \tag{12}$$

It may easily be checked from the field eqs. (Eqs. 10) that the boundary conditions at $\theta = \theta_o$ are satisfied if n_i and l_i are solutions to the equations

$$\begin{aligned} P_{n_i}^{1}(\cos\theta)\Big|_{\theta=\theta_o} &= 0 \\ \frac{\partial}{\partial\theta}\left[P_{l_i}^{1}(\cos\theta)\right]\Big|_{\theta=\theta_o} &= 0 \end{aligned} \tag{13}$$

Equations 11 and 12 are total solutions consisting of the sum of incident and scattered fields. To determine the expansion coefficients B_i and C_i the implication of the second boundary condition may be utilized to recognize the incident part of these solutions as the incoming plane wave at very large r. Then an expansion of the incident field in terms of orthogonal $P_{n_i,l_i}(\cos\theta)$ functions is in order.

The potential functions for the incident field will be of the same form as total field

$$\psi_a^i = \sum_{i=1}^{\infty} U_{n_i}(kr) \; P_{n_i}^1(\cos\theta) \; \sin\phi \tag{14}$$

$$\psi_f^i = \sum_{i=1}^{m} V_{1_i}(kr) \; P_{1_i}^1(\cos\theta) \; \cos\phi \; . \tag{15}$$

The spherical radial functions $U_{n_i}(kr)$ and $V_{1_i}(kr)$ may be determined by finding E_r^i and H_r^i from Eqs. 14 and 15 using field relations and comparing them with the radial components of the incident field:

$$E_r^i = \sin\theta \sin\phi \, E_y^i = E_o \sin\theta \sin\phi \; e^{jkr\cos\theta}$$

$$H_r^i = \sin\theta \cos\phi \, H_x^i = \frac{E_o}{\eta} \sin\theta \cos\phi \; e^{jkr\cos\theta}$$

Making use of the differential equation

$$\left[\frac{d^2}{dr^2} + k^2 - \frac{n_i(n_i+1)}{r^2}\right] (kr) \, b_{n_i}(kr) = 0$$

the result for E_r^i becomes

$$E_o \, e^{jkr\cos\theta} \sin\theta = \frac{1}{\tilde{y}r} \sum_i n_i(n_i+1) \, U_{n_i}(kr) \, P_{n_i}^1(\cos\theta)$$

Multiplying both sides by $P_{n_i}^1(\cos\theta)\sin\theta\, d\theta$ and integrating over $(0, \theta_o)$, one has

$$\frac{1}{\tilde{y}r} U_{n_i}(kr)\, n_i(n_i+1) \int_0^{\theta_o} [P_{n_i}^1(\cos\theta)]^2 \sin\theta\, d\theta$$

$$= E_o \int_0^{\theta_o} e^{jkr\cos\theta} P_{n_i}^1(\cos\theta)\sin^2\theta\, d\theta$$

$$\longrightarrow -\frac{E_o e^{jkr}}{(kr)^2} n_i(n_i+1) \qquad r\longrightarrow\infty$$

but

$$\int_0^{\theta_o} [P_{n_i}^1(\cos\theta)]^2 \sin\theta\, d\theta = -\frac{(1-\nu_o^2)}{(2n_i+1)} \left[\frac{dP_{n_i}^1(\nu_o)}{d\nu}\right]\left[\frac{dP_{n_i}^1(\nu_o)}{dn_i}\right]$$

if n_i are determined from $P_{n_i}^1(\nu_o) = 0$, and where $\nu = \cos\theta$, $\nu_o = \cos\theta_o$. Then $U_{n_i}(kr)$ is given by

$$U_{n_i}(kr) = \frac{\tilde{y} E_o e^{jkr} (2n_i+1)}{k^2 r (1-\nu_o^2) \left[\frac{dP_{n_i}^1(\nu_o)}{d\nu}\right]\left[\frac{dP_{n_i}^1(\nu_o)}{dn_i}\right]}$$

Substitution into the eq. (14) gives

$$\Psi_a^i = \frac{\tilde{y}E_o \sin\phi}{k^2} \left[\frac{e^{ikr}}{r}\right] \sum_i \frac{(2n_i+1)\, P_{n_i}^1(\nu)}{(1-\nu_o^2)\left[\frac{dP_{n_i}^1(\nu_o)}{d\nu}\right]\left[\frac{dP_{n_i}^1(\nu_o)}{dn_i}\right]} \qquad (16)$$

The asymptotic form of Ψ_a may be obtained by making use of the asymptotic form of the spherical Bessel's functions

$$j_{n_i}(kr) \rightarrow \frac{1}{kr} \cos\left(kr - \frac{n_i+1}{2}\pi\right) \qquad kr \gg n_i$$

$$\Psi_a \Big|_{r\to\infty} = \frac{\sin\phi}{2k}\left[\frac{e^{jkr}}{r}\right] \sum_i B_i\, e^{-j(n_i+1)\frac{\pi}{2}}\, P_{n_i}^{1}(\nu)$$

$$+ \frac{\sin\phi}{2k}\left[\frac{e^{-jkr}}{r}\right] \sum_i B_i\, e^{j(n_i+1)\frac{\pi}{2}}\, P_{n_i}^{1}(\nu)$$

Comparing the incident part of this equation with Eq.(16), one obtains

$$B_i = \frac{2\tilde{y}\, E_o (2n_i+1)\, e^{j(n_i+1)\frac{\pi}{2}}}{k(1-\nu_o^2)\left[\frac{dP_{n_i}^{1}(\nu_o)}{d\nu}\right]\left[\frac{dP_{n_i}^{1}(\nu_o)}{dn_i}\right]}$$

The potential A_r now becomes:

$$A_r = \frac{2\tilde{y}\, E_o\, r \sin\phi}{k} \sum_{i=1}^{\infty} \frac{(2n_i+1)\, e^{j(n_i+1)\frac{\pi}{2}}\, P_{n_i}^{1}(\nu)\, j_{n_i}(kr)}{(1-\nu_o^2)\left[\frac{dP_{n_i}^{1}(\nu_o)}{d\nu}\right]\left[\frac{dP_{n_i}^{1}(\nu_o)}{dn_i}\right]} \qquad (17)$$

The expression for F_r may be obtained in much the same way except for a different normalizing factor for Legendre polynonimals

$$F_r = -2\,j\,E_o\,r\cos\phi \sum_{i=1}^{\infty} \frac{(2l_i+1)\,e^{j(l_i+1)\frac{\pi}{2}}\,P_{l_i}^{1}(\nu)\,j_{l_i}(kr)}{(1-\nu_o^2)\,P_{l_i}^{1}(\nu_o)\,\dfrac{\partial^2 P_{l_i}^{1}(\nu_o)}{\partial\nu\partial l_i}} \qquad (18)$$

The components of the total electric field in the space may be computed from Eqs. (17) and (18) using field relations.

Let

$$H_{n_i} = \frac{(2n_i+1)\,e^{j(n_i+1)\frac{\pi}{2}}}{(1-\nu_o^2)\left[\dfrac{dP_{n_i}^{1}(\nu_o)}{d\nu}\right]\left[\dfrac{dP_{n_i}^{1}(\nu_o)}{dn_i}\right]}$$

$$G_{l_i} = \frac{(2l_i+1)\,e^{j(l_i+1)\frac{\pi}{2}}}{(1-\nu_o^2)\,P_{l_i}^{1}(\nu)\,\dfrac{\partial^2 P_{l_i}^{1}(\nu_o)}{\partial\nu\partial l_i}}$$

Then

$$E_r = \frac{1}{\tilde{y}}\left(\frac{\partial^2}{\partial r^2} + k^2\right) A_r$$

$$= \frac{2\,E_o \sin\phi}{kr} \sum_i H_{n_i}\, n_i(n_i+1)\, P_{n_i}^{1}(\nu)\, j_{n_i}(kr)$$

$$E_\theta = -\frac{1}{r \sin\theta}\frac{\partial F_r}{\partial \phi} + \frac{1}{\tilde{y} r}\frac{\partial^2 A_r}{\partial r \partial \theta}$$

$$= -\frac{2 j E_o \sin\phi}{\sin\theta}\sum_i G_{l_i} P_{l_i}^1(\nu)\, j_{l_i}(kr)$$

$$+\frac{2 E_o \sin\phi}{kr}\sum_i H_{n_i}\frac{d}{d\theta}\left[P_{n_i}^1(\nu)\right] j_{n_i}(kr)$$

$$+\frac{2 E_o \sin\phi}{k}\sum_i H_{n_i}\frac{d}{d\theta}\left[P_{n_i}^1(\nu)\right]\frac{d}{dr}\left[j_{n_i}(kr)\right]$$

$$E_\phi = \frac{1}{r}\frac{\partial F_r}{\partial \theta} + \frac{1}{\tilde{y} r \sin\theta}\frac{\partial^2 A_r}{\partial r \partial \phi}$$

$$= -2 j E_o \cos\phi \sum_i G_{l_i}\frac{d}{d\theta}\left[P_{l_i}^1(\nu)\right] j_{l_i}(kr)$$

$$+\frac{2 E_o \cos\phi}{kr \sin\theta}\sum_i H_{n_i} P_{n_i}^1(\nu)\, j_{n_i}(kr)$$

$$+\frac{2 E_o \cos\phi}{k \sin\theta}\sum_i H_{n_i} P_{n_i}^1(\nu)\frac{d}{dr}\left[j_{n_i}(kr)\right]$$

An expression for the y-component of the total electric field, E_y, may now be computed from

$$E_y = E_r \sin\theta \sin\phi + E_\theta \cos\theta \sin\phi + E_\phi \cos\phi$$

$$E_y = \frac{2 E_o \sin\theta \sin^2\phi}{kr} \sum_i H_{n_i} n_i(n_i+1) P_{n_i}^1(\nu) j_{n_i}(kr)$$

$$- \frac{2 j E_o \cos\theta \sin^2\phi}{\sin\theta} \sum_i G_{1_i} P_{1_i}^1(\nu) j_{1_i}(kr)$$

$$+ \frac{2 E_o \cos\theta \sin^2\phi}{kr} \sum_i H_{n_i} \frac{d}{d\theta} [P_{n_i}^1(\nu)] j_{n_i}(kr)$$

$$+ 2 E_o \cos\theta \sin^2\phi \sum_i H_{n_i} \frac{d}{d\theta} [P_{n_i}^1(\nu)] \frac{d}{dr} [j_{n_i}(kr)]$$

$$- 2 j E_o \cos^2\phi \sum_i G_{1_i} \frac{d}{d\theta}[P_{1_i}^1(\nu)] j_{1_i}(kr)$$

$$+ \frac{2 E_o \cos^2\phi}{kr \sin\theta} \sum_i H_{n_i} P_{n_i}^1(\nu) j_{n_i}(kr)$$

$$+ \frac{2 E_o \cos^2\phi}{\sin\theta} \sum_i H_{n_i} P_{n_i}^1(\nu) \frac{d}{dr}[j_{n_i}(kr)] \qquad (19)$$

Equation (19) gives the y-component of the total electric field in space arising from the so-called tip diffraction of the semi-infinite cone. Although no specialization to the back-scattered field has been made during the derivation of Eq. (19) the accuracy of the result as applied to the region near the cone tip requires some consideration. This results from the asymptotic evaluation of certain integrals in order to synthesize the solution. Nevertheless the series involved in Eq. (19) converges very rapidly near the cone tip and it may be used to approximate the field there if the eigenvalues and the corresponding eigenfunctions and normalizing integrals could be obtained numerically. In relation with the previous work on the cone problem some data have already been computed at the Institute for Numerical Analysis; however, they are limited to the certain range of values of the cone parameters. The Bessel's functions of small arguments may be computed directly from their power series expansion.

On the axis of the cone the total solution for the electric field vector, $\bar{E}$, should reduce to the y-component only, as required from symmetry conditions. To check this, let

$$\bar{E}(\underline{r}) = \hat{u}_r E_r + \hat{u}_\theta E_\theta + \hat{u}_\phi E_\phi$$

and making use of the relations

$$P^1_{n_i}(1) = 0$$

$$\left.\frac{P^1_{n_i}(\nu)}{\sin\theta}\right|_{\theta=0} = \frac{1}{2} n_i(n_i+1)$$

$$\left.\frac{d}{d\theta} P^1_{n_i}(\nu)\right|_{\theta=0} = \frac{1}{2} n_i(n_i+1)$$

$$J_{n_i}(kr) = \frac{1}{kr} \hat{J}_{n_i}(kr)$$

one has

$$\overline{E}(\underline{r})\Big|_{\theta=0} = \hat{u}_y \frac{E_o}{kr} \left[\sum_i H_{n_i} \; n_i(n_i+1) \; \hat{J}'_{n_i}(kr) + \frac{1}{j} \sum_i G_{l_i} \; l_i(l_i+1) \hat{J}_{l_i}(kr) \right] \tag{20}$$

Hence for an axial plane-wave incidence the total field on the axis has only a y - component as expected. Eq. (20) is in agreement with the result derived by Felsen[16] from the spherical transmission line theory.

In the actual case of a finite cone the total field results from both tip and base scattering. However, if the base does not contain a sharp edge and is rounded in an unsymmetrical manner the main contribution comes from the tip[13].

In summary, the near-field distributions of a flat based finite cone may be approximated in different regions by specializing to the different problems. Near the tip the series solution of a semi-infinite cone is useful. A wedge solution may be employed in the vicinity of the base edge. In the regions away from the tip and the edge the solutions using the geometric optics methods may be used.

VI. EXPERIMENTAL RESULTS

VI-1. Cone Design Considerations

Three different cones were employed in the experiments having half apex angles $\gamma = 20^{\circ}$, 45° and 67° respectively. All the cones were right circular cones with the same base diameter of 5λ (λ=3.2 cm.). The cone angles were chosen in an arbitrary manner to represent typical small, average and large angle cones. If it was intended to extract some numerical results from the analytical formulations more suitable angles might have been chosen for which some numerical data already have been computed. The equality of base diameters for the different cones permits a comparison between tip and base scatterings at small and large cone angles. The corresponding heights of the cones were 6.86λ, 2.50λ and 1.04λ. In addition, some experiments were conducted on a thin circular plate of the same diameter for the limiting case of $\gamma = 90^{\circ}$. This also provided a check on the validity of the experimental data by comparing the results with the ones obtained previously[23].

Cones were machined from 2024T aluminum with a surface finish of 13 micro-inches RMS.

VI-2. Measurement of Diffraction Fields in the H-plane

Most of the measurements concerning electric field distributions were made for the y-component of the total electric field around the scattering cone. The experimental set up was the same as described earlier in relation to the circular aperture experiment. Cones were placed in the field as their axis coincides with the axis of the radiating antenna, a 20 db horn and 68λ away from the horn aperture.

The geometry of the measurement space is illustrated in Fig. 13.

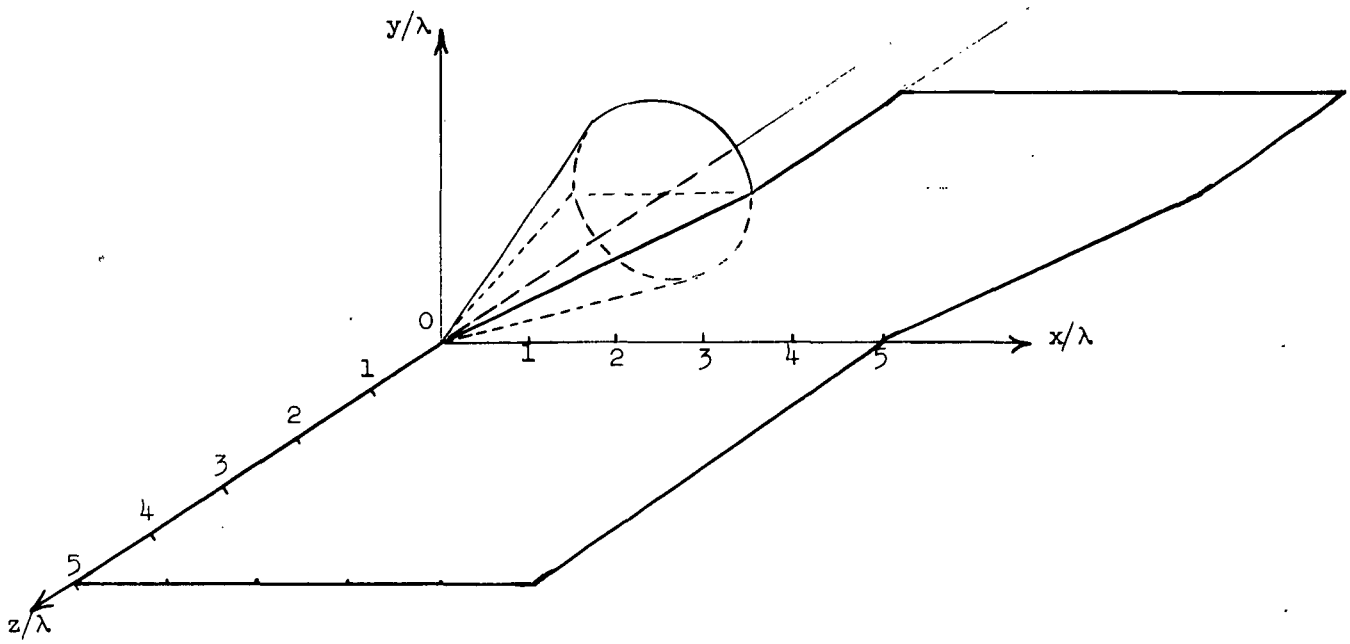

Fig. 13. Geometry of measurement space

Measurements began at z = 5λ in front of the cone tip and extended back as far as 2λ behind the cone base in discrete steps. At each step the scatterer was moved along the x - axis over a distance of 5λ.

Figs. 14-17 show the results of measurements for 20, 45, 67 and 90 degree cones along the x - axis in the principal H-plane (y=0). Results are plotted as normalized squares $\left|\frac{E_y}{E_i}\right|^2$.

The results of the principal H-plane measurements of the electric field distributions are also summarized in the 3-dimensional plots of Figs. 18-20 for 20, 45 and 67 degree cones.

Some data were also taken for distributions in the planes of constant y in parallel with the principal H-plane. Fig. 21 shows the results of these measurements.

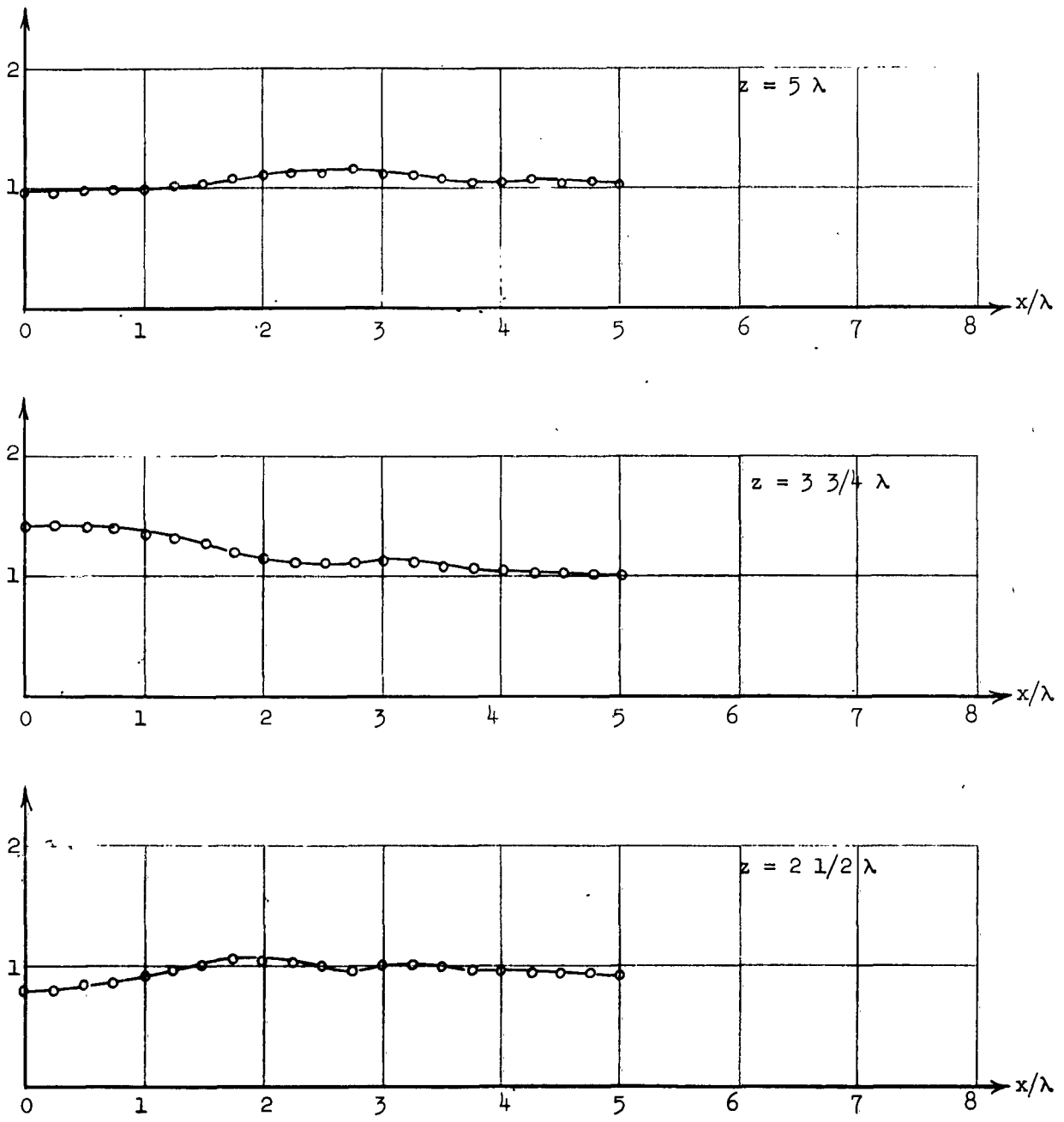

Fig. 14. Distribution of $\left|\frac{E_y}{E_i}\right|^2$ for 20° cone at various values of z in the principal H-plane (y=0).

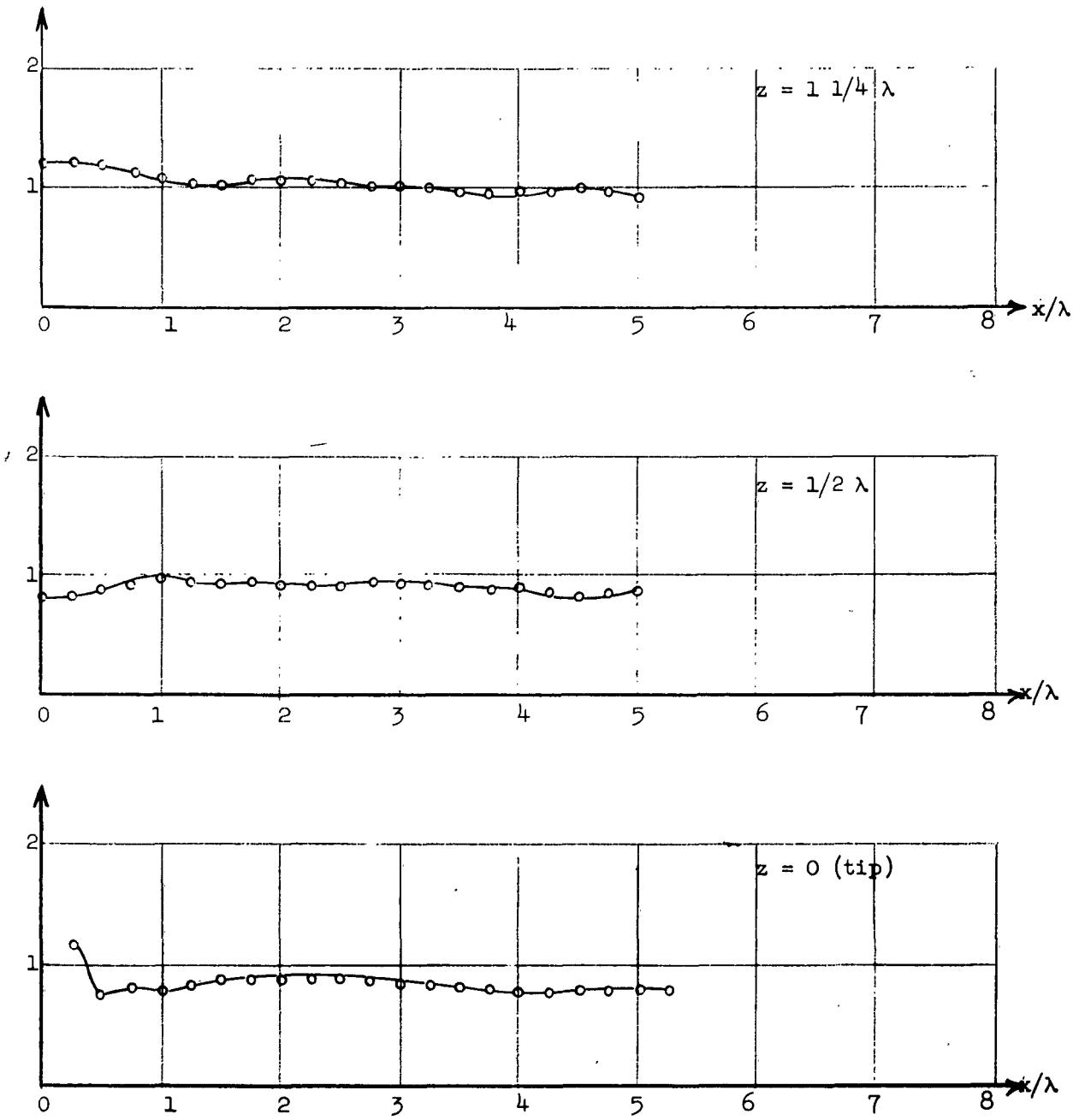

Fig. 14 (continued)

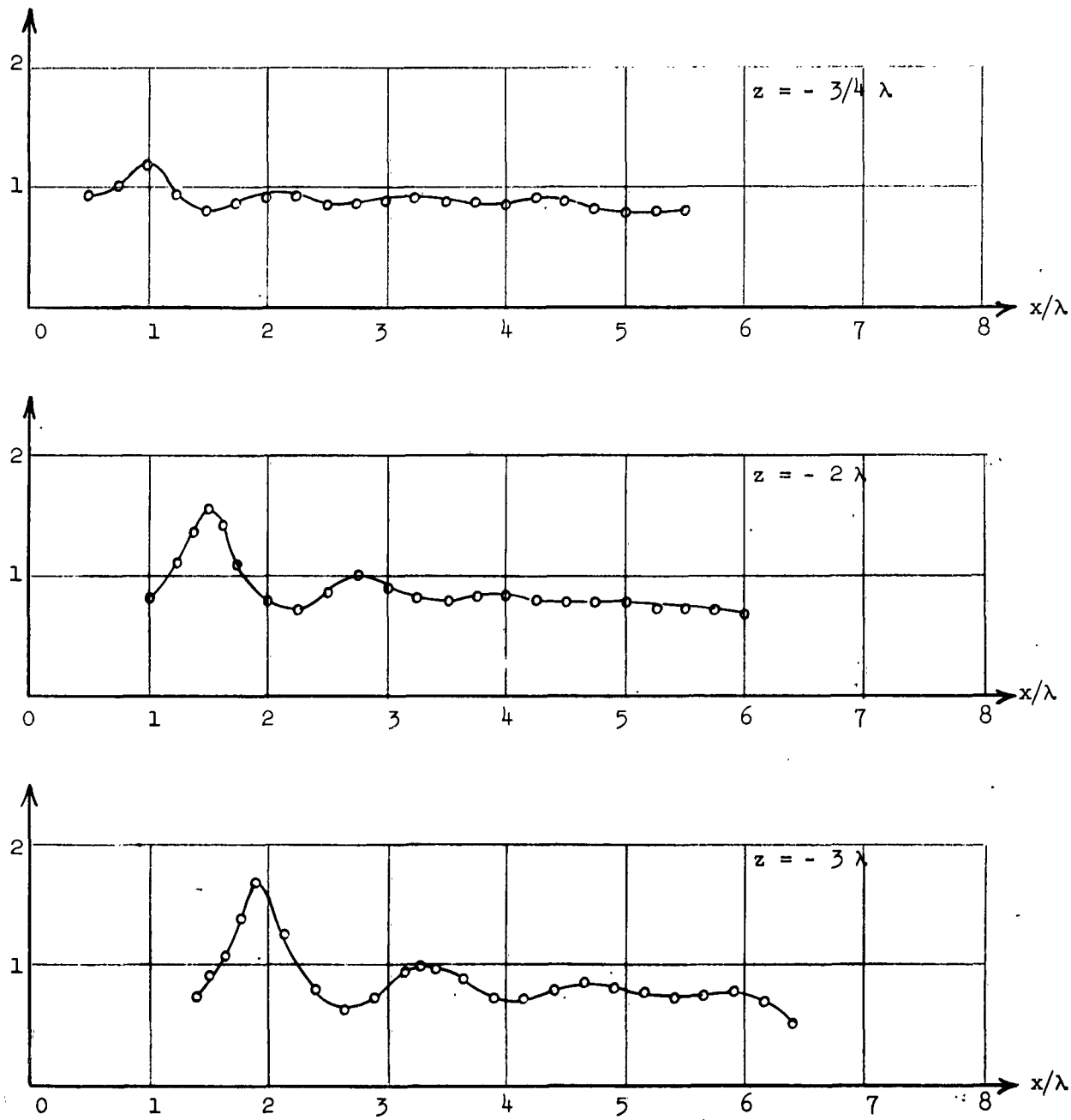

Fig. 14. (continued)

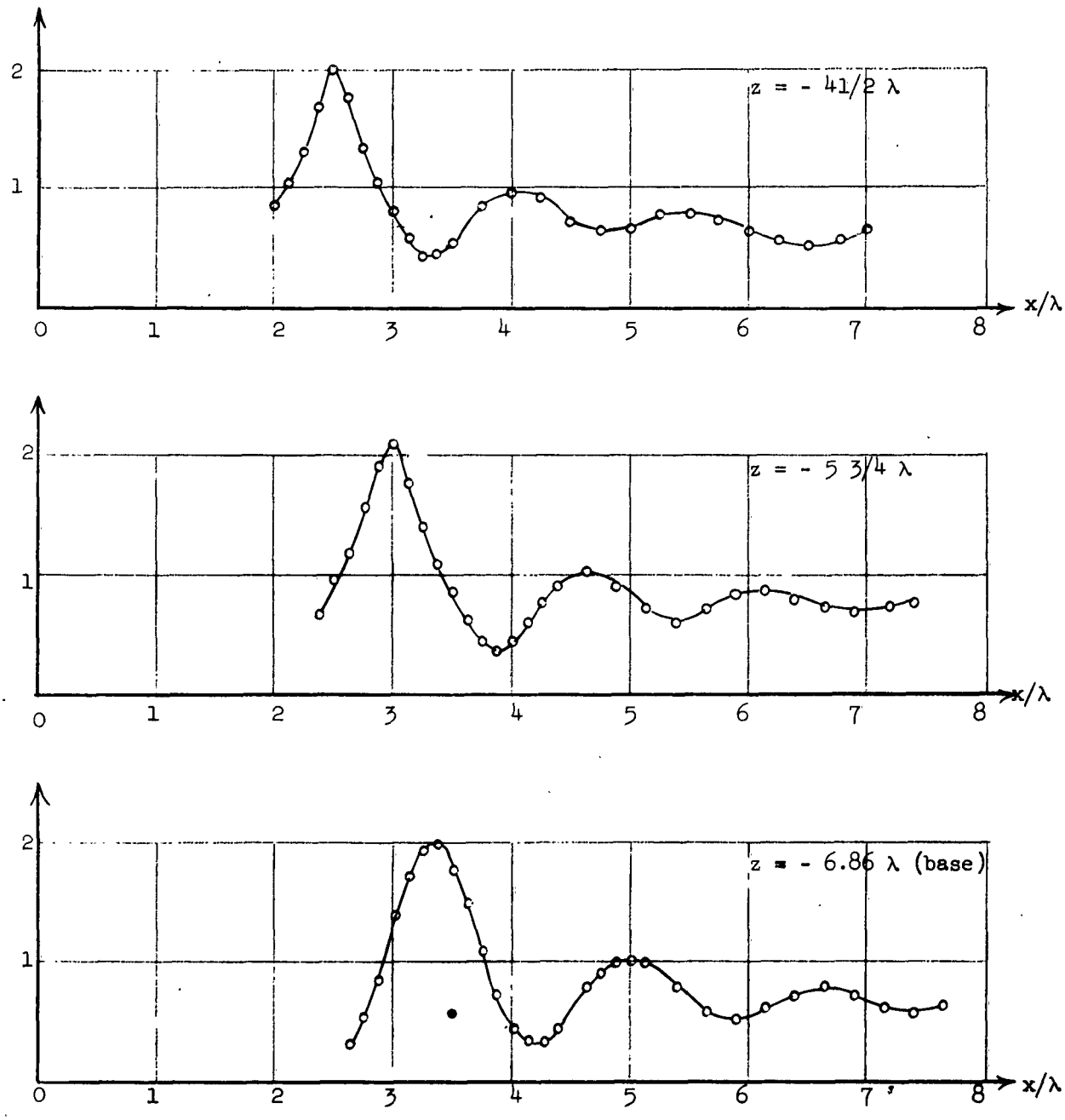

Fig. 14. (continued)

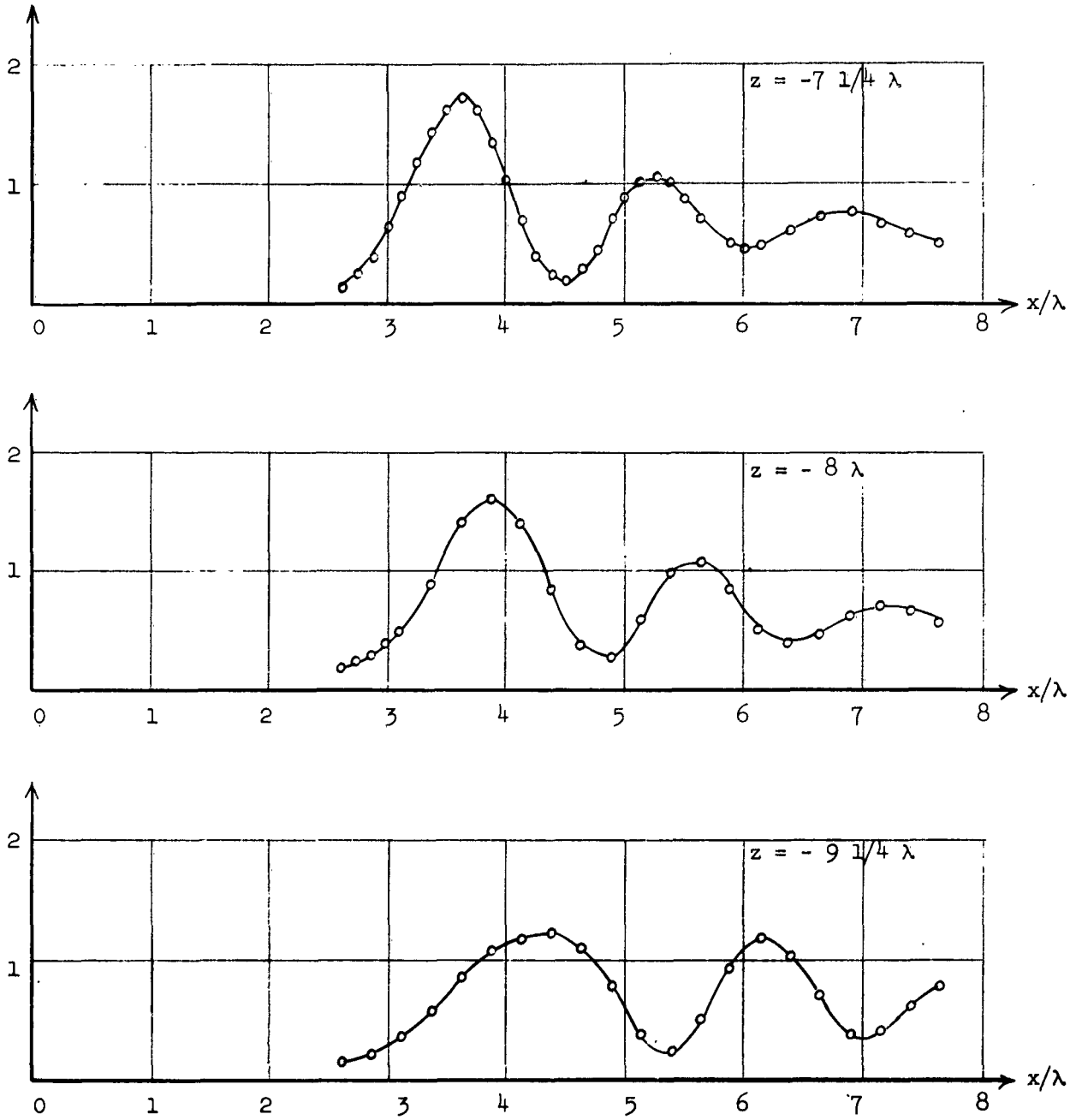

Fig. 14. (continued)

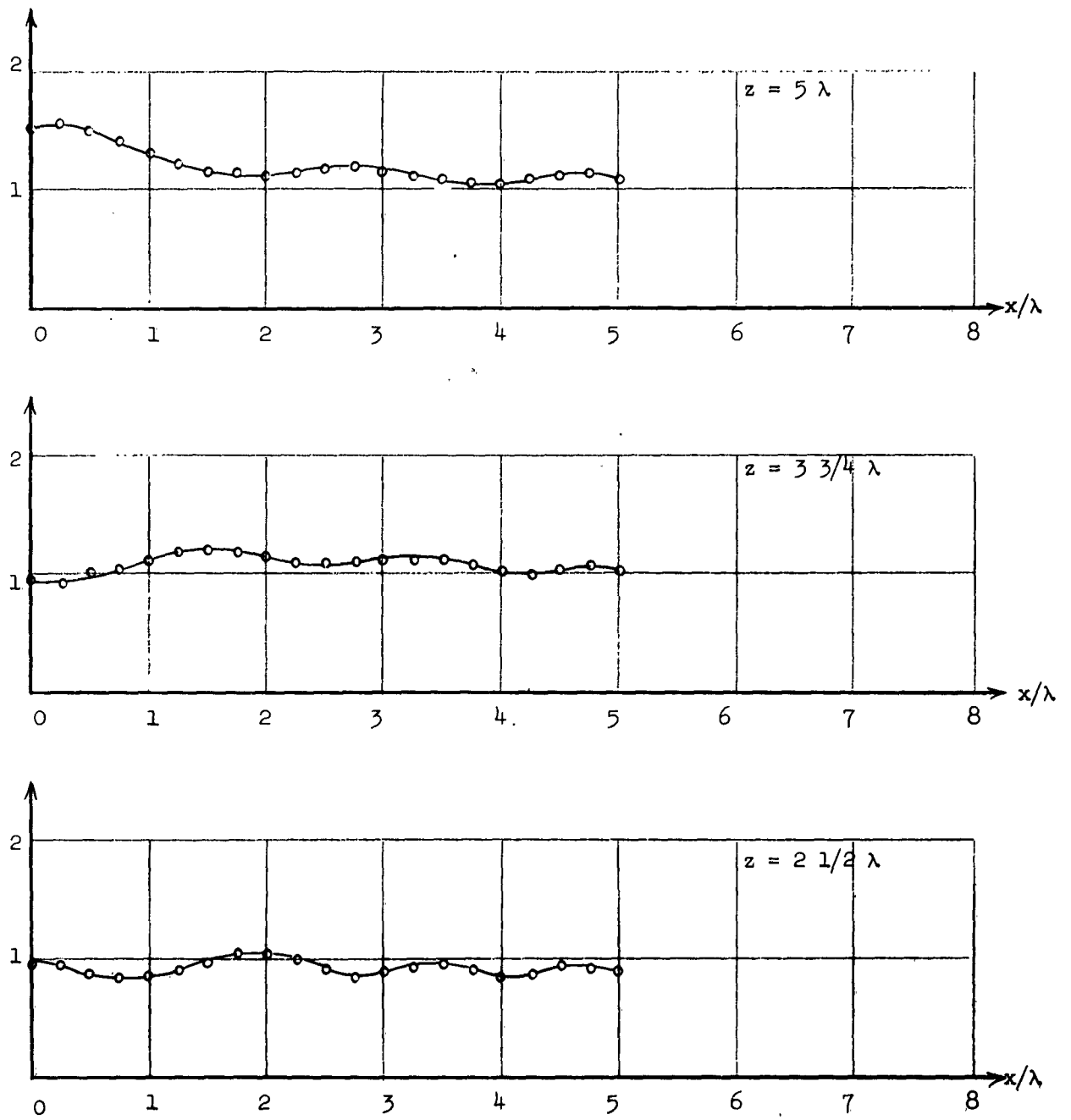

Fig. 15. Distribution of $\left|\frac{E_y}{E_i}\right|^2$ for 45° cone at various values of z in the principal H-plane (y=0).

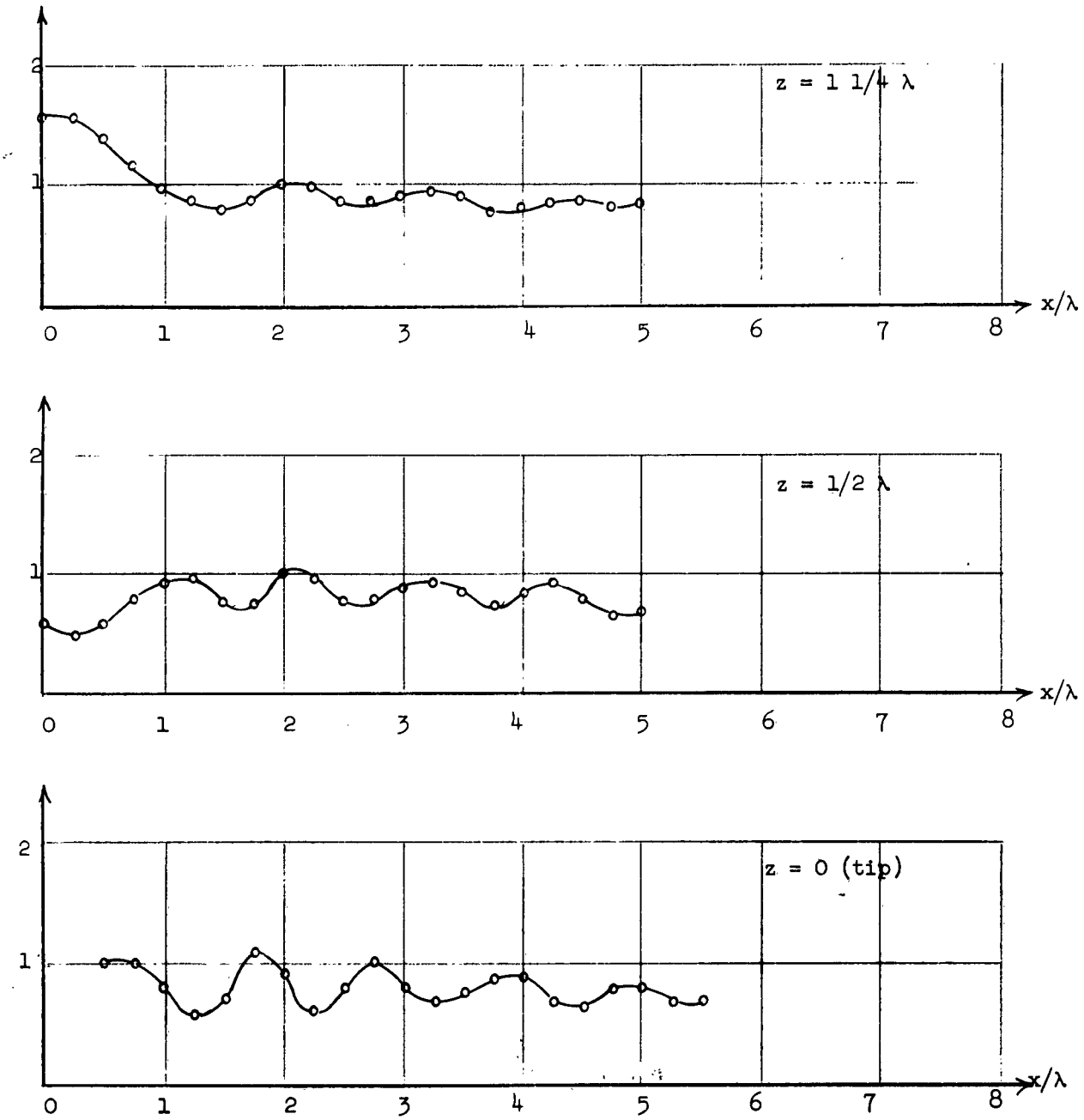

Fig. 15. (continued)

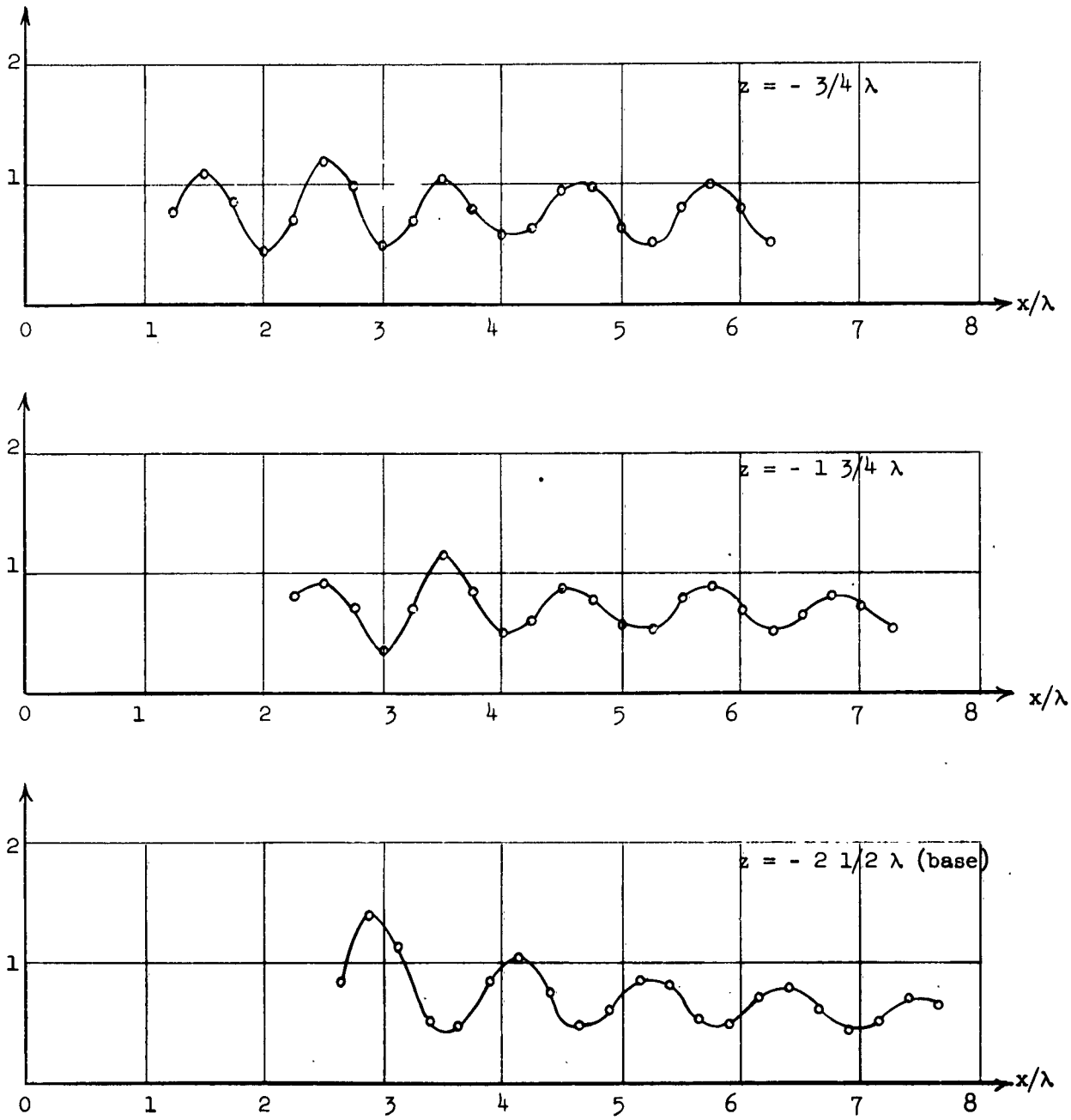

Fig. 15. (continued)

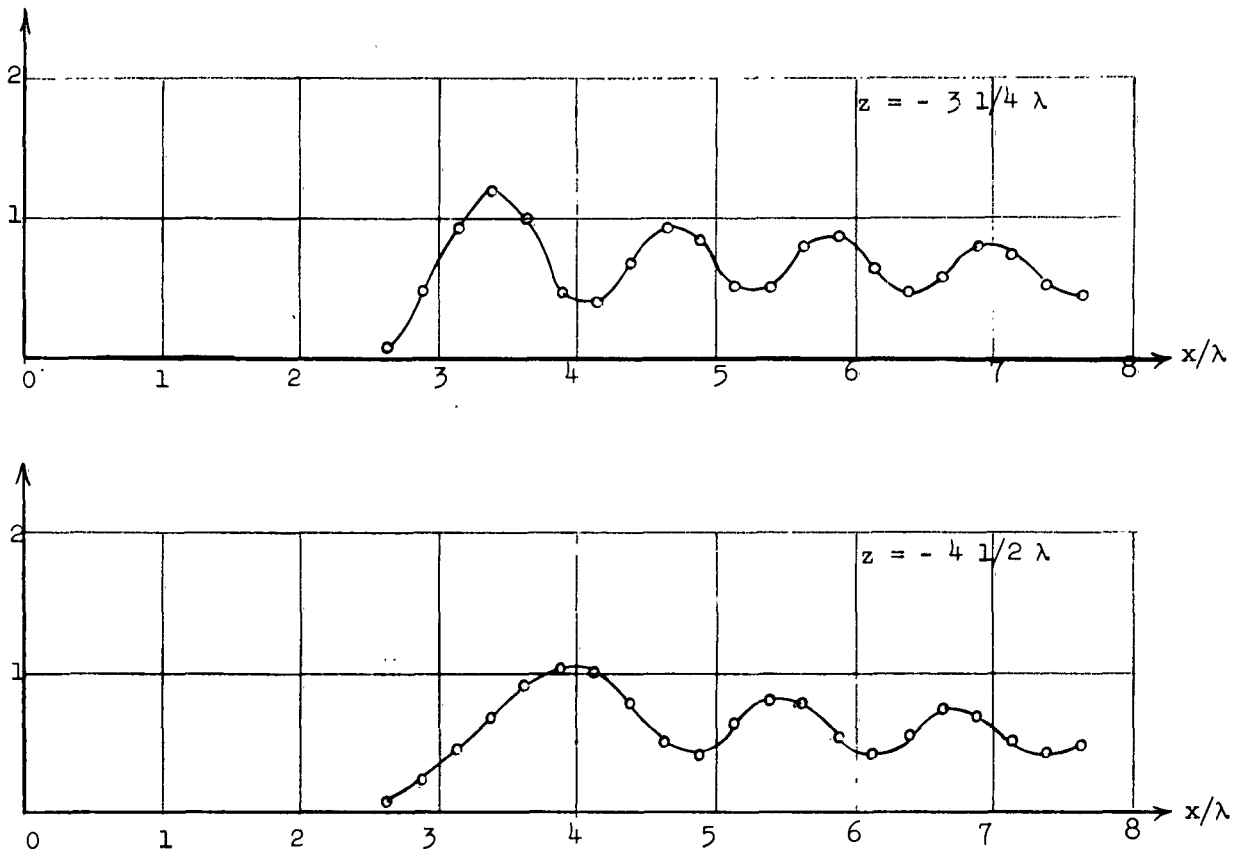

Fig. 15. (continued)

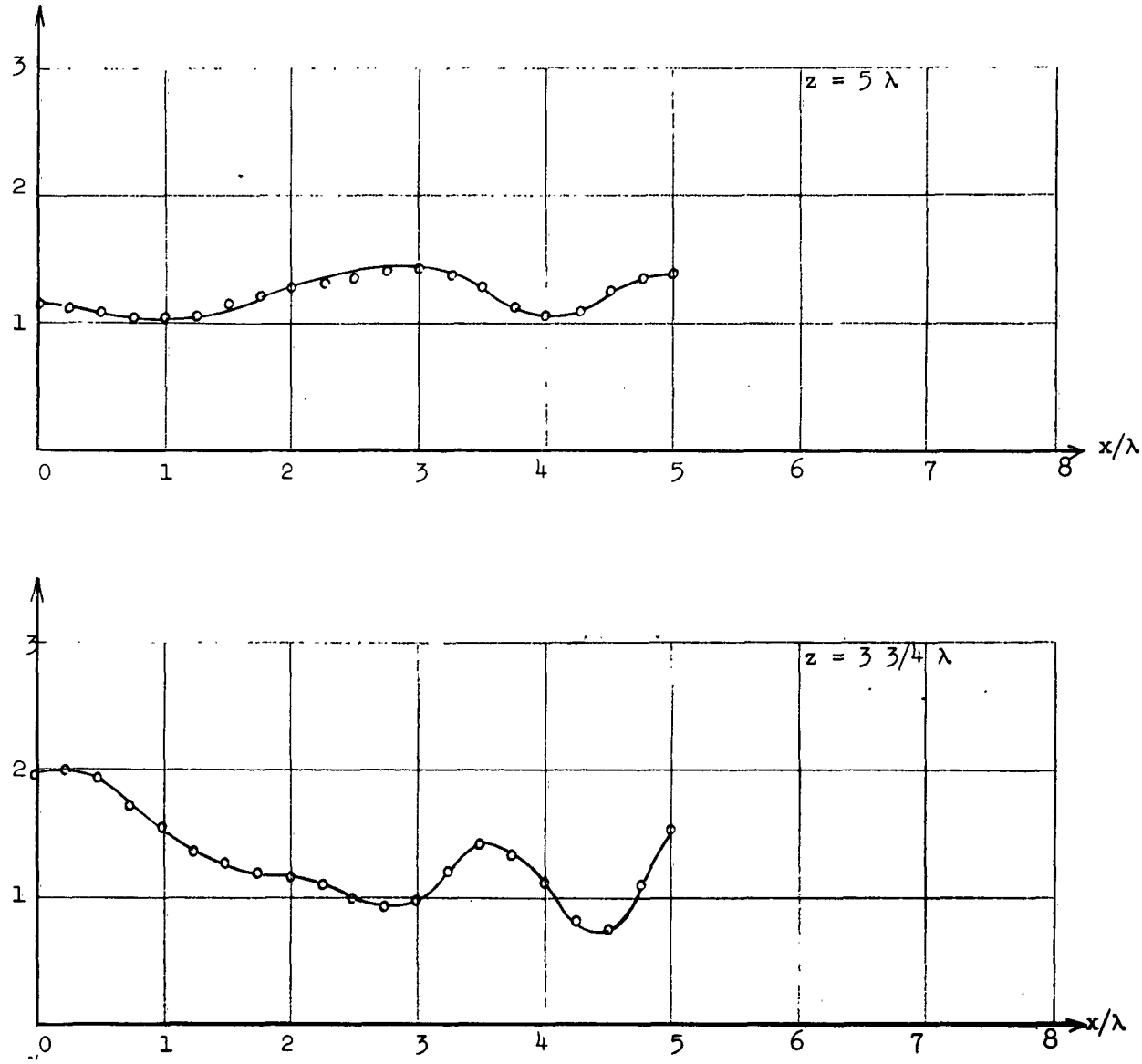

Fig. 16. Distribution of $\left|\frac{E_y}{E_i}\right|^2$ for 67° cone at various values of z in the principal H-plane (y=0).

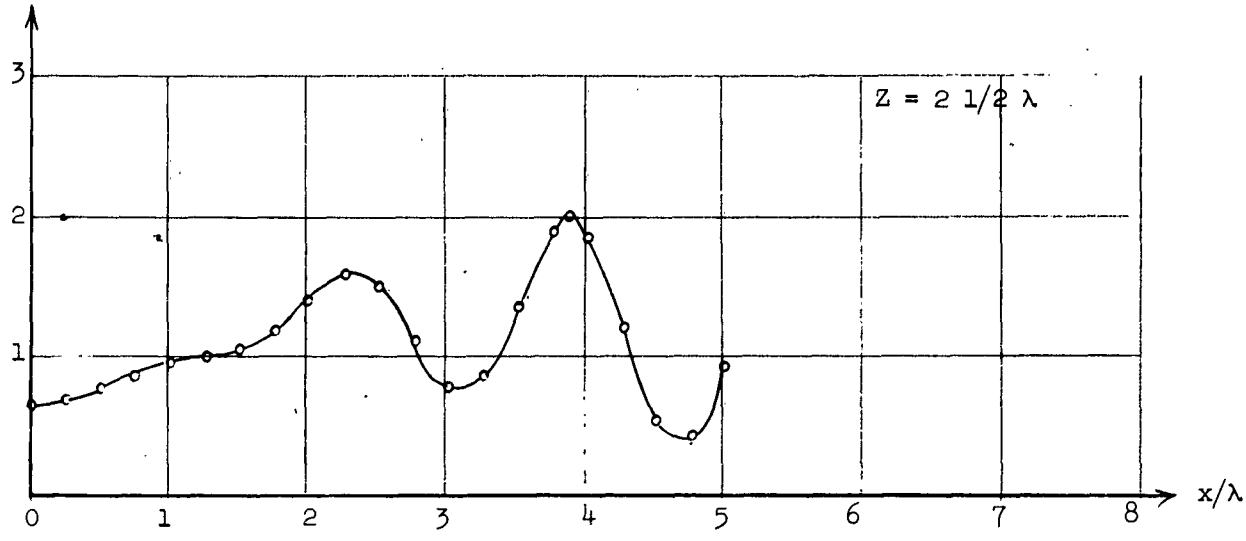

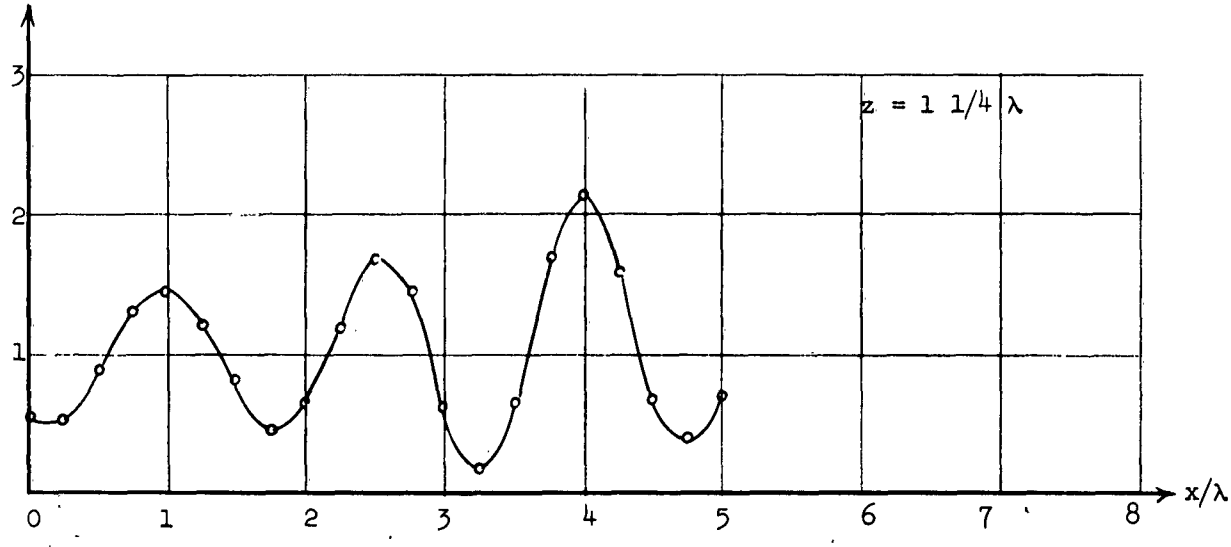

Fig. 16. (continued)

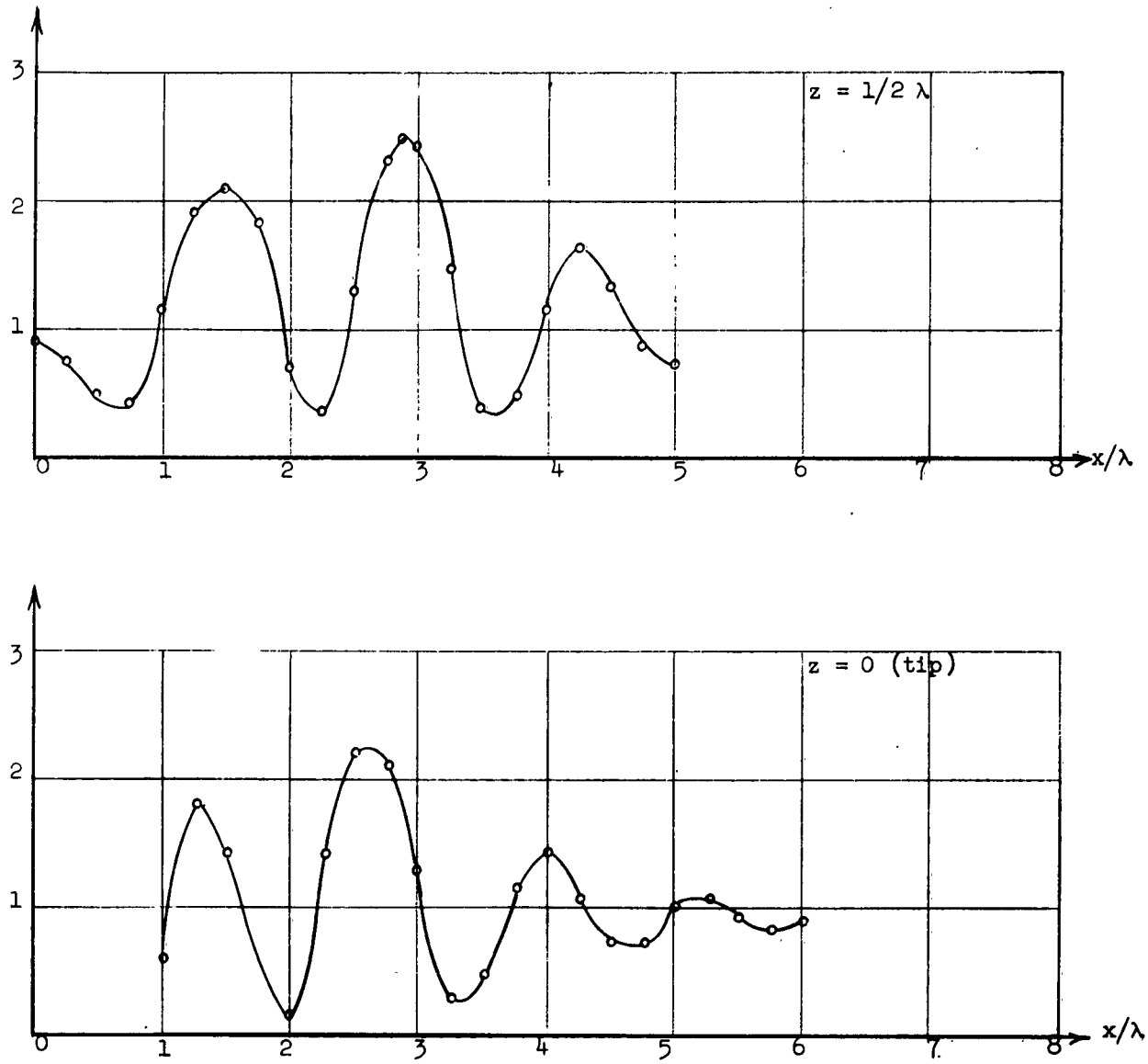

Fig. 16. (continued)

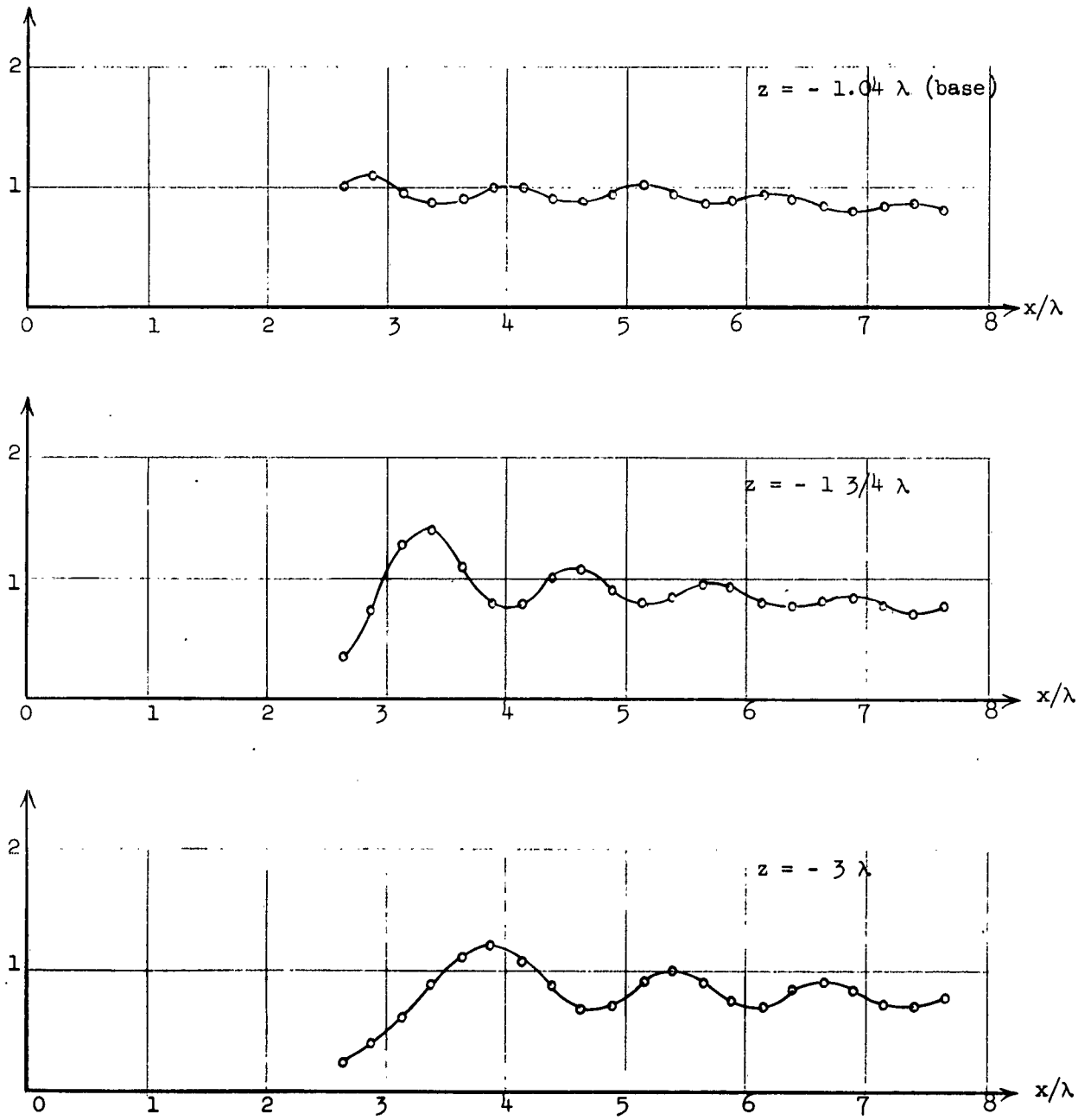

Fig. 16. (continued)

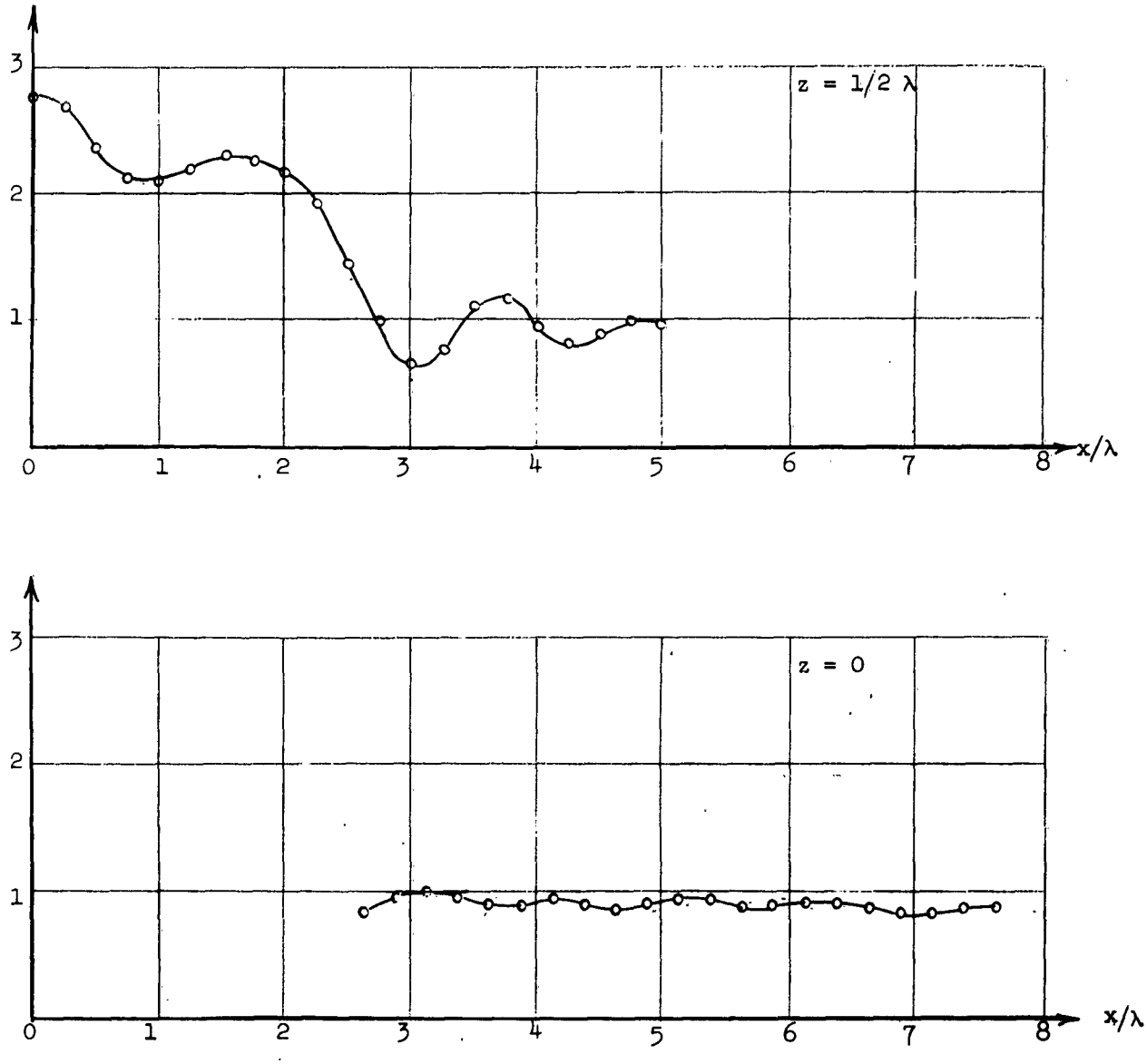

Fig. 17. Distribution of $\left|\frac{E_y}{E_i}\right|^2$ for 90° cone (circular plate) at various values of z in the principal H-plane (y=0).

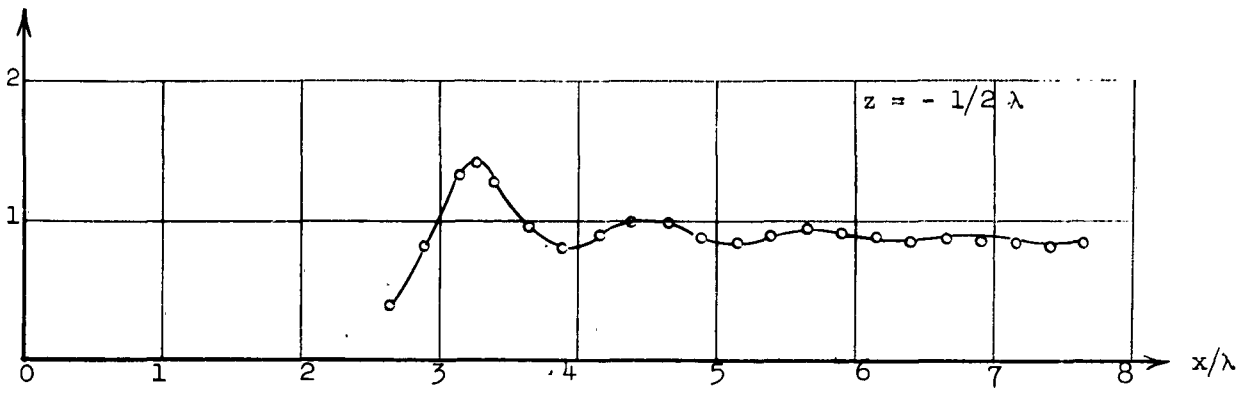

Fig. 17. (continued)

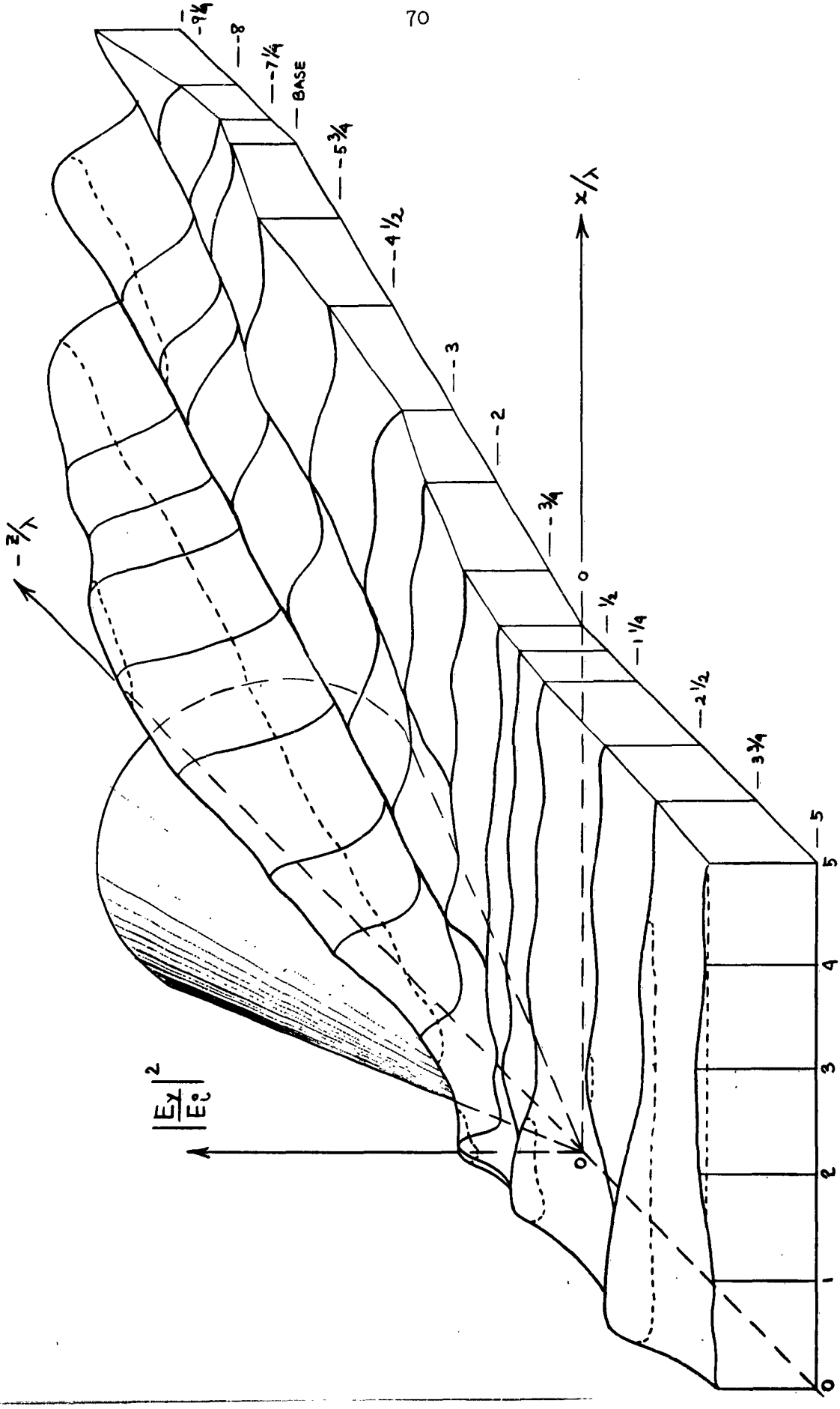

Fig. 18. Three dimensional plot of $\left|\frac{E_y}{E_i}\right|^2$ in the principal H-plane for 20° cone

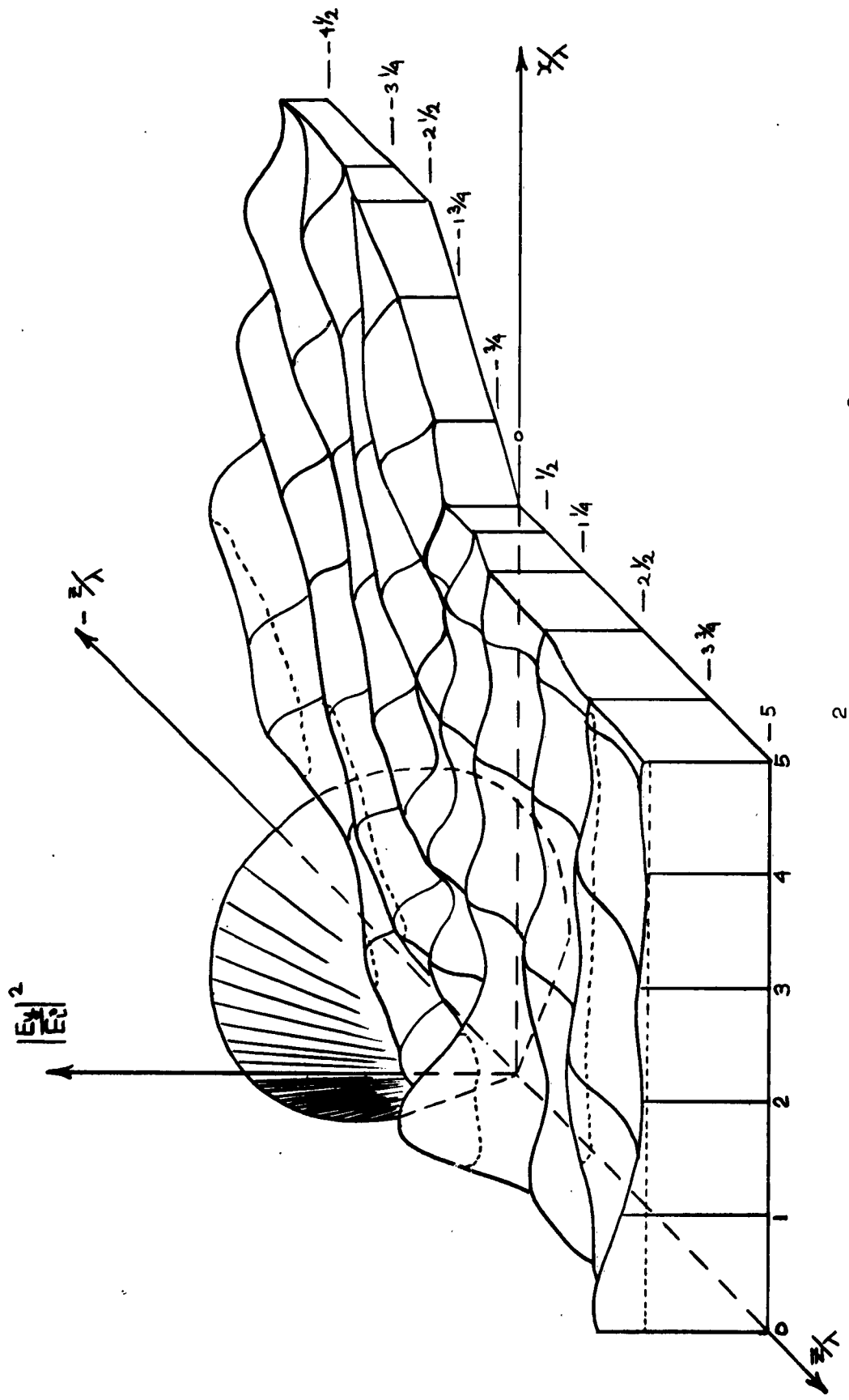

Fig.19—Three-dimensional plot of $|E_y/E_i|^2$ in principal H-plane (45° cone)

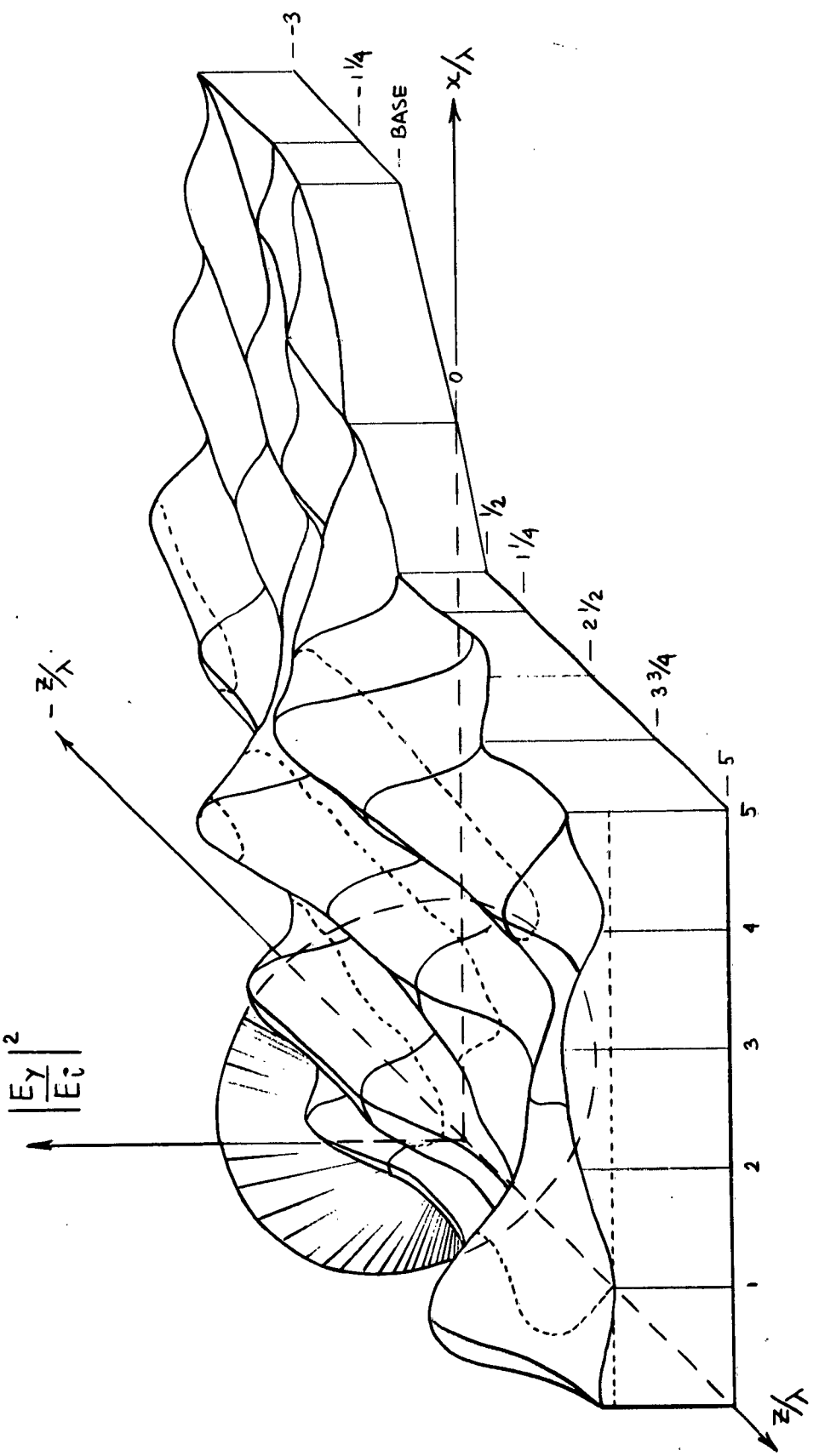

Fig. 20. Three dimensional plot of $\left|\frac{E_y}{E_i}\right|^2$ in the principal H-plane for 67° cone.

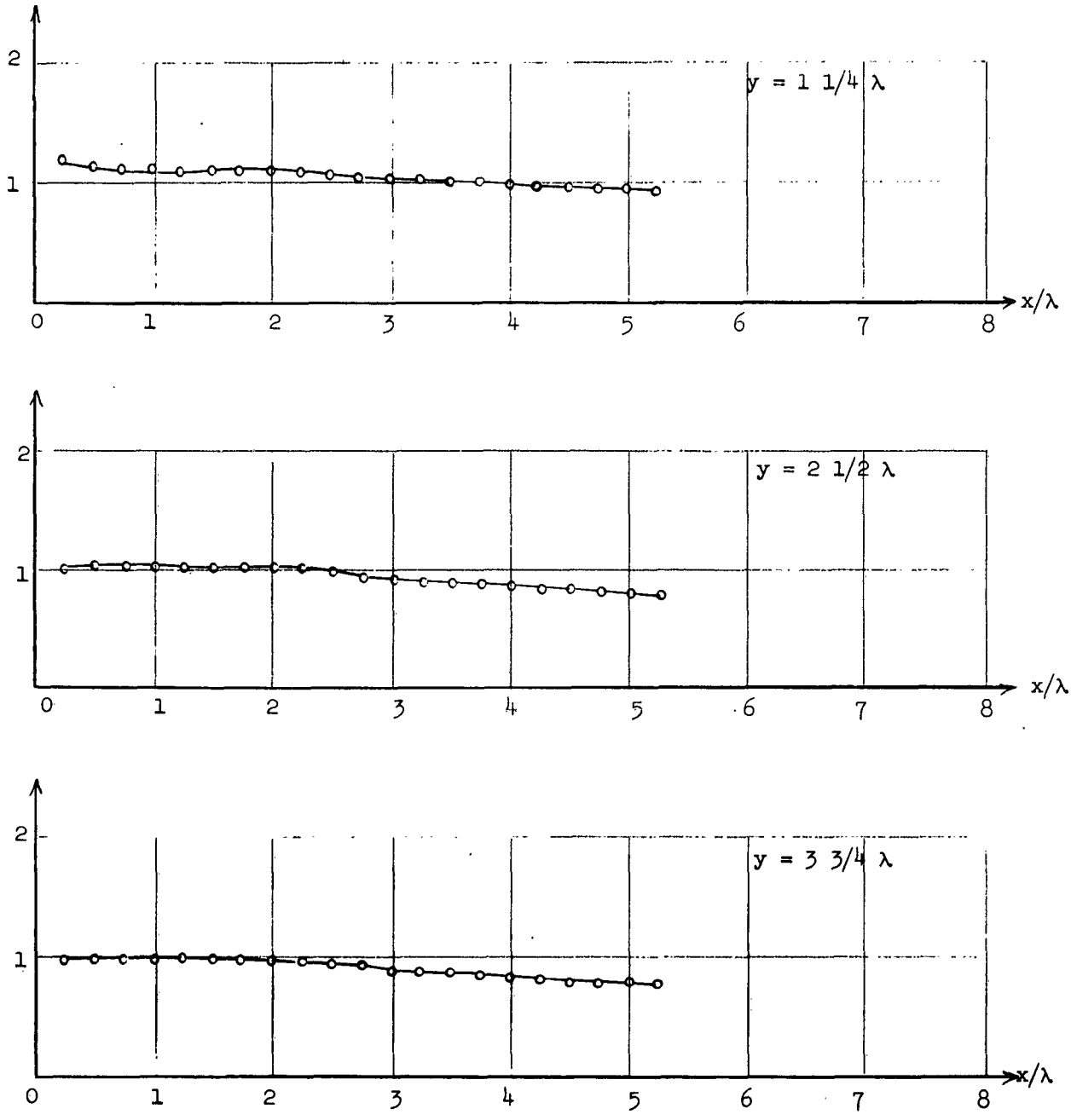

$\gamma = 20^{\circ}$; z = 0 (Cone tip)

Fig. 21. Distribution of $\left|\frac{E_y}{E_i}\right|^2$ for 20°, 45°, 67° cones, at various values of z, in the planes y = 1 1/4λ, 2 1/2λ 3 3/4λ parallel to the principal H-plane.

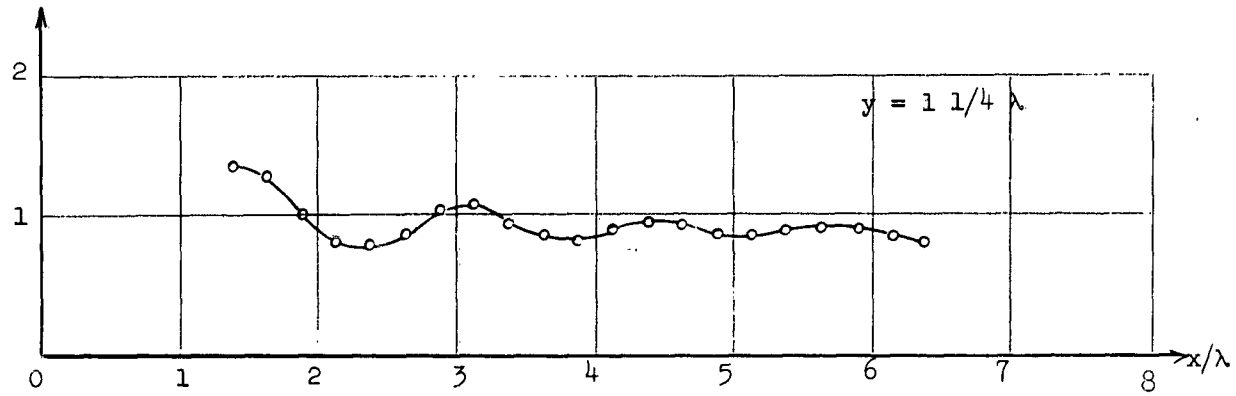

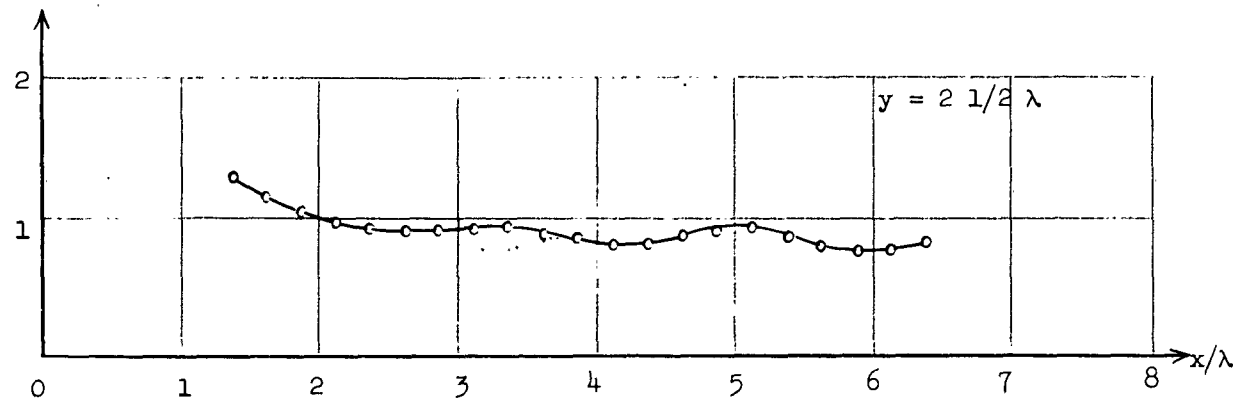

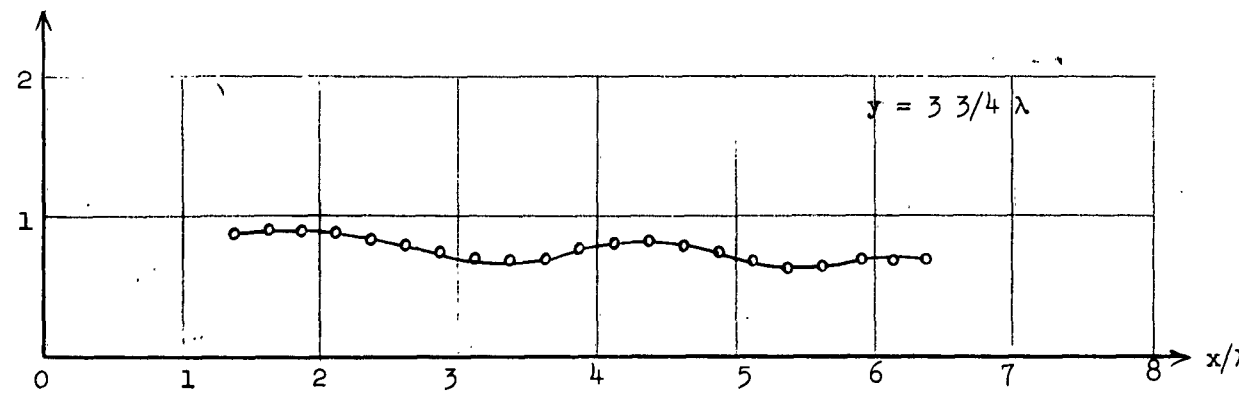

$\gamma = 20^{\circ}$; $z = -3\lambda$

Fig. 21. (continued)

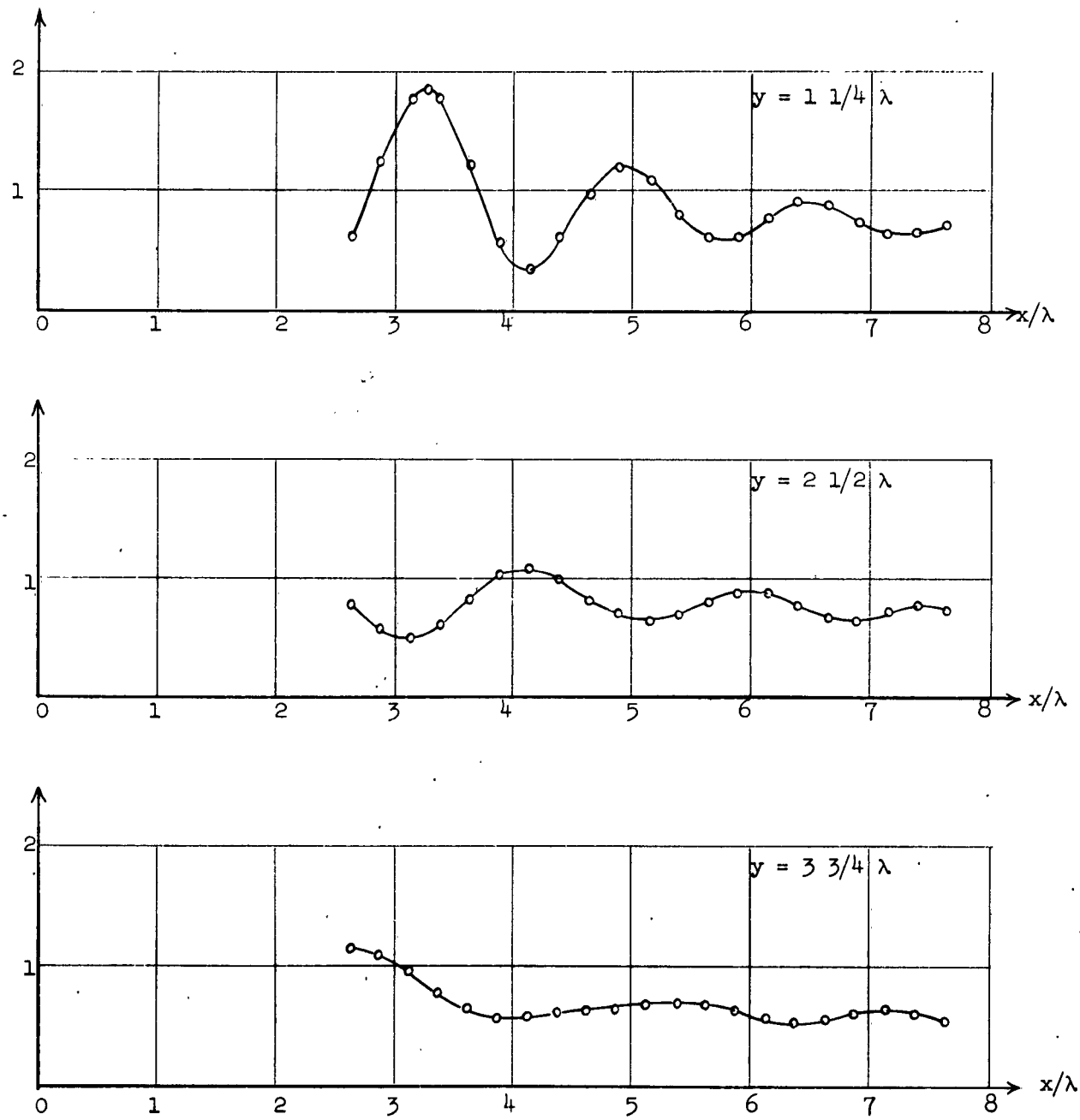

$\gamma = 20^{\circ}$; z = - 6.86λ (Cone tip)

Fig. 21. (continued)

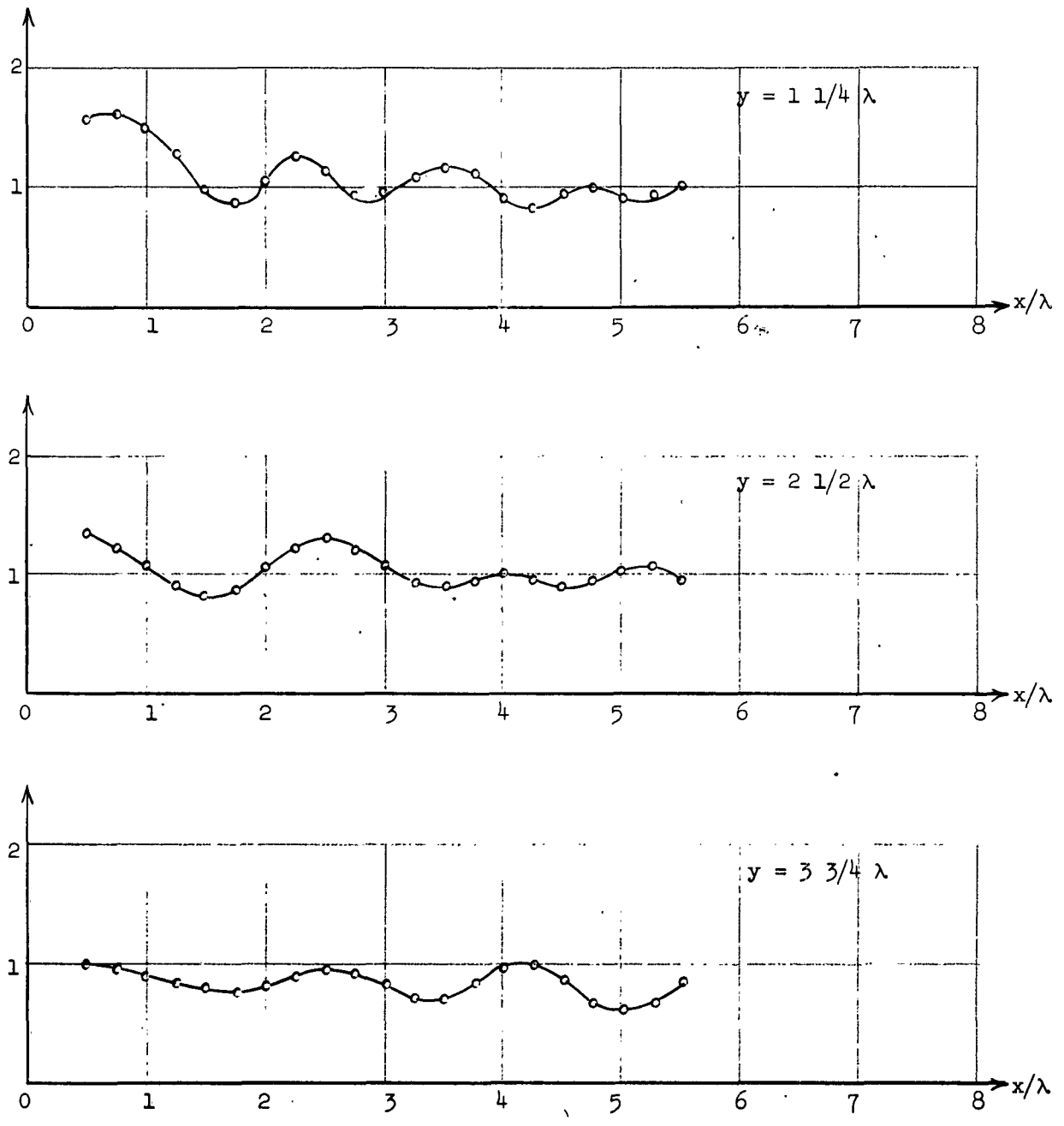

$\gamma = 45^{\circ}$; z = 0 (Cone tip)

Fig. 21. (continued)

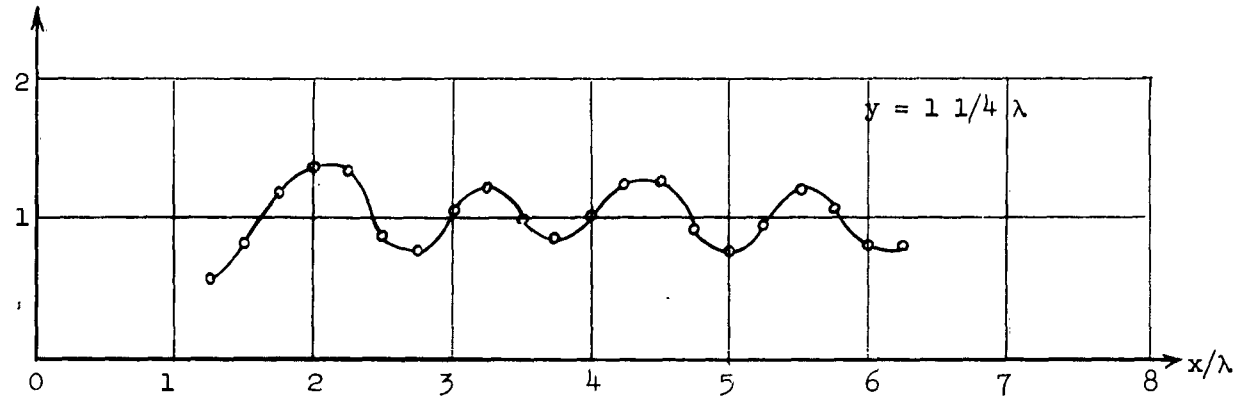

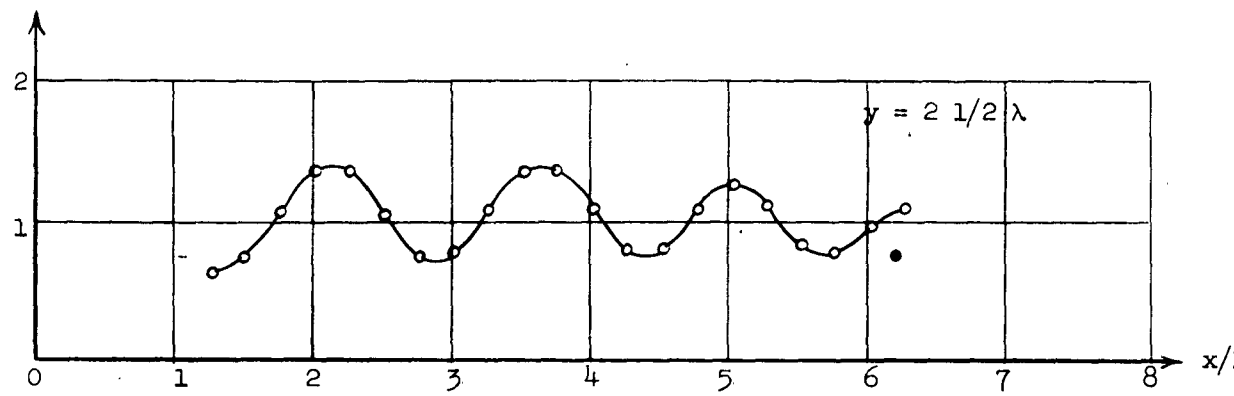

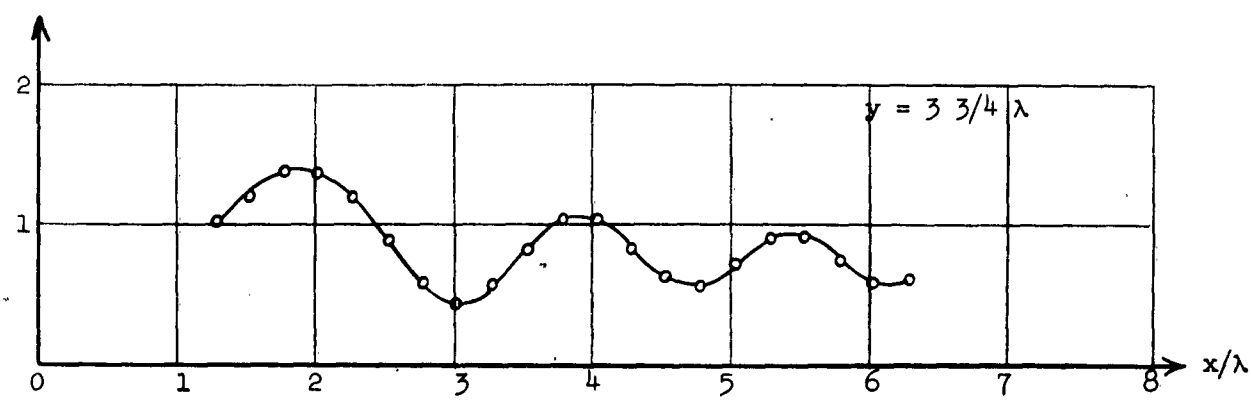

$\gamma = 45^{\circ}$; $z = -3/4\lambda$

Fig. 21. (continued)

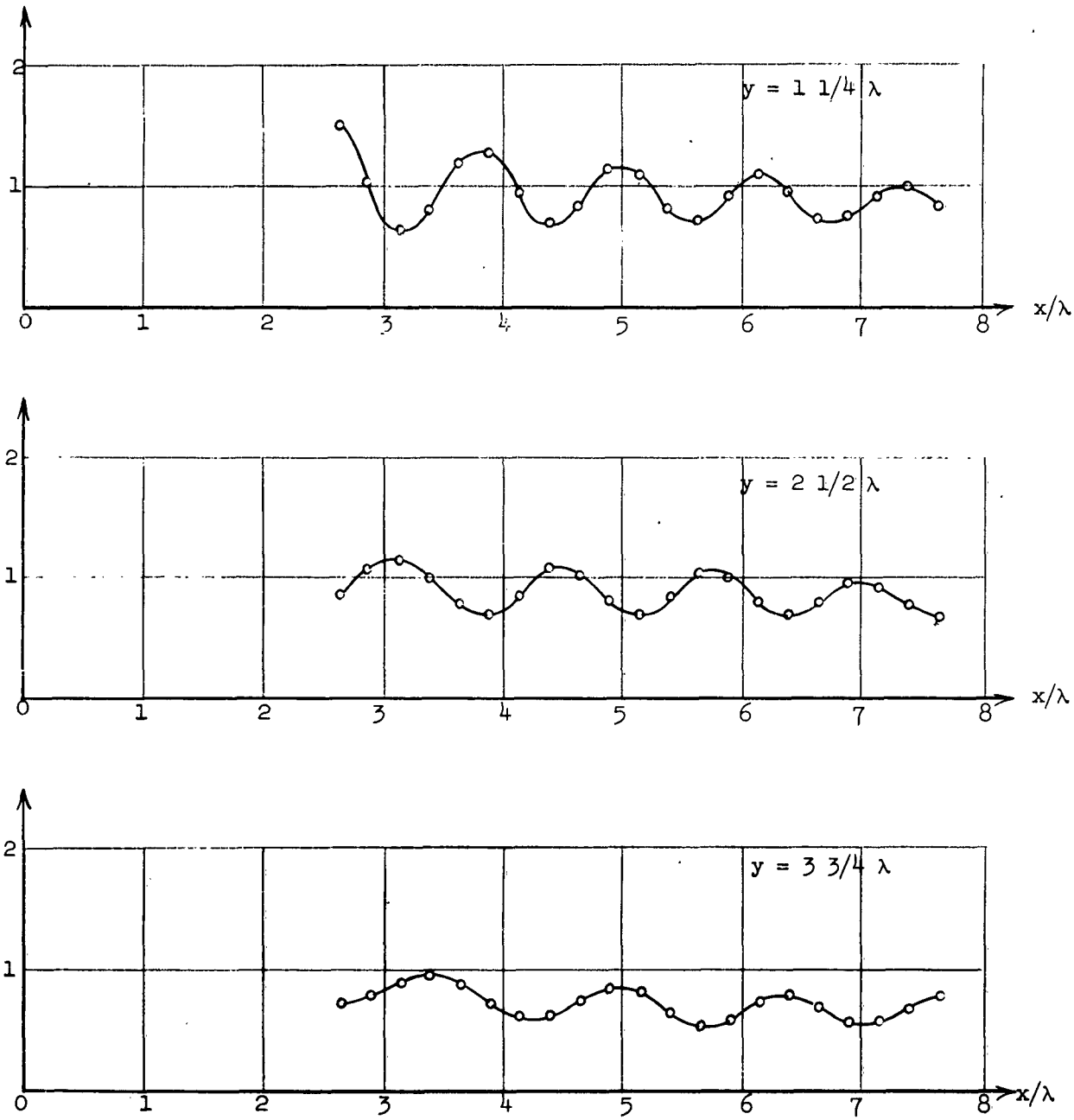

$\gamma = 45^{\circ}$; z = - 2 1/2λ (Cone base)

Fig. 21. (continued)

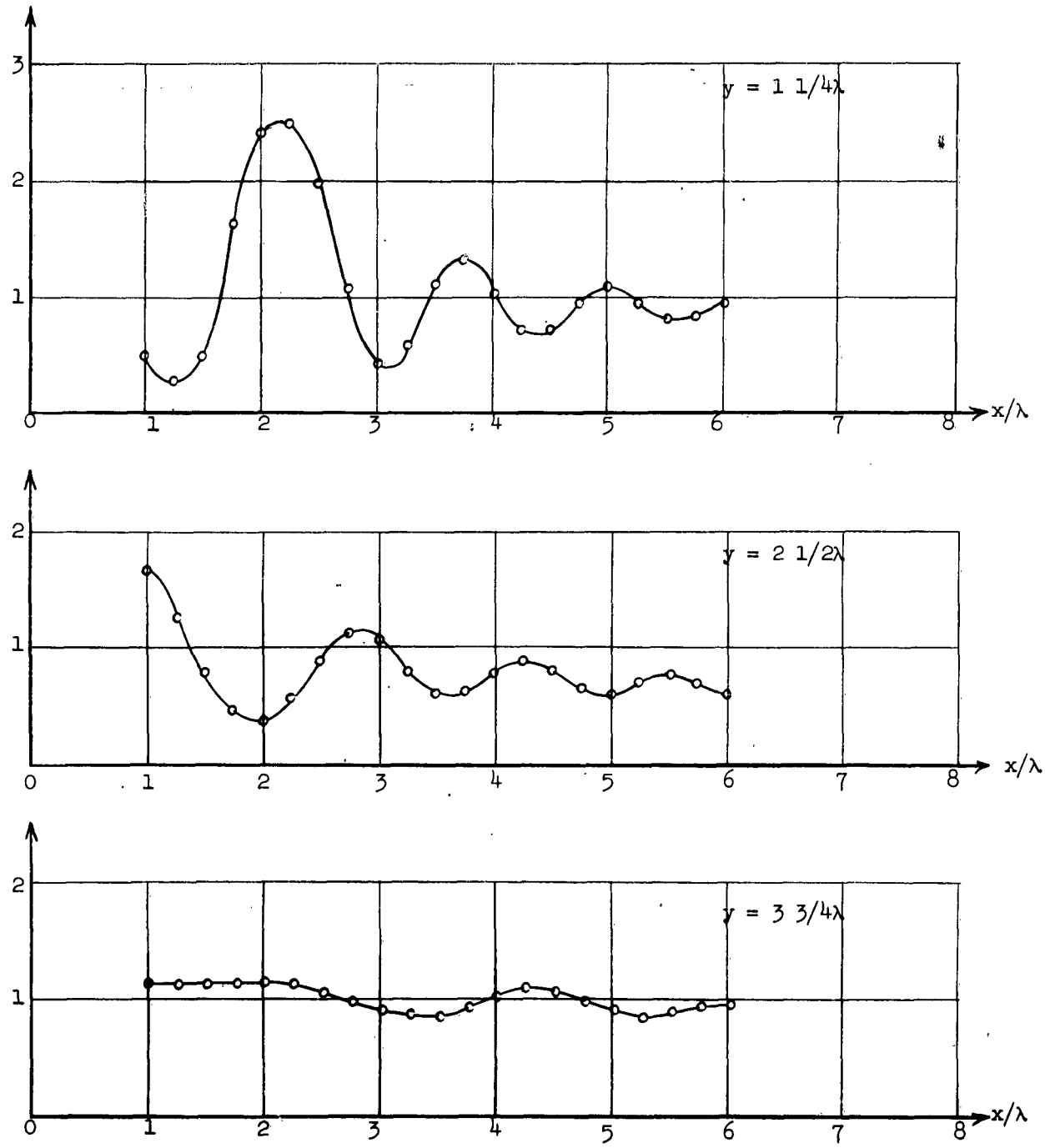

$\gamma = 67^{\circ}$; z = 0 (Cone tip)

Fig. 21. (continued)

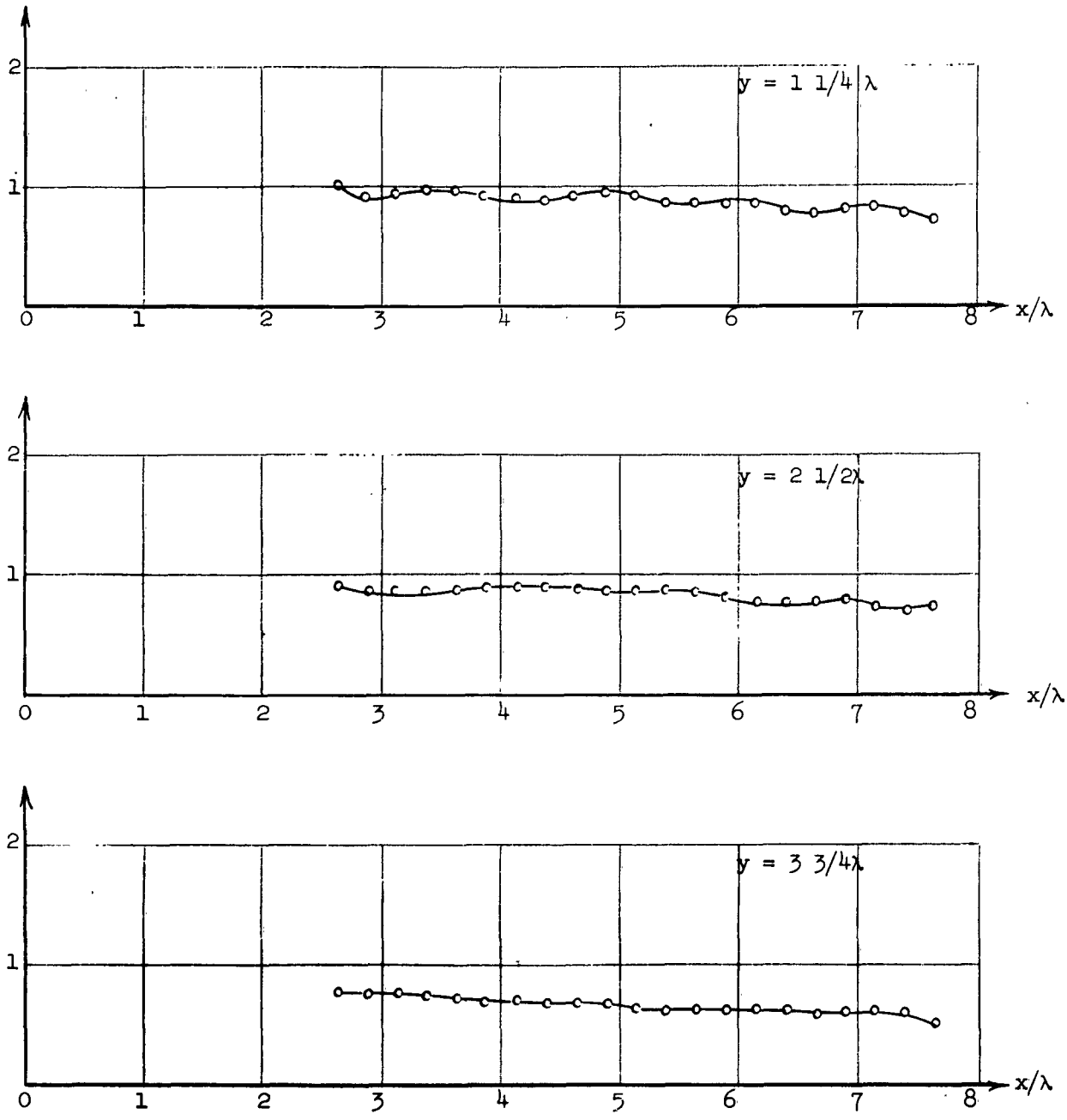

$\gamma = 67^{\circ}$; z = - 1.04λ (Cone base)

Fig. 21. (continued)

In the derivation of Eq. 20 in section V-2 it was shown that the total electric field along the cone axis has only a y-component due to symmetry. At field points away from the axis the electric field has also an x-component. However, as might be suspected from a physical argument, this component is very weak in comparison with the y-component. Fig. 22 shows this comparison between the normalized squares of x and y components in the case of a 20-degree cone. At most places the magnitude of the x-component was below the noise level of the receiving apparatus so that variation of this component could not be determined.

VI-3. On-Axis Field Measurements

To determine the behavior of the electric field on the cone axis, a set of measurements were performed for the different cones. Fig. 23 shows the results of these measurements.

In the case of axial incidence the cone axis is the caustic of the geometrical optic rays diffracted from the edge. The effect of this interference on the amplitude of the variation becomes more emphasized as the cone angle gets larger. This may be seen from the plots of axial distributions.

VI-4. Discussion of Results

Near-zone electric field distributions for finite conducting cones have been obtained. These curves have not hitherto been available. Only the y-component of the $\bar{E}$ field was found to be of significance in the study of cone diffraction patterns.

The study of the diffracted fields near the tip and the edge show that the base scattering is more important for small-angle cones. However, as

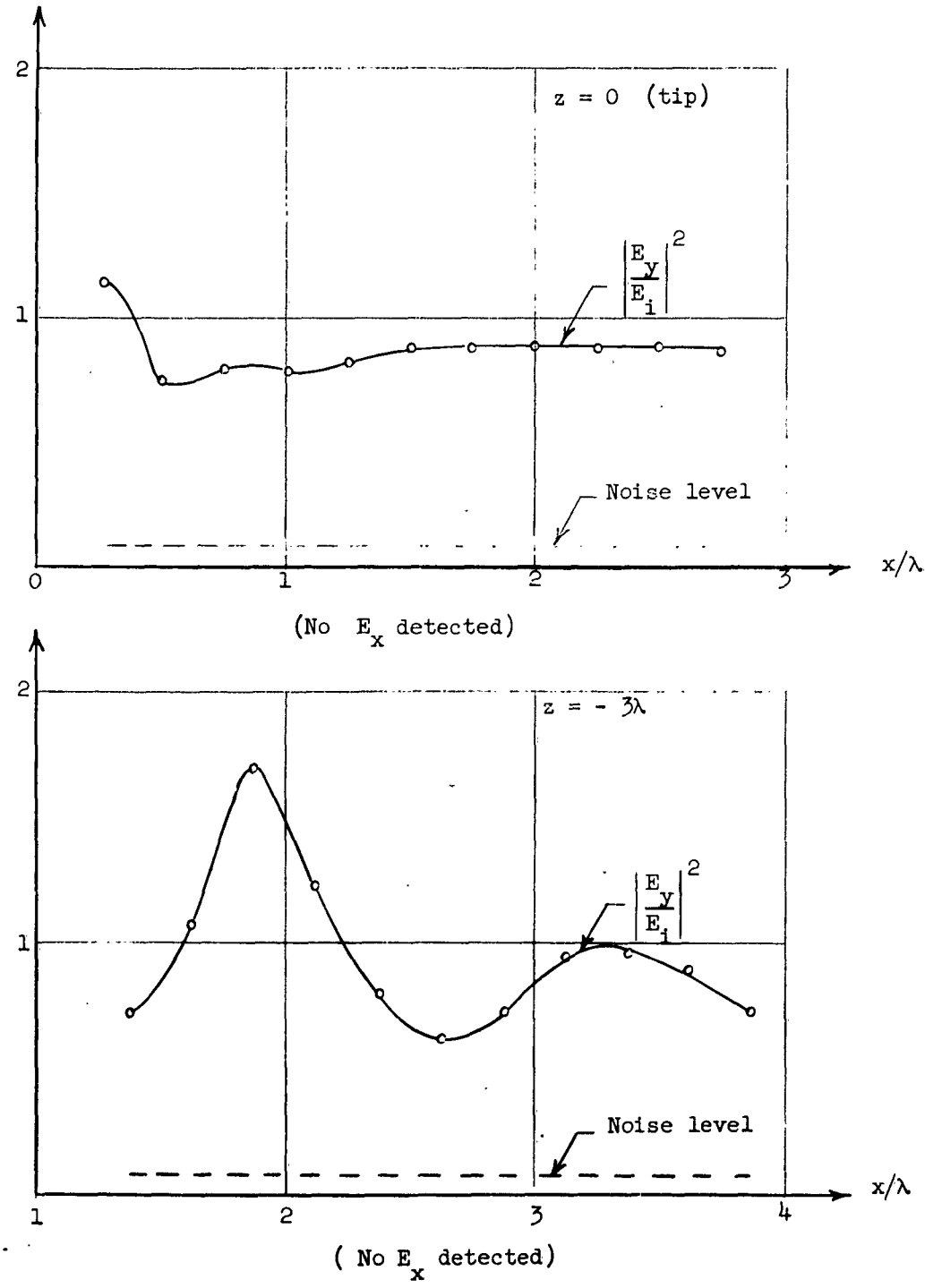

Fig. 22. Comparison between $\left|\frac{E_y}{E_i}\right|^2$ and $\left|\frac{E_x}{E_i}\right|^2$ for 20° cone at various values of z in the principal H-plane.

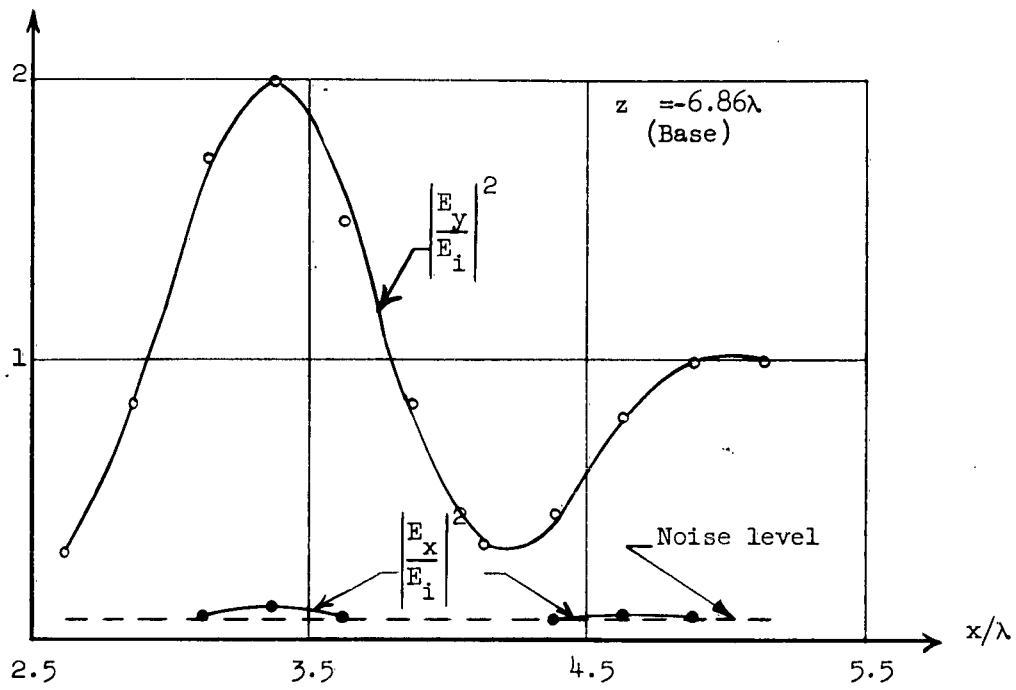

Fig. 22. (continued)

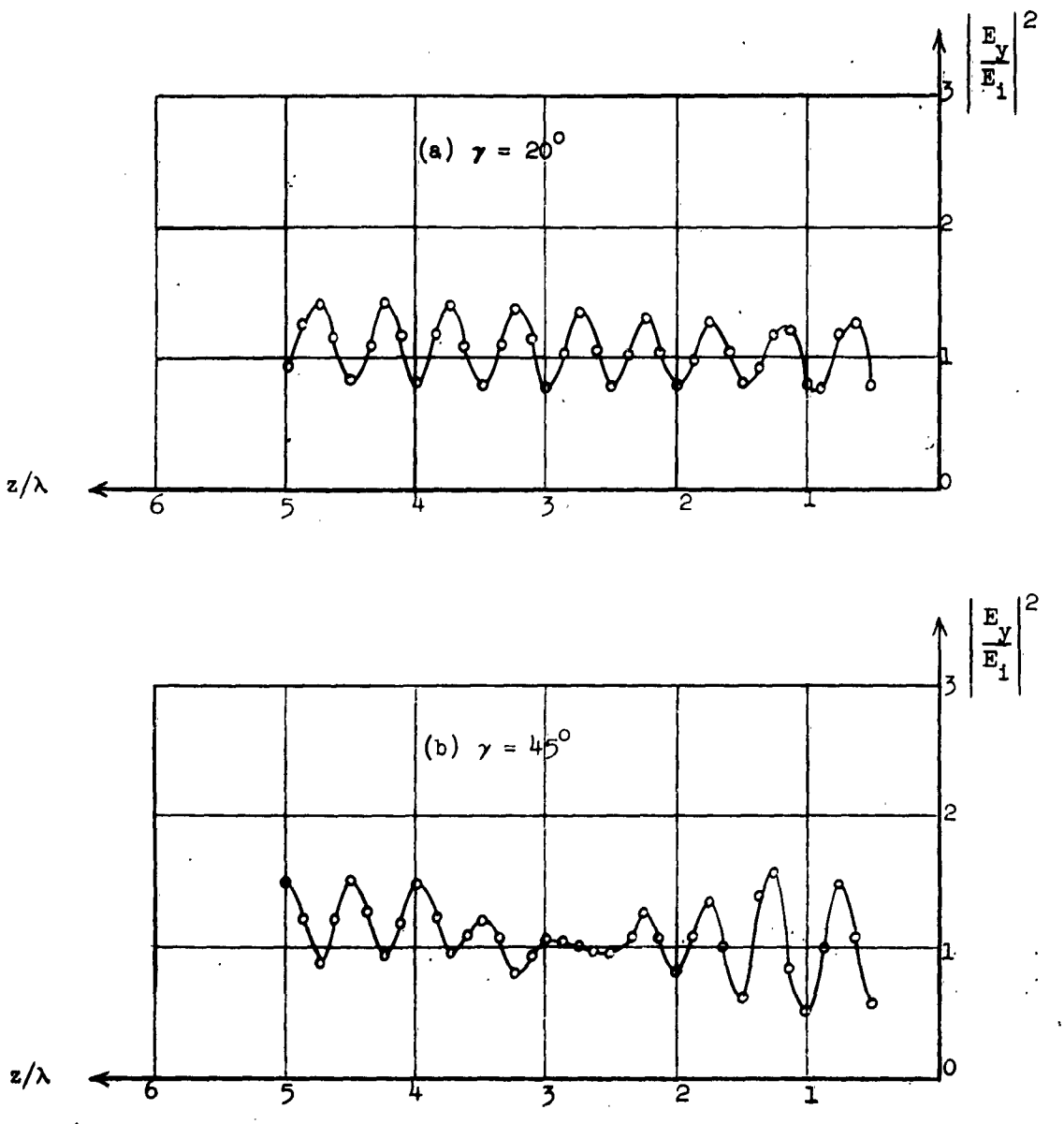

Fig. 23. The distribution of $\left|\frac{E_y}{E_i}\right|^2$ on the axis of the cone for different values of the cone angle.

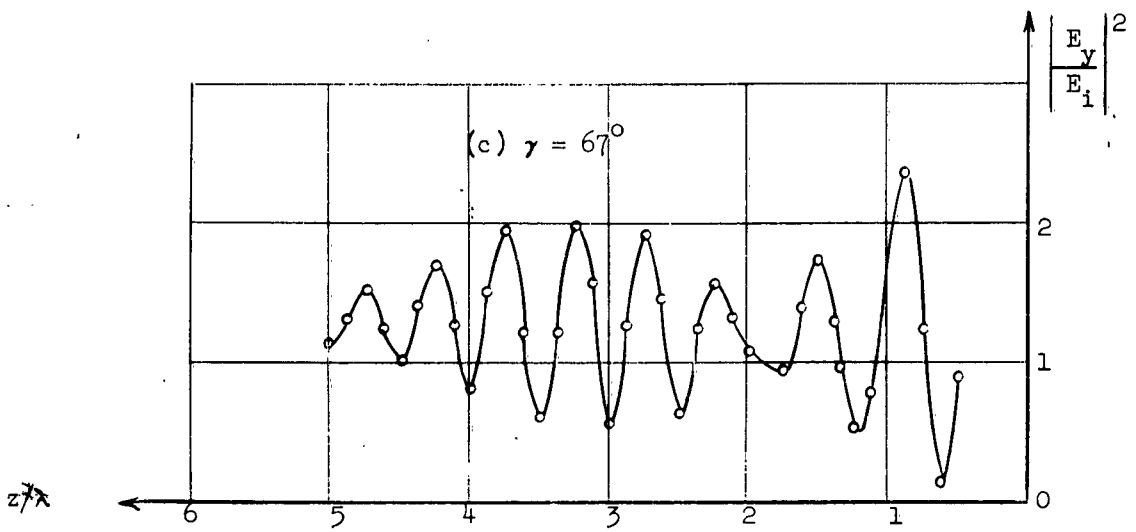

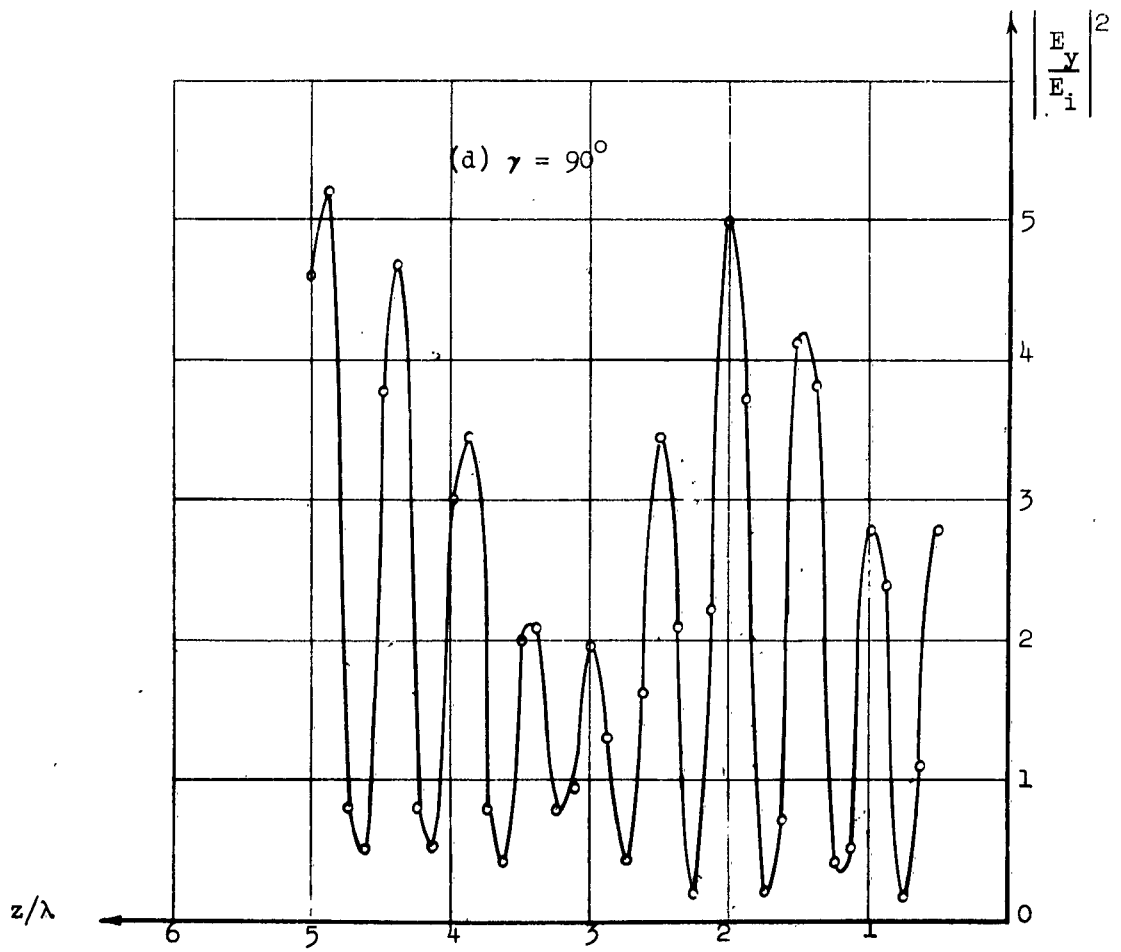

Fig. 23. (continued)

the cone angle gets larger the scattering is dominated by the contribution from the tip when the base diameter is held constant. The same argument was concluded in the study of radar cross sections of finite cones[13] in the case of axial plane wave incidence. It was shown that for large values of kz_o, where z_o is the height of the cone, the cross section is dominated by scattering from the base and when $kz_o \geq 10$ a relative error of less than 10% results if only the base contribution was accounted for. This indicates the existence of a close correlation between the near-field distributions and the radar cross sections under identical situations.

The near-field measurements in the neighborhood of a circular plate using the photoconductive modulation system checked very well with previously obtained results using other methods. Fig. 24 shows a comparison of the results using the light-modulated scattering techniques with those obtained by Ehrlich and Silver[23] under the same conditions using the conventional probing technique.

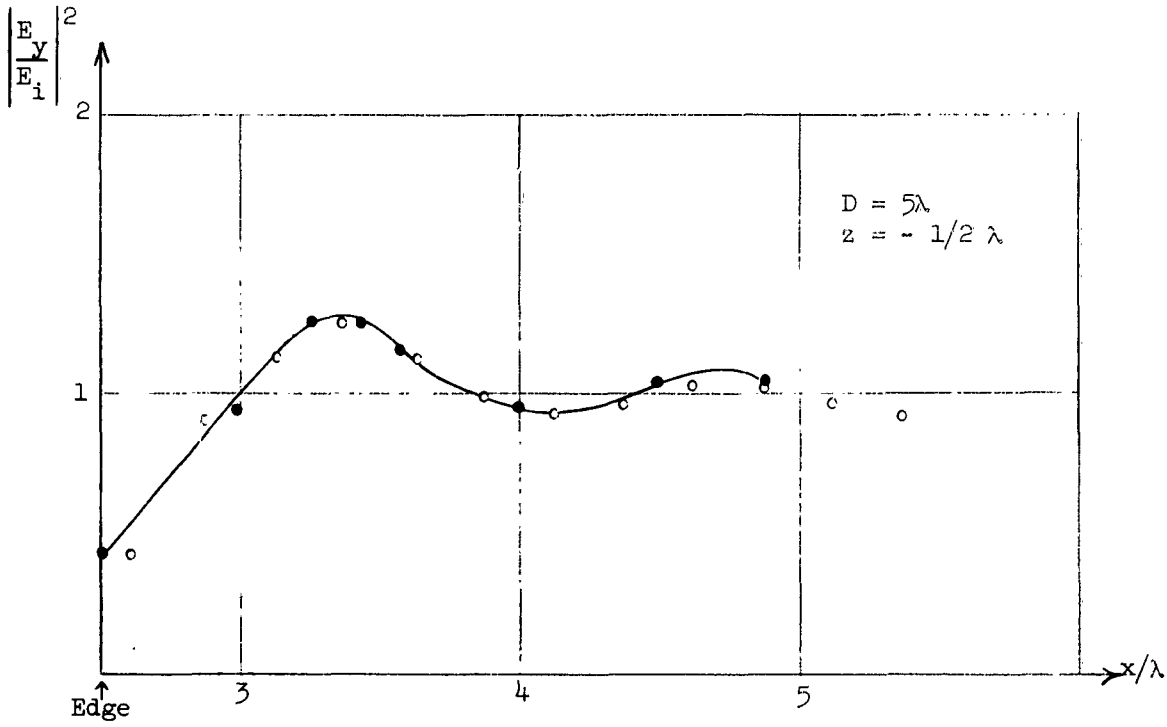

Measured by Ehrlich and Silver

c o c Measured by photoconductive modulation system

Fig. 24. A comparison of the results obtained for the near-field distribution of a circular disk.

VII. CONCLUSIONS

A new method for measuring microwave diffraction fields has been described. It employs a small photoconductive scatterer in a light-modulated scattering technique which dispenses with connecting circuits to the scatterer entirely. Since the scatterer is now completely isolated electrically, all complications and sources of error due to connection disturbance and scatterer movement are eliminated.

Measurements with the circular aperture and the circular disk using light-modulation method checked very well with the published data of Strait[3] and Ehrlich et al[23].

The scattering technique using light modulation was adapted to measuring the diffraction fields of finite conducting cones. Near-zone electric field distributions for three cones (half apex angles 20°, 45° and 67°) and a circular disk of the same diameter were mapped in detail. The experimental results verified the advantages and usefulness of this method.

No measurement of the near-zone magnetic field distribution was made in this study. This was due to the difficulty in constructing a small loop scatterer of photoconductive material having accurate geometry. However, the extension of the light-modulation principle to independent measurements of microwave H-field distributions is straight forward.

APPENDIX

Effect of the Chopper Blade Modulation

The coherent detector used in the experiments is illustrated in Fig. A-1.

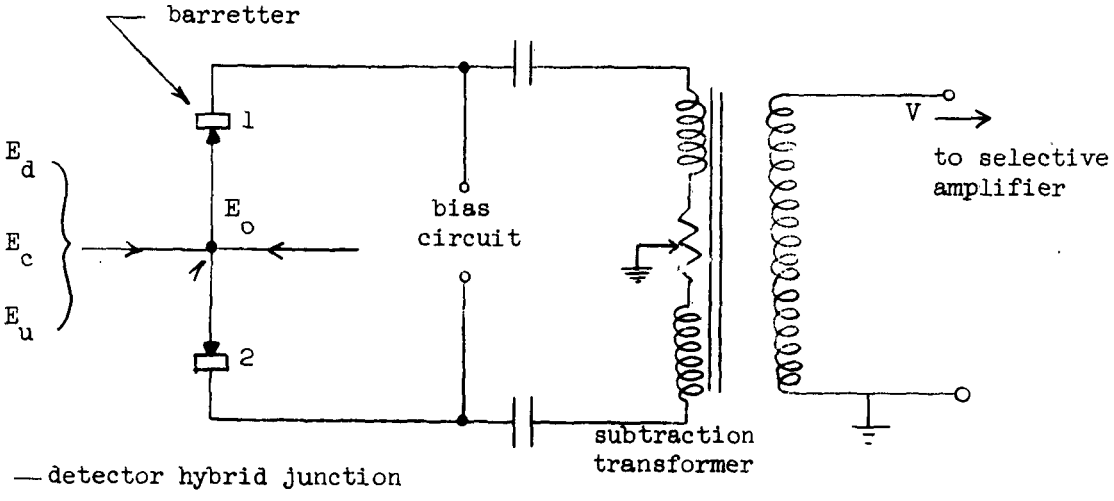

Fig. A-1 Basic diagram of the coherent detector

If a signal is modulated from the rotation of the chopper blade it arrives at the detector hybrid junction together with a signal from the scatterer and an error signal.

Let the different signals be denoted by

$E_d \cos(\omega t + \gamma)$ = Modulated signal from scatterer

$E_c \cos(\omega t + \alpha)$ = " " from chopper blade

$E_u \cos(\omega t + \eta)$ = Un modulated error signal

$E_o \cos(\omega t + \beta)$ = Reference signal

$m(t)$ = Modulation function

As a result of the properties of the hybrid junction the signals E_1 and E_2 arrive at barreters 1 and 2 in phase in one arm and out of phase in the other arm of the junction.

$$E_1 = E_o \cos(\omega t+\beta) + E_u \cos(\omega t+\eta) + [E_d \cos(\omega t+\gamma) + E_c \cos(\omega t+\alpha)]\, m(t)$$

$$E_2 = E_o \cos(\omega t+\beta) - E_u \cos(\omega t+\eta) - [E_d \cos(\omega t+\gamma) + E_c \cos(\omega t+\alpha)]\, m(t)$$

These signals are squared by the square law barreters 1 and 2 respectively. Since the power is proportional to E^2, the modulated components of the powers arriving at detectors 1 and 2 are given by

$$P_{1,2} = [E_d^2 \cos^2(\omega t+\gamma) + E_c^2 \cos^2(\omega t+\alpha) + 2 E_u E_d \cos(\omega t+\eta) \cos(\omega t+\gamma)$$
$$\mp 2 E_o E_d \cos(\omega t+\beta) \cos(\omega t+\gamma) \mp 2 E_o E_c \cos(\omega t+\beta) \cos(\omega t+\alpha)$$
$$+ 2 E_u E_c \cos(\omega t+\eta) \cos(\omega t+2) + 2 E_d E_c \cos(\omega t+\gamma) \cos(\omega t+\alpha)]\, m(t)$$

where upper sign belongs to P_2. The audio response V_1 and V_2 are found by averaging $P_{1,2}$ over one cycle:

$$V_{1,2} = \frac{1}{2} E_d^2 + \frac{1}{2} E_c^2 + E_u E_d \cos(\gamma-\eta) \mp E_o E_d \cos(\gamma-\beta)$$
$$\mp E_o E_c \cos(\alpha-\beta) + E_u E_c \cos(\alpha-\eta) + E_d E_c \cos(\alpha-\gamma)$$

The audio transformer takes the difference of there signals. Hence the

output of the coherent detector becomes

$$V = E_o E_d \cos(\gamma-\beta) + E_o E_c \cos(\alpha-\beta)$$

Hence, the amount contributed by chopper modulation is an additive term to the final reading.

BIBLIOGRAPHY

1. R.Justice and V.H.Rumsey, "Measurement of Electric Field Distributions," IRE Trans.on Antennas and Propagation,Vol.AP-3,pp.177-180;October,1955.

2. J.H.Richmond, "A Modulated Scattering Technique for Measurement of Field Distributions," IRE Trans.on Microwave Theory and Techniques,Vol.MTT-3, pp.13-15;April,1955.

3. B.J.Strait and D.K.Cheng, "Microwave Magnetic-Field Measurements by a Modulated Scattering Technique," Proc. IEE,Vol.109,pt.B,pp.33-40; January,1962.

4. A.Cullen and J.Parr, "A New Perturbation Method for Measuring Microwave Fields in Free Space," Proc.IEE.Vol.102B,paper No.1921R,pp.836, November,1955.

5. R.F.Harrington, "Small Resonant Scatterers and Their Use for Field Measurements," Syracuse University Research Institute,Report No.EE492-6201T13;January,1962.

6. M.K.Hu,"On Measurements of E and H Field Distributions by Using Modulated Scattering Methods," IRE Trans.,Vol MTT-8,pp.295-300,May,1960.

7. W.E.Bulman and B.C.Potts, "Photoconductive Modulation of Microwave Electric Fields," IRE trans.on Antennas and Propagation,Vol.AP-9, pp.193-199;March,1961.

8. R.H.Bube, "Photoconductivity of the Sulfide, Selenide, and Telluride of Zinc or Cadmium," Proc.IRE,Vol.43,No.12,pp.1836-1848,December,1955.

9. R.B.McQuistan, "On Radiation Modulation," Journal of the Optical Society of America,Vol.49,pp.70-74,January,1959.

10. H.S.Carslaw, "The Scattering of Sound Waves by a Cone," Mathematische Annalen,Vol.75,pp.133-147,1914.

11. W.W.Hansen and L.I.Schiff, "Theoretical Study of Electromagnetic Waves Scattered from Shaped Metal Surfaces," Quarterly Report No.4,Stanford University,Microwave Laboratory,1948.

12. C.E.Schensted, "Application of Summation Techniques to the Radar Cross Section of a Cone," Symp. on Microwave Optics, McGill University,Montreal, Canada;June, 1953.

13. K.M.Siegel and H.A.Alperin, "Studies in Radar Cross-Sections-III: Scattering by a Cone," Willow Run Research Center Engineering Research Institute, University of Michigan, Res.Dept. UMM-87,January,1952.

14. K.M.Siegel et al, "Studies in Radar Cross-Sections-IV: Comparison Between Theory and Experiment of the Cross-Section of a Cone," Willow Run Research Center Engineering Research Institute, University of Michigan, Res.Rept.UMM-92,February,1953.

15. L.B.Felsen, "Back Scattering from Wide-Angle and Narrow-Angle Cones," Symp. on Microwave Optics,McGill University,Montreal,Canada;June,1953.

16. L.B.Felsen, "Back Scattering from Wide-Angle and Narrow-Angle Cones," J.Appl.Phys.,Vol.26,pp.138-151,February,1955.

17. L.B.Felsen, "Plane-wave Scattering by Small-Angle Cones," IRE Trans. on Antennas and Propagation,Vol.AP-5,pp.121-129,January,1957.

18. L.B.Felsen,"Back Scattering from a Semi Infinite Cone," Microwave Research Inst.Polytechnic Inst. of Brooklyn, N.Y.,memo.43,R-675, PIB-603,July,1958.

19. J.B.Keller, "The Geometric Optics Theory of Diffraction," Symp.on Microwave Optics,McGill University,Montreal,Canada,June,1953.

20. J.B.Keller, "Backscattering from a Finite Cone," IRE Trans.on Antennas and Propagation,Vol.AP-8,pp.175-182,March,1960.

21. J.R.Mentzer, "Scattering and Diffraction of Radio Waves," Pergamon Press, Ltd.pp.81-94,1955.

22. R.F.Harrington, "Time-Harmonic Electromagnetic Fields," McGraw-Hill Book Company,Inc.,Chapter 6,1961.

23. M.J.Ehrlich,S.Silver,G.Held, "Studies of the Diffraction of Electromagnetic Waves by Circular Apertures and Complementary Obstacles: The Near-Zone Field," J.Appl.Phys.,Vol.26,pp.336-345,March,1955.

ACKNOWLEDGEMENT

The author wishes to express his gratitude to Dr. David K. Cheng, the project director and thesis advisor, for suggesting this task and for his valuable advice and consultation throughout its completion, and to B. Strait for his assistance whose previous work formed the basis of this investigation. Appreciation is also extended to D. Spurling for helping with experimental data, F. Cummings for his mechanical work, and Mrs. R. Daigle for typing this report.

	No. of Copies
RADC (RALTM/Mr. Potenza) Griffiss AFB NY	3
RADC (RAAPT) Griffiss AFB NY	1
RADC (RAALD) Griffiss AFB NY	1
GEEIA (ROZMCAT) Griffiss AFB NY	1
RADC (RAIS/Mr. Malloy) Griffiss AFB NY	1
U S ARMY Electronics R and D Labs Liaison Officer RADC Griffiss AFB NY	1
AUL (3T) Maxwell AFB Ala	1
ASD (ASAPRD) Wright-Patterson AFB Ohio	1
Chief, Naval Research Lab ATTN: Code 2027 Wash 25 DC	1
Air Force Field Representative Naval Research Lab ATTN: Code 1010 Wash 25 DC	1
Commanding Officer U S Army Electronics R and D Labs ATTN: SELRA/SL-ADT Ft Monmouth NJ	1
National Aeronautics and Space Admin Langley Research Center Langley Station Hamption Virginia ATTN: Librarian	1

AFSC (SCSE) Andrews AFB Wash 25 DC	1
Commanding General US Army Electronic Proving Ground ATTN: Technical Documents Library Ft Huachuca Ariz	1
ASTIA (TISIA-2) Arlington Hall Station Arlington 12 Va	10
Hq USAF (AFCOA) Wash 25 DC	1
AFOSR (SRAS/Dr. G.R. Eber) Holloman AFB NMex	1
Commander US Naval Air Dev Center (NADC Lib) Johnsville Pa	1
Commander Naval Missile Center Tech Library (Code No 3022) Pt Mugu Calif	1
Commanding General ATTN: Technical Library US Army Missile Command Redstone Arsenal, Alabama	1
Commander US Naval Ordnance Lab (Tech Lib) White Oak, Silver Springs Md	1
Commanding General ATTN: Technical Library White Sands Missile Range New Mexico	1
Director US Army Engineer R and D Labs Technical Documents Center Ft Belvoir Va	1
ESD(ESRL) LG Hanscom Fld Bedford, Mass.	1

Commanding Officer and Director 1
US Navy Electronics Lab (LIB)
San Diego 52 Calif

ESD (ESAT) 1
LG Hanscom Fld
Bedford Mass

APGC (PGAPI) 1
Eglin AFB Fla

AFSWC (SWOI) 1
Kirtland AFB NMex

AFMTC (Tech Library MU-135) 1
Patrick AFB Fla

RADC (RAWED/Mr. Blymiller) 1
Griffiss AFB NY

RADC (RALSS/Mr. Diab) 1
Griffiss AFB NY

Martin Company 1
Electronic Systems and Products Div.
ATTN: Mr. Harry Sefton
Mail No.355
Baltimore 3 Md

Commander 1
Air Force Cambridge Research Laboratory
ATTN: Mr. C. E. Ellis
Bedford Mass.

Director 1
National Security Agency
ATTN: Code C124 (Mr. W. G. Fink)
Fort George G. Meade, Md.

Director 1
National Security Agency
ATTN: Code K31 (Mr. J. B. Norvell)
Fort George G. Meade, Md.

Commanding Officer 1
US Army Ordnance
Ballistics Research Laboratory
ATTN: ORDBG-BRL-M (Mr. V. Richard)
Aberdeen Proving Ground, Md.

Chief 1
National Bureau of Standards
Boulder Laboratories
ATTN: Mr. H. V. Cottony
Boulder, Colorado

Commander 1
Aeronautical Systems Division
Air Force Systems Command
ATTN: ASRNRE-4 (Mr. E. Turner)
Wright-Patterson AFB Ohio

Commander 1
US Air Force Security Service
ATTN: Mr. Art Martinez
San Antonio, Texas